ERDC TR-16-13

US Army Corps
of Engineers®
Engineer Research and
Development Center

ERDC
INNOVATIVE SOLUTIONS
for a safer, better world

Force Protection Basing; TeCD 1a

Equipment and Protocols for Quasi-Static and Dynamic Tests of Very-High-Strength Concrete (VHSC) and High-Strength High-Ductility Concrete (HSHDC)

Brett A. Williams, Robert D. Moser, William F. Heard,
Carol F. Johnson, Dylan A. Scott, Thomas R. Slawson,
Henry L. Blake, R. Nicholas Boone, and Thomas D. White

August 2016

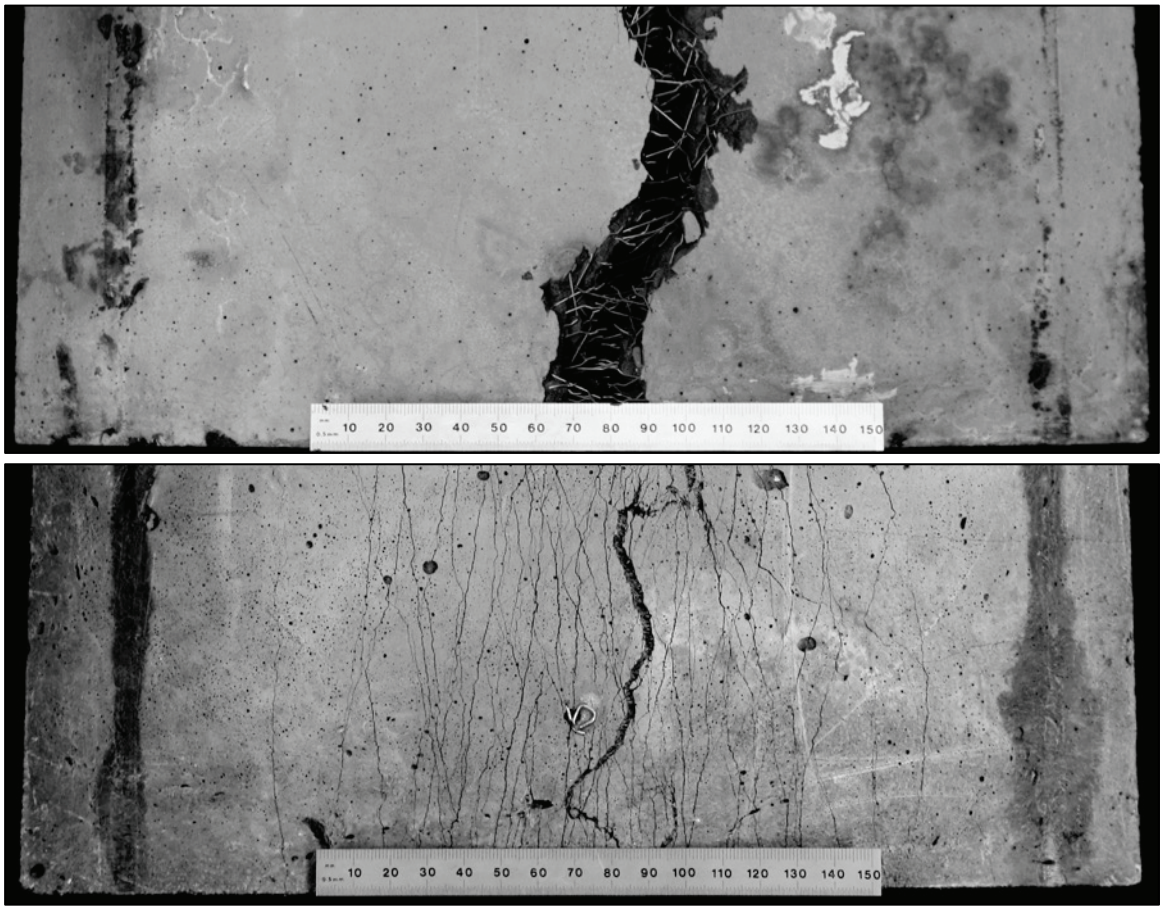

Engineer Research and Development Center

The U.S. Army Engineer Research and Development Center (ERDC) solves the nation's toughest engineering and environmental challenges. ERDC develops innovative solutions in civil and military engineering, geospatial sciences, water resources, and environmental sciences for the Army, the Department of Defense, civilian agencies, and our nation's public good. Find out more at www.erdc.usace.army.mil.

To search for other technical reports published by ERDC, visit the ERDC online library at http://acwc.sdp.sirsi.net/client/default.

ERDC TR-16-13
August 2016

Equipment and Protocols for Quasi-Static and Dynamic Tests of Very-High-Strength Concrete (VHSC) and High-Strength High-Ductility Concrete (HSHDC)

Brett A. Williams, Robert D. Moser, William F. Heard, Carol F. Johnson, Dylan A. Scott Thomas R. Slawson, and R. Nicholas Boone

Geotechnical and Structures Laboratory
U.S. Army Engineer Research and Development Center
3909 Halls Ferry Road
Vicksburg, MS 39180-6199

Henry L. Blake

Information Technology Laboratory
U.S. Army Engineer Research and Development Center
3909 Halls Ferry Road
Vicksburg, MS 39180-6199

Thomas D. White

Department of Civil and Environmental Engineering
Mississippi State University
501 Hardy Road
Mississippi State, MS 39762-9546

Final report

Prepared for Office of the Assistant Secretary of the Army for Acquisition, Logistics and Technology, Research and Technology (SAAL-ZT)

Under Work Unit BT007–Survivability Material Development, “Force Protection Basing; TeCD 1a”

Abstract

This research developed the quasi-static and dynamic equipment and protocols for tests of both very-high-strength concrete (VHSC) and high-strength high-ductility concrete (HSHDC) to predict blast performance. VHSC was developed for high compressive strength (> 200 MPa). Using VHSC as the baseline material, HSHDC was developed and exhibits comparable compressive strength (> 150 MPa) and high tensile ductility (> 3 percent tensile strain). This research investigated quasi-static material properties including compression, tension, and flexure (third-point and pressure loadings). Additionally, dynamic blast load simulator (shock tube) tests were performed on simply supported one-way panels in flexure. Subsequently, the material response in flexure was predicted using the Wall Analysis Code (WAC). Although VHSC has a higher peak flexural strength capacity, HSHDC exhibits higher ductility through multiple parallel micro-cracks transverse to loading. The equipment and test protocols proved to be successful in providing ways to test scaled concrete specimens quasi-statically and dynamically.

Contents

Abstract ii

Figures and Tables vi

Preface ix

Unit Conversion Factors x

1 Introduction 1

1.1 Problem 1
1.2 Potential solution 1
1.3 Research objectives 2
1.4 Research scope 2

2 Review of Literature 4

2.1 Introduction 4
2.2 Development of high-strength high-ductility concrete (HSHDC) 4
2.2.1 Engineered cementitious composites (ECC) 4
2.2.2 Very-high-strength concrete (VHSC) 5
2.2.3 High-strength high-ductility concrete (HSHDC) 5
2.3 Standard quasi-static test methods 6
2.4 Characterization of FRC under blast loading 7
2.4.1 Quasi-static characterization 7
2.4.2 Blast load simulator (BLS) experiments 8
2.5 Prior testing and results 9
2.6 Wall Analysis Code (WAC) 11

3 Materials 12

3.1 Very-high-strength concrete (VHSC) 12
3.2 High-strength high-ductility concrete (HSHDC) 12

4 Scaling Production and Fabrication of HSHDC 15

4.1 Introduction 15
4.2 Scaling mixing action 15
4.3 Batching sequence 16
4.4 Placement techniques 17
4.5 Finishing techniques 18
4.6 Curing regime and specimen preparation 18

5 Quasi-Static 20

5.1 Introduction 20
5.2 Compressive strength 20
5.2.1 Comparison between VHSC and HSHDC 21
5.2.2 Comparison to previous HSHDC data 22
5.3 Splitting tensile strength 22

5.3.1 Comparison between VHSC and HSHDC 23
5.3.2 Comparison to previous HSHDC splitting tensile data 23
5.4 Direct tensile strength 24
5.4.1 Comparison between VHSC and HSHDC 26
5.4.2 Comparison to previous HSHDC data 26
5.5 Third-point flexure strength 27
5.5.1 Flexure tests of VHSC and HSHDC 29
5.5.2 Comparison to previous HSHDC data 29

6 Equipment and Test Method Development 30
6.1 Introduction 30
6.2 Simply supported, pressure-loaded one-way panels 30
6.3 Importance of resistance function for dynamic calculations 31
6.4 Water chamber equipment and test method development 31
6.4.1 Physical design and setup 31
6.4.2 Data acquisition and instrumentation 33
6.5 Blast load simulator equipment and test method development 34
6.5.1 Physical design and setup 34
6.5.2 Achieving consistent test pressures for replicates 37
6.5.3 Data acquisition and instrumentation 38

7 Testing of Simply Supported Pressure-Loaded Panels 40
7.1 Introduction 40
7.2 Centerline displacement measurements 40
7.3 Strain and strain rate calculations 41
7.4 Quasi-static water chamber tests 42
7.4.1 Results 42
7.4.2 Discussion 44
7.5 Resistance function 45
7.6 Dynamic blast data 46
7.6.1 Results 46
7.6.2 Discussion 47

8 Wall Analysis Code (WAC) 49
8.1 Introduction to WAC 49
8.1.1 Procedure for using WAC 49
8.1.2 Specified load case 50
8.2 WAC calculations with quasi-static resistance function 52
8.2.1 Results 52
8.2.2 Discussion 52
8.3 WAC calculations with dynamic resistance function 53
8.3.1 Developing dynamic resistance function 53
8.3.2 Results 54
8.3.3 Discussion 55

9 Conclusions and Recommendations 58
9.1 Scope 58
9.2 Conclusions 58

9.2.1 Quasi-static material properties *58*
9.2.2 Dynamic test method development *58*
9.2.3 Testing of simply supported, pressure-loaded one-way panels *58*
9.2.4 Wall Analysis Code (WAC) *59*
9.3 Recommendations 59
9.3.1 Quasi-static material properties *59*
9.3.2 Test method development *59*
9.3.3 Testing of simply supported, pressure-loaded one-way bending panels *60*
9.3.4 Wall Analysis Code (WAC) *60*
9.4 Summary 60

References 61

Appendix A: Photographs of Tested Panels 64

Report Documentation Page

Figures and Tables

Figures

Figure 1.1. Optical microscopy images of HSHDC (a, c) and VHSC (b, d). 2
Figure 1.2. Flow chart displaying research scope. 3
Figure 2.1. Illustration of micro-cracking and fiber interactions in SHCC[9]. 5
Figure 2.2. Positive pressure water test chamber designed for testing fourth-scale CMU block walls 80 cm high by 160 cm wide (32 x 64 in).[19,20] 8
Figure 2.3. Third-scale Blast Load Simulator at the U.S. Army Engineer Research and Development Center (ERDC). 9
Figure 2.4. HSHDC specimen 163x86x8 cm (64x34x3 in.) tested in the ERDC's 1/3-scale blast load simulator. 10
Figure 2.5. HSHDC specimen 163x86x8 cm (64x34x3 in.) tested using quasi-static positive water pressure loading. 11
Figure 3.1. Dramix 3D 55/30BG hooked steel fiber. 12
Figure 3.2. Spectra 1000 375d Chopped UHMWPE Fiber, single fiber (a), bulk fibers (b), fiber morphology (c). 14
Figure 4.1. Hobart paddle mixer (Hobart 2015) (a), and Eirich high-shear mixer (Eirich Mixing Technology 2015) (b). 15
Figure 4.2. Weigh raw materials prior to batching. 16
Figure 4.3. HSHDC images showing the following visual cues of the mixing progression: mixed dry materials (a), darkened color as water/HRWRA are distributed throughout (b), clumps begin to form (c), the material starts to roll over in large folds (d), the mixture becomes fluid (e), and then fibers are added and dispersed (f). 17
Figure 4.4. Finished HSHDC samples being sprayed with evaporation retardant to prevent moisture loss. 18
Figure 5.1. Tested uniaxial compressive specimen of VHSC (a), HSHDC (b), and test setup (c). 20
Figure 5.2. Compression data from VHSC 102x203 mm (4x8 in.) cylinders (a) and HSHDC 51 mm (2 in.) cubes (b). 21
Figure 5.3. VHSC (a) and HSHDC (b) split tensile specimens, HSHDC specimen displays failure modes compressive crushing (flattened region at the bottom of specimen); ASTM test setup (c) (ASTM 2012). 22
Figure 5.4. Splitting tensile data from VHSC and HSHDC 102x203 mm (4x8 in.) cylinders. 23
Figure 5.5. Direct Tension setup from Japanese Society of Civil Engineers (JSCE) "Testing Method for Uniaxial Tensile Strength" showing a dimensioned drawing (a) (JSCE 2008) and the actual test setup (b) (Scott et al. 2014); 30 mm (1.18-in.) thickness used in this study. 24
Figure 5.6. LVDT setup used for JSCE "Testing Method for Uniaxial Tensile Strength." 25
Figure 5.7. VHSC (top) and HSHDC (bottom) direct tension specimens, HSHDC specimen exhibits multiple parallel cracking pattern causing pseudo-strain-hardening behavior. 25
Figure 5.8. Direct tension data for VHSC and HSHDC specimens. 26
Figure 5.9. Tested third-point flexure specimens of VHSC (a) and HSHDC (b), HSHDC specimen shows multiple cracking radiating back to the center of the beam. 28
Figure 5.10. Flexure data comparing VHSC to HSHDC. 28

Figure 6.1. Modular Protective System (MPS) utilizing armor panels for rapidly deployable blast and ballistic protection. 30
Figure 6.2. Initial water chamber design (WC1) for quasi-static pressure loading capable of testing a 305x305x25 mm (12x12x1 in.) square specimen underneath the support rails at the top of the chamber. 32
Figure 6.3. Drain milled in the bottom of the high-density polyethylene (HDPE) base of water chamber. 33
Figure 6.4. Water chamber test fixture (WC2) capable of flexure testing 305x305x25-mm (12x12x1-in.) concrete panel with a 254 mm (10-in.) span. 33
Figure 6.5. Graphical user interface showing customized virtual instrument in National Instruments LabVIEW program. 34
Figure 6.6. Complete test setup for small-scale blast load simulator (BLS). 35
Figure 6.7. Reaction frame providing simply supported loading conditions with appropriate cutouts and windows for instrumentation, lighting, and video (dimensions in inches). 35
Figure 6.8. Modified BLS with stiffened supports and tension members (a) and Red Head Tapcon anchors through angle iron into the slab (b). 36
Figure 6.9. Pressure gauge layout showing gauges P1-P9 as configured for calibration shots, gauges P1, P2, P8, and P9 were used during concrete panel testing. 37
Figure 6.10. Small-scale BLS test setup showing accelerometer positions and scales used for high-speed video measurements. 39
Figure 7.1. Centerline displacement of HSHDC simply supported one-way panel specimen. 40
Figure 7.2. High-speed video length measurements (yellow lines), pretest image (left), and peak centerline deflection image (right). 42
Figure 7.3. Quasi-static positive water pressure loading of simply supported one-way panels. 43
Figure 7.4. Image of HSHDC-18 panel after testing with quasi-static pressure loading. 44
Figure 7.5. Image of VHSC-20 panel after testing with quasi-static pressure loading. 45
Figure 7.6. Quasi-static positive water pressure loading of simply supported panels and calculated resistance functions (RF). 46
Figure 7.7. Panel VHSC-6 image taken from high-speed video showing hairline cracking (inside the boxed region) observed during dynamic testing. 47
Figure 7.8. Panel HSHDC-16 image taken from high-speed video showing multiple, parallel cracks from dynamic testing. 48
Figure 8.1. Wall Analysis Code (WAC) graphical user interface (GUI). 51
Figure 8.2. Difference in quasi-static (dotted) and dynamic (solid) resistance functions calculated for material response of VHSC and HSHDC. 51
Figure 8.3. WAC predicted deflections vs. measured deflections for individual test panels from dynamic testing using quasi-static resistance functions. 53
Figure 8.4. Difference in quasi-static (dotted) and dynamic (solid) resistance functions calculated for material response of VHSC and HSHDC. 54
Figure 8.5. WAC predicted deflections vs. measured deflections from dynamic testing using quasi-static resistance functions and dynamic resistance functions. 55

Tables

Table 3.1. VHSC mixture proportions by weight. 12
Table 3.2. HSHDC mixture proportions by weight. 13

Table 5.1. Uniaxial compression test results. 21
Table 5.2. Splitting tensile test results. 23
Table 5.3. Direct tension test results. 26
Table 5.4. Third-point flexure test results. 29
Table 7.1. VHSC results from quasi-static testing of simply supported one-way panels. 43
Table 7.2. HSHDC results from quasi-static testing of simply supported one-way panels. 43
Table 7.3. Dynamic blast data. 47
Table 8.1. Results from WAC analysis using quasi-static resistance function. 52
Table 8.2. Results from WAC analysis using dynamic resistance function. 55

Preface

This study was conducted for the Office of the Assistant Secretary of the Army for Acquisition, Logistics and Technology, Research and Technology (SAAL-ZT) under Work Unit BT007-Survivability Material Development.

The work was performed by the Concrete and Materials Branch (CMB) of the Engineering Systems and Materials Division (ESMD), U.S. Army Engineer Research and Development Center, Geotechnical and Structures Laboratory (ERDC-GSL). The Principal Investigator for this research was Brett A. Williams, CMB. Williams prepared this report, which is essentially his thesis submitted to the faculty of Mississippi State University in partial fulfillment of the requirements for the degree of Master of Science in Civil Engineering in the Department of Civil and Environmental Engineering.

The authors would also like to recognize technical assistance from Jason Morson, Kevin Taylor, Rudolph Andreatta, Dan Wilson, Mickey Blackmon, and Christopher Ables. Helpful conversations with Brian Green, Mare Dockery, Dr. Stanley Woodson, Dr. Philip Gullett, Dr. Ravi Ranade, and Dr. Victor Li are also gratefully acknowledged.

At the time of publication, C.M. Moore was Chief, CEERD-GMC; B.A. Steed was Chief CEERD-GSM; Omar-Perez Flores was Acting Chief, CEERD-GSV; Dr. G.W. McMahon was Chief, CEERD-GM; J.L. Davis was Acting Chief, CEERD-GS; and P.G. Kinnebrew, CEERD-GZT, was the Technical Director for Survivability and Protective Structures research area. The Deputy Director of ERDC-GSL was Dr. W.P. Grogan and the Director was B.P. Durst.

COL Bryan S. Green was the Commander of ERDC, and Dr. Jeffery P. Holland was the Director.

Unit Conversion Factors

Multiply	By	To Obtain
cubic feet	0.02831685	cubic meters
cubic yards	0.7645549	cubic meters
degrees Fahrenheit	(F-32)/1.8	degrees Celsius
feet	0.3048	meters
inches	0.0254	meters
microns	1.0 E-06	meters
pounds (force)	4.448222	newtons
pounds (force) per square inch	6.894757	kilopascals

1 Introduction

1.1 Problem

The United States military continues to investigate technologies to protect personnel and facilities. One important technology is related to material development. Currently, the Army utilizes concrete armor panels as barrier walls to protect soldiers and military assets. However, the current panels are relatively heavy for a two-man team to install. Benefits would be realized from panels that were lighter and provided an equivalent level of blast protection. On one side, an improved material could result in a panel that ships easier, reduces manpower requirements, and assembles more rapidly. On the other side a thicker panel of an equivalent, lighter material could improve protection.

1.2 Potential solution

High-strength high-ductility concrete (HSHDC) has been developed through a joint partnership between the U.S. Army Engineer Research and Development Center (ERDC) and the Materials Science and Engineering department at the University of Michigan. This material is comprised of the constituent materials used in very-high-strength concrete (VHSC) that has been used by the U.S. Army Corps of Engineers for many years. The components of VHSC consist of class H cement, manufactured silica sand, silica fume, silica flour, fly ash, and hooked steel fibers. HSHDC uses the same constituent materials as VHSC, yet different mixture proportions, and has ultra-high molecular weight polyethylene (UHMWPE) fibers rather than steel fibers. This material combines the high compressive strength of VHSC (used as the control in this study) with the strain hardening and strain capacity found in lower strength Engineered Cementitious Composite (ECC) materials. Although HSHDC has been characterized very well quasi-statically (slower rates where material response appears to be static), dynamic material performance is still relatively unknown. For the Army to benefit from this material, higher strain rate testing must be conducted. Optical microscopy images of HSHDC and VHSC are presented in Figure 1.1.

Figure 1.1. Optical microscopy images of HSHDC (a, c) and VHSC (b, d).

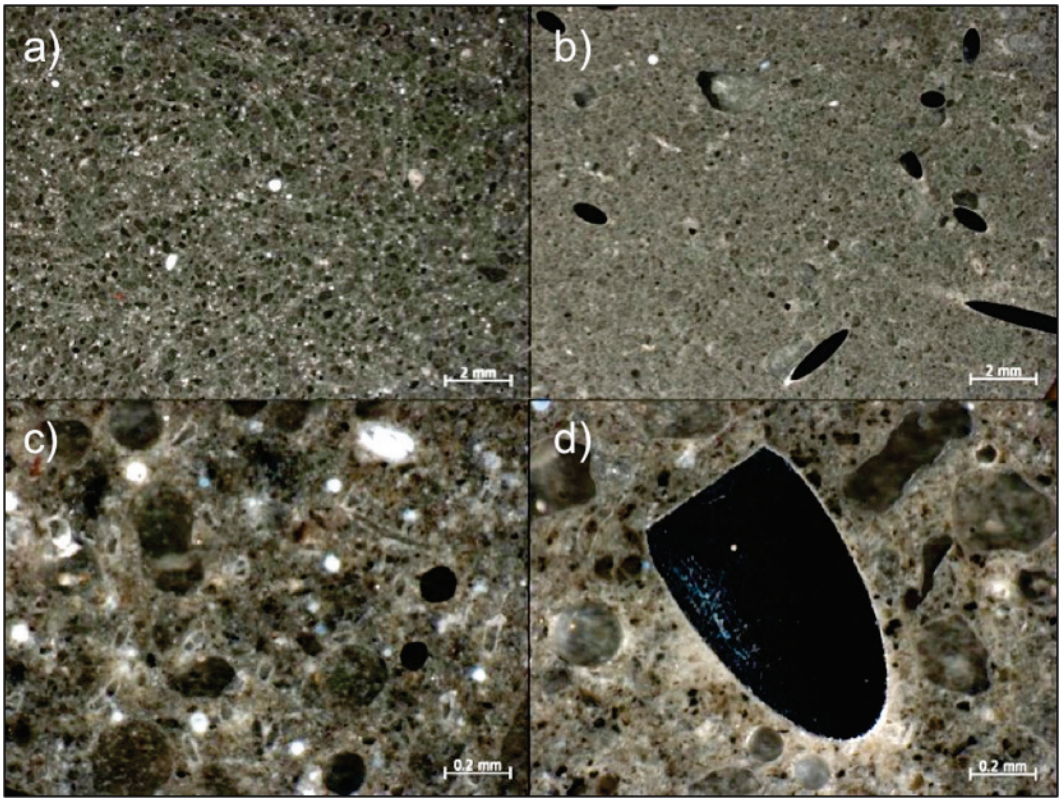

1.3 Research objectives

In determining the application of HSHDC for protective structures, fundamental mechanisms of the material must be discovered. This leads to the following research objectives:

1. Identify the critical quasi-static mechanical properties, deformation behavior, and damage mechanisms in HSHDC and compare the behavior with VHSC.
2. Develop experimental apparatus and test protocols for quasi-static and dynamic pressure loadings of simply supported one-way panels.
3. Compare the measured material response to known design methodologies used in the Wall Analysis Code (WAC).
4. Study the high strain rate behavior of HSHDC and compare it with damage mechanisms observed quasi-statically.

1.4 Research scope

Quasi-static material testing will be conducted and includes: unconfined compressive strength, splitting tensile strength, third-point flexure

strength, and direct tensile strength. Results from these tests will be used as a baseline to compare results from the same tests previously published on HSHDC.

An important part of this study will be in comparing the flexural response of HSHDC and the control VHSC due to blast loading. In order to examine the flexural response of these materials, a resistance function is determined from load/deflection data from quasi-statically loading specimens using water pressure. After these tests, additional concrete panels will be tested on the small-scale Blast Load Simulator (BLS) using identical samples and support conditions as those in the quasi-static tests. This will allow for a direct comparison of the failure modes as the strain rate increases. An overview of this research scope is presented in Figure 1.2.

Figure 1.2. Flow chart displaying research scope.

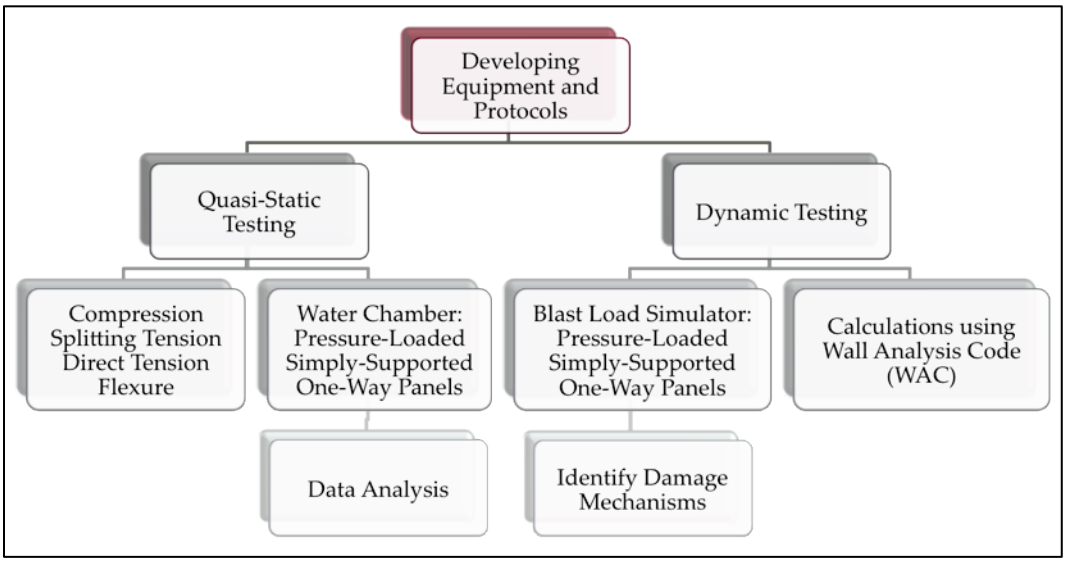

2 Review of Literature

2.1 Introduction

The review of literature includes background information on development of the two concretes used in this study: high-strength high-ductility concrete (HSHDC) and very-high-strength concrete (VHSC). Test methods are also reviewed that include ASTM International standards, Japanese Society of Civil Engineers (JSCE) standard, and new test methods developed in current research for quasi-static and dynamic pressure loadings of cementitious specimens.

2.2 Development of high-strength high-ductility concrete (HSHDC)

High-strength high-ductility concrete (HSHDC) results from combining attributes from two distinct materials: engineered cementitious composite (ECC) and very-high-strength concrete (VHSC). Li (1993) began initial development stages of ECC in 1993 in an attempt to maximize the ductile response of concrete. Meanwhile, O'Neil (2008) developed a VHSC focused on attaining maximum compressive strength. His approach involved particle packing and an optimized curing regime. Ranade and co-workers (Ranade et al. 2012) developed a material, HSHDC, which combined the ductility of ECC with the compressive strength of VHSC. Background information on the development of HSHDC is described below, while details for the exact mixture proportions used for this research are described in Chapter 3.

2.2.1 Engineered cementitious composites (ECC)

ECC is a strain-hardening cementitious composite (SHCC). It exhibits apparent ductility through microcracking in tension. The microcracks are parallel (transverse to loading direction) and bridged by polyvinyl alcohol (PVA) fibers distributed throughout the concrete matrix. The ECC is characterized by an average tensile strain of up to 5 percent (500 times higher than conventional concrete) and compressive strengths of approximately 40 MPa (5.8 ksi) (Li 2003). ECC was developed using a micromechanics based design concept developed by Li and co-workers (Lin et al. 1999; Li et al. 2001; Li et al. 2002). These design principles are based on "deliberate selection of fiber, matrix, and their interface" (Ranade et al. 2013). This approach combines the material structure-property

relationships at the macroscopic scale with the materials science approach of focusing on processing and formation of microstructures. Figure 2.1 illustrates the multiple cracking patterns observed in SHCC resulting in strain hardening behavior under direct tensile loadings.

Figure 2.1. Illustration of micro-cracking and fiber interactions in SHCC[9].

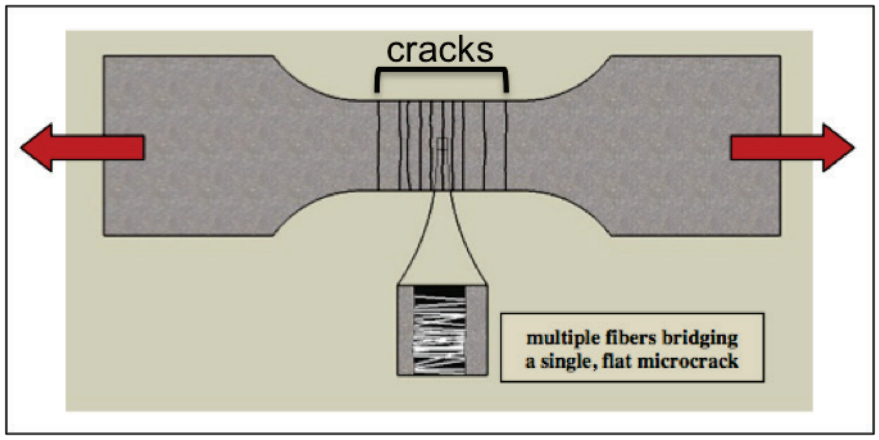

2.2.2 Very-high-strength concrete (VHSC)

Very-high-strength concrete (VHSC) is taken to be a concrete with compression strength that exceeds 200 MPa (29.0 ksi) (Ranade et al. 2013). This study focuses on one particular VHSC developed at the ERDC by O'Neil (2008), which is being used as the control in the current study. VHSC was also used as the baseline for developing HSHDC. In previous work (Ranade et al. 2009), the compressive strength of this VHSC ranged from 190-244 MPa (27.6-35.4 ksi). This compressive strength was achieved by using particle-packing methods. As a result, the porosity is reduced and compressive strength increased. However, the material exhibits brittleness similar to ceramics. Historically, this shortcoming has been addressed by adding steel fibers to bridge cracks and maintain structural integrity.

2.2.3 High-strength high-ductility concrete (HSHDC)

High-strength high-ductility concrete (HSHDC) applies the results from the micromechanical design approach of ECC to the VHSC matrix. The product of this approach is a concrete that has an average tensile ductility of 3.4 percent and an average ultimate compressive strength of 166 MPa (24.1 ksi). The combination of these two properties allows for maximum energy absorption by increasing the area underneath the stress-strain curve.

The development of HSHDC involved adjusting the fresh properties of VHSC to optimize fiber distribution. The adjustments include reducing the sand/cement ratio and increasing the high-range water-reducing (HRWA) admixture. At the same time, the w/c ratio is unchanged. The mixture remains workable with good fiber dispersion. Also, HSHDC compressive strength is comparable to that of VHSC.

Fiber selection was also important. Since the VHSC matrix has minimal water content at a w/c of 0.22, the polymer fiber needed to be hydrophobic so as not to require additional water in the final mixture. Ultra-high molecular weight polyethylene (UHMWPE) fibers were selected for tests based on their aspect ratio, strength, and hydrophobic properties. Fiber selection and optimization is discussed in great detail by Ranade (Ranade et al. 2013). The final fiber selection was a Honeywell Spectra 1000 fiber chopped to 0.5-in. length.

2.3 Standard quasi-static test methods

ASTM International Standards were used to characterize commonly reported material properties for the concrete specimens produced in this study. These test methods include: ASTM C 39 ((ASTM 2012) Standard Test Method for Compressive Strength of Cylindrical Concrete Specimens), ASTM C 109 ((ASTM 2013) Standard Test Method for Compressive Strength of Hydraulic Cement Mortars), ASTM C 496 ((ASTM 2012) Standard Test Method for Splitting Tensile Strength of Cylindrical Concrete Specimens), and ASTM C 1609 ((ASTM 2012) (Standard Test Method for Flexural Performance of Fiber-Reinforced Concrete).

Direct uniaxial tension tests of VHSC and HSHDC adopted dumbbell-shaped specimens recommended by the Japanese Society of Civil Engineers (JSCE) (Testing Method Appendix (JSCE 2008)) for standardized testing of high performance fiber reinforced cement composites (HPFRCC). In initial studies with HSHDC (Ranade et al. 2012), tension tests were performed with a pin-supported (hinged) load end. Later on, the JSCE method was modified to include fixed-fixed support conditions (Ranade et al. 2013). Although the JSCE method allows for specimen thickness of 13 or 30 mm (0.51 or 1.18 in.), only 13 mm specimen thicknesses have been reported in previously published research on HSHDC.

Although ASTM C496 (splitting tensile strength) is a common tensile test for concrete, it provides a non-conservative estimation (Ranade et al.

2013) of actual tensile strength of HSHDC, which is approximately 19 percent higher than direct tension test results (Ranade et al. 2013).

2.4 Characterization of FRC under blast loading

As discussed in the following section, dynamic flexural response of concrete is a focus area for the U.S. military. An informative reference for structural dynamics has been provided by Biggs (1964). The development of quasi-static resistance functions combined with the use of shock tube experiments provides material performance predictions using single degree-of-freedom (SDOF) models.

2.4.1 Quasi-static characterization

For the purpose of predicting and modeling blast response of concrete in flexure, quasi-static data are needed to produce resistance functions for a given type of support conditions. Initial test methods used positive air pressure to apply loads to masonry walls (Yokel et al. 1971). Similarly, vacuum is still being used to apply these types of loads (Salim et al. 2013). Where pressure loadings are impractical, loading trees have also been designed in various ways to distribute point loads across wall systems (Dennis et al. 2002). At the ERDC, Woodson developed a quasi-static chamber for testing walls using positive water pressure chamber (Dennis et al. 2002). This work is the basis for the design of the water chamber used in this study as detailed in Chapter 6.

A conceptual design of Woodson's apparatus is shown in Figure 2.2. This design focused on testing concrete masonry unit (CMU) walls. The CMU walls were built in place. Water is introduced simultaneously on both sides of the panel so that differential pressure does not develop as the water level increases. This ensures that the panel is at a state of equilibrium when testing begins. City water pressure is used to fail the wall specimens using pressures of approximately 60 kPa (8.5 psi) chamber (Dennis et al. 2002).

Figure 2.2. Positive pressure water test chamber designed for testing fourth-scale CMU block walls 80 cm high by 160 cm wide (32 x 64 in).[19,20]

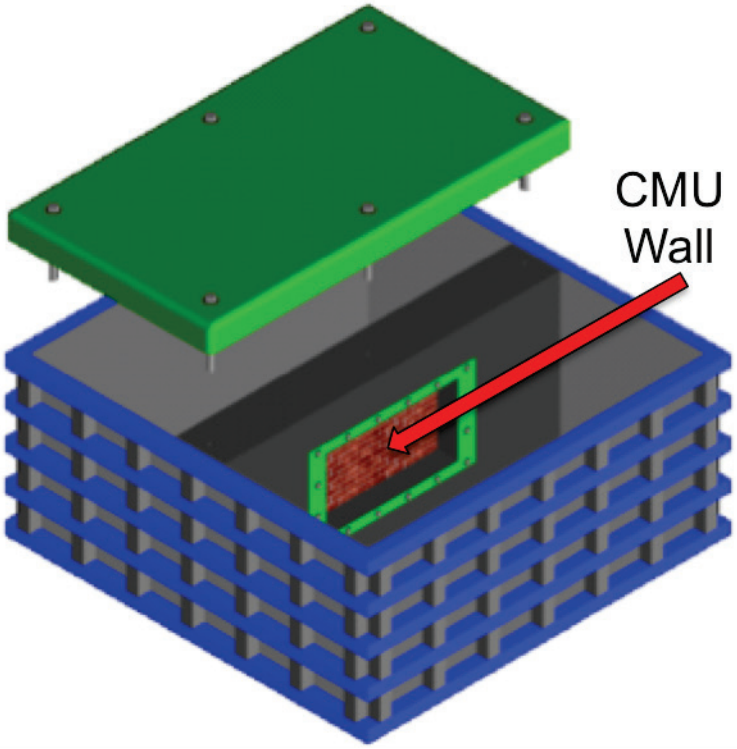

2.4.2 Blast load simulator (BLS) experiments

A blast load simulator (BLS) at the ERDC can be utilized to provide loading conditions found in explosive events with a controlled environment. The BLS is a gas-driven air blast of compressed air. It applies pressure load with compressed air that is quickly released from a pressurized tank and directed in a uniform pressure wave toward the desired specimen surface. Dimensions for the BLS used in the current study are presented in Section 6.5.

The ERDC's Blast Load Simulator (BLS) facility is designed to house three different scale blast load simulators (also known as gas-driven shock tubes). The full-scale design will be capable of testing a structural wall up to 3.66 x 3.66 m (12 x 12 ft). The construction of this full-scale shock tube is not completed. The other two shock tubes are functional and were developed at one-third and one-twelfth of the full scale.

During initial developments of the BLS facility, the small-scale (1/12-scale) shock tube was built for calibration shots and proof of concept prior to designing the 1/3-scale shock tubes. Subsequently, the 1/3-scale facility

was built and has been used for all BLS experimentation to date. This 1/3-scale shock tube has the capability to vary target pressure (loading on specimen) and impulse (duration of loading). This is accomplished by controlling tank pressure and tank volume while providing adjustable air vents. As a result, a desired loading history (simulating a given explosive at a given standoff distance) can be imposed on the specimen. This shock tube is shown in Figure 2.3.

Figure 2.3. Third-scale Blast Load Simulator at the U.S. Army Engineer Research and Development Center (ERDC).

The small-scale BLS required modifications to transition from a proof-of-concept to a fully functional testing device. The small-scale BLS configuration was selected for the reduced length scale to test the 305x305x25 mm (12x12x1 in.) panel specimens in the current study. Prior work at this facility on the 1/3-scale shock tube is discussed in greater detail in the literature Johnson (2013) and Robert et al. (2011).

2.5 Prior testing and results

In my prior unreported testing at the ERDC, HSHDC batches were mixed in a twin-shaft mixer with a capacity of 1 cubic meter. The batches were large enough to cast 163x86x8 cm (64x34x3 in.) one-way slab specimens for testing in the ERDC's 1/3-scale Blast Load Simulator (BLS). These panels exhibited reduced flexural strength as compared to the control VHSC tested in the same manner. Also, they did not fail in a ductile manner as expected. An HSHDC specimen is shown in Figure 2.4 showing that some cracks were formed parallel to the simple supports, but microcrack saturation was lower than expected in the center of the specimen (where maximum displacement is observed).

Figure 2.4. HSHDC specimen 163x86x8 cm (64x34x3 in.) tested in the ERDC's 1/3-scale blast load simulator.

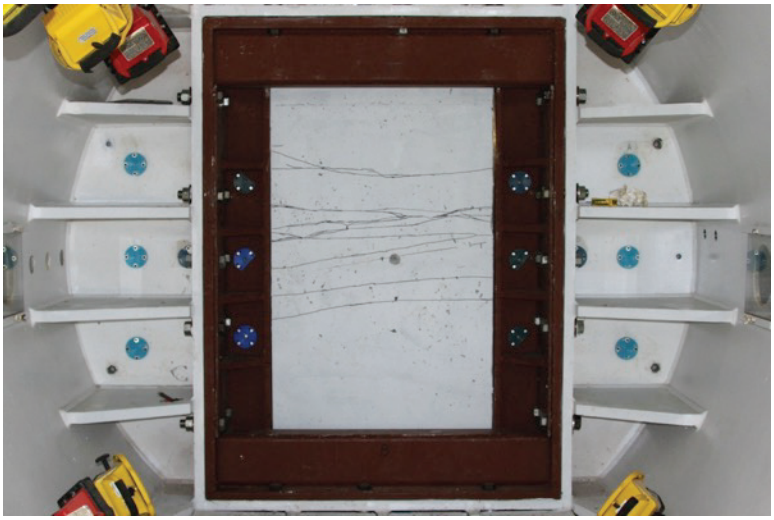

The initial premise was that this failure to initiate microcracking was related to the influence of high strain rate and a potential transition in plastic deformation mechanisms between quasi-static and dynamic strain rates. Subsequent tests of 1/3-scale VHSC and HSHDC slabs were conducted using a water chamber. These specimens were simply supported one-way slabs as in the initial blast tests. However, water pressure provides quasi-static loading rather than impulse loading with air pressure. Panels tested in the water chamber also failed to exhibit the ductility expected from HSHDC. An HSHDC specimen from the water chamber tests is shown in Figure 2.5. Although some parallel cracks are visible, the crack separation was much larger than the saturated cracking patterns observed in smaller flexural beam specimens.

The conclusion from these test results was that numerous factors affected the tests and therefore the results. Factors that changed comparing previously published tests on HSHDC to the unreported 1/3-scale tests presented here included: the mixer type (tabletop paddle vs. twin-shaft batch plant), placement procedure (hand vs. shovels/rakes), curing condition (as presented in Section 4.6 vs. steam), test specimen size, and batch size. In order to pursue this research further, these factors need to be controlled so that the influence of material and processing variables can be quantified.

Figure 2.5. HSHDC specimen 163x86x8 cm (64x34x3 in.) tested using quasi-static positive water pressure loading.

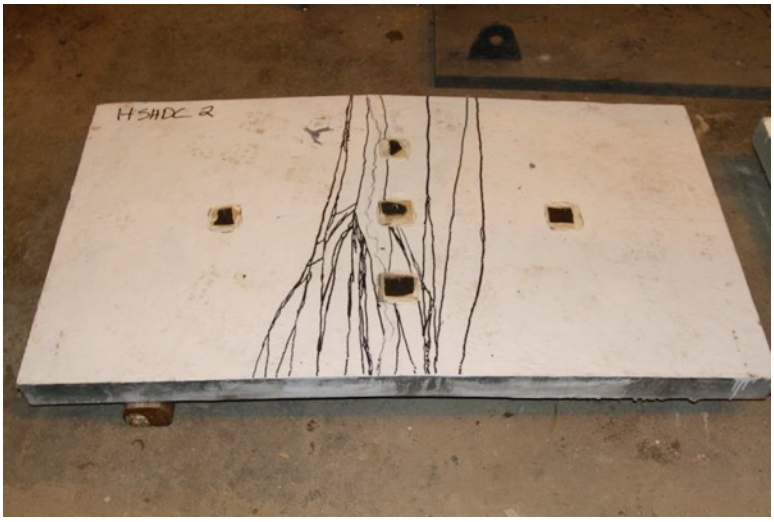

2.6 Wall Analysis Code (WAC)

Wall Analysis Code (WAC) (Slawson 1995) is an analysis program. The model incorporated in the program is a single degree-of-freedom (SDOF) model and incorporates piece-wise linear functions for the wall (concrete specimen) resistance and loading. A resistance function is input to the program to provide a relationship between the specimen load and centerline deflection. This is established using quasi-static testing with the same loading and support conditions that will be observed during blast testing. The input to WAC is a text file with X (deflection) and Y (pressure) values.

The program can be used to simulate the centerline deflection response of test panels subjected to impulse loading in the gas-driven shock tube. Subsequently, the analysis can be used to compare predicted and actual results for a given load-time pressure history.

3 Materials

3.1 Very-high-strength concrete (VHSC)

O'Neil (2008) describes the development of VHSC in great detail. The constituents and mixture proportion for this concrete are listed in Table 3.1. Constituent materials are outlined in greater detail in the literature (Williams et al. 2009; Roth et al. 2010). This material is being used as the control in this study. This concrete uses hooked steel fibers as shown in Figure 3.1. This fiber is made by Bekaert and is denoted as Dramix 3D 55/30BG where: 55 – aspect ratio (length/diameter), 30 – length in mm, B – bright (uncoated), G – glued (bundled, glue dissolves in water).

Table 3.1. VHSC mixture proportions by weight.

Cement (LaFarge, Class H)	Silica Fume (Elkem, ES900W)	Silica Sand (US Silica, F-50)	Silica Flour (US Silica, Sil-co-sil 75)	Water (Tap)	Steel Fibers (Bakaert, 3D 55/30 BG) 3.15% Vf	HRWRA (WR Grace, ADVA 190)
1	0.389	0.967	0.277	0.208	0.270	0.00855

Figure 3.1. Dramix 3D 55/30BG hooked steel fiber.

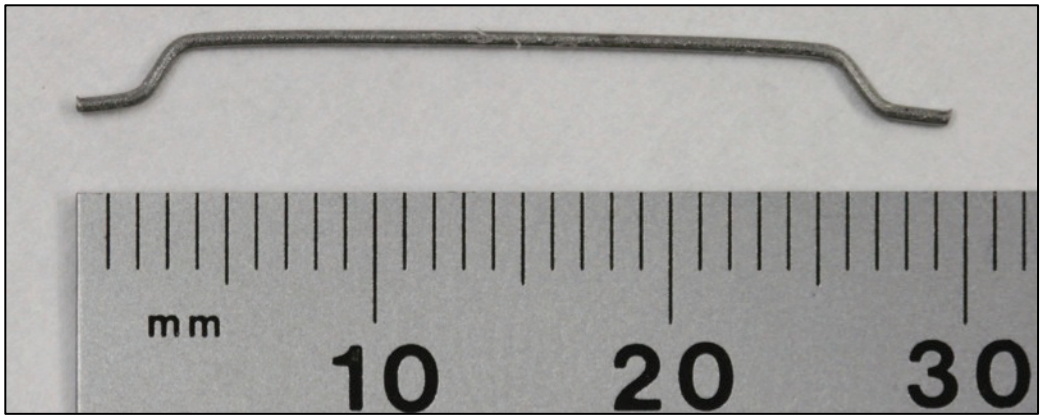

3.2 High-strength high-ductility concrete (HSHDC)

Ranade describes the development of HSHDC and its variances from VHSC in prior ACI publications (Ranade et al. 2013, 2013). The constituents are the same with slight changes made to the proportions. These changes include a reduction in sand and fibers with an increase in water reducing admixture. The main difference between these two fiber reinforced concretes is that the fibers used in HSHDC are relatively small

(diameter = 38 microns) (Rushing et al. 2012) polyethylene fibers as opposed to the larger steel fibers (diameter = 0.55 mm) used in the control VHSC. Table 3.2 details the constituents and mixture proportions of HSHDC. The mechanical properties of HSHDC include average tensile strengths of 14.5 MPa (2.1 ksi) and tensile strain of 3.5 percent (Ranade et al. 2012). A pseudo-strain hardening (ductile) behavior identified for HSHDC is the apparent result of parallel micro-cracking occurring transverse to the loading direction. Based on these test results, HSHDC has potential for increased energy absorption as compared to VHSC because the ultimate tensile strain increases by an order of magnitude (from an average of 0.2 percent for VHSC to 3.5 percent for HSHDC) with only a minor reduction in compressive strength (200 MPa for VHSC and 160 MPa for HSHDC) (Ranade et al. 2012).

Table 3.2. HSHDC mixture proportions by weight.

Cement (LaFarge, Class H)	Silica Fume (Elkem, ES900W)	Silica Sand (US Silica, F-50)	Silica Flour (US Silica, Sil-co-sil 75)	Water (Tap)	PE Fibers (Spectra 1000) 2% Vf	HRWRA (WR Grace, ADVA 190)
1	0.389	0.700	0.277	0.208	0.214	0.018

Figure 3.2. Spectra 1000 375d Chopped UHMWPE Fiber, single fiber (a), bulk fibers (b), fiber morphology (c).

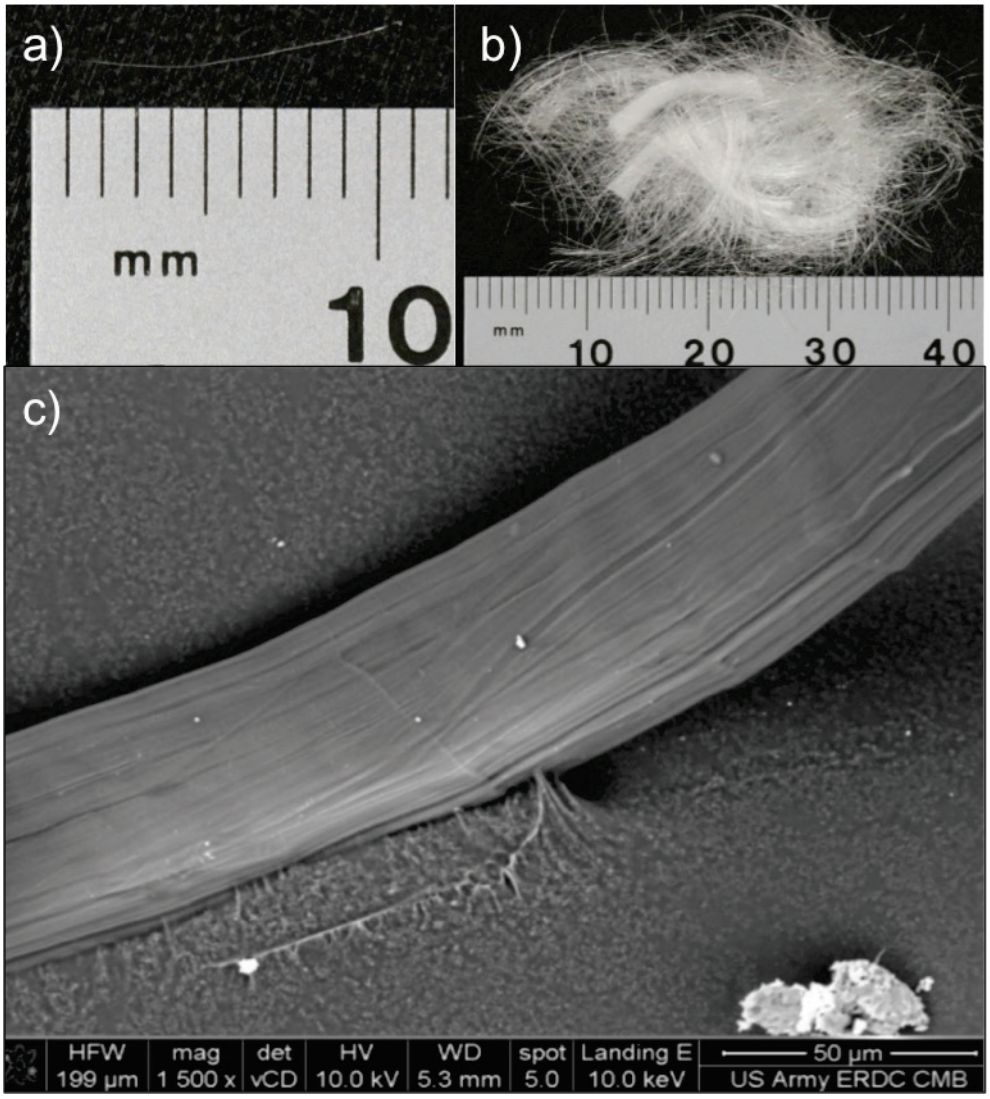

4 Scaling Production and Fabrication of HSHDC

4.1 Introduction

This section describes the process used for production and fabrication of HSHDC specimens used in this study. The process includes batching, mixing, placement, finishing and curing.

4.2 Scaling mixing action

Until this research effort, all published work related to HSHDC has been of a given mixture on small batch sizes (≤1 ft^3). In the current study, all specimens were cast from a single batch. As a result, a larger mixer was required. Also, all prior research used commercial kitchen paddle-style mixers. In the current study a high-shear mixer type was utilized (Eirich, Model R09). These two mixer types are illustrated in Figure 4.1.

Figure 4.1. Hobart paddle mixer (Hobart 2015) (a), and Eirich high-shear mixer (Eirich Mixing Technology 2015) (b).

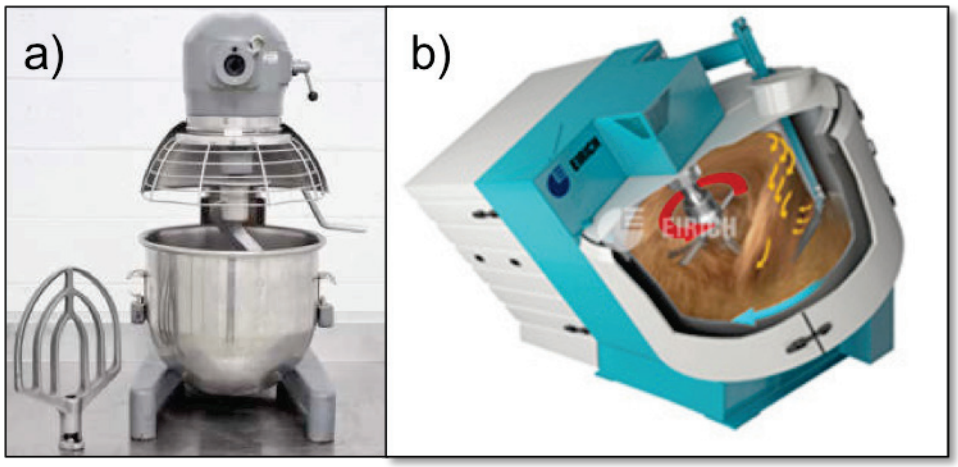

The Eirich mixer has a shearing action created by a rotating mixing pan and an internal rotor (variable speed) that spins in the opposite direction. A bottom/wall scraper prevents buildup and provides additional mixing action. The high-shear action prevents the fibers from clumping and achieves uniform fiber dispersion.

4.3 Batching sequence

Batching sequence was controlled to make use of the mixer's full capacity. For standard concrete mixtures, the mixer is rated for up to 5.3 ft^3. However, prior to mixing the VHSC, the volume of dry materials is approximately 50 percent higher than the volume of mixed concrete. After mixing and consolidation the VHSC's volume was 3.0 ft^3.

1. Weigh appropriate amounts of dry materials, water, admixture, and fibers as shown in Figure 4.2. Specific mixture proportions and constituent materials are outlined in Chapter 3.

Figure 4.2. Weigh raw materials prior to batching.

2. Load silica fume, silica flour, cement (preferably with less dense materials loaded first). With only these constituents loaded, the material volume approaches the 5.3 ft3 capacity of the machine.
3. Mix dry materials for 1 min at low speed (~70 RPM) to achieve dispersion while not losing fines.
4. While the mixer is rotating at 50 RPM, gradually add water and high-range water-reducing admixture (HRWRA). As the mixture's dry materials absorb water, the volume decreases.
5. Silica sand should be added slowly as additional space becomes available until all of the sand has been added to the mixer.
6. Once all of these components (excluding fibers) have been added, the mixer speed is increased to ~200 RPM.
7. At this stage, the mixture needs to be observed to determine when the mixture will "break over." The visual progression consists of the powder material gradually turning a darker shade of gray. Then it will start to form small clumps, which turn into larger balls of clumped material. With

continued mixing, the mixture begins folding over and gradually become fluid. This progression will take approximately 20-30 min.

8. Once the material appears to be fairly homogeneous, the mixer should be opened and inspected. Any dry or clumped material stuck to the mixer should be scraped off by hand and placed in the center of the mixer.
9. At this point, mixing should continue at 200 RPM for 5 min or until uniform.
10. Once the batch is uniform, fibers are added to the mix. In order to help prevent clumping, fibers should be distributed slowly by hand as the mixer is rotating at 200 RPM. An additional 5 min of mixing time at 200 RPM is required for adequate fiber dispersion.

Figure 4.3 illustrates visual cues described in steps 2-10 that were used to achieve the target batch size of 3.0 ft^3.

Figure 4.3. HSHDC images showing the following visual cues of the mixing progression: mixed dry materials (a), darkened color as water/HRWRA are distributed throughout (b), clumps begin to form (c), the material starts to roll over in large folds (d), the mixture becomes fluid (e), and then fibers are added and dispersed (f).

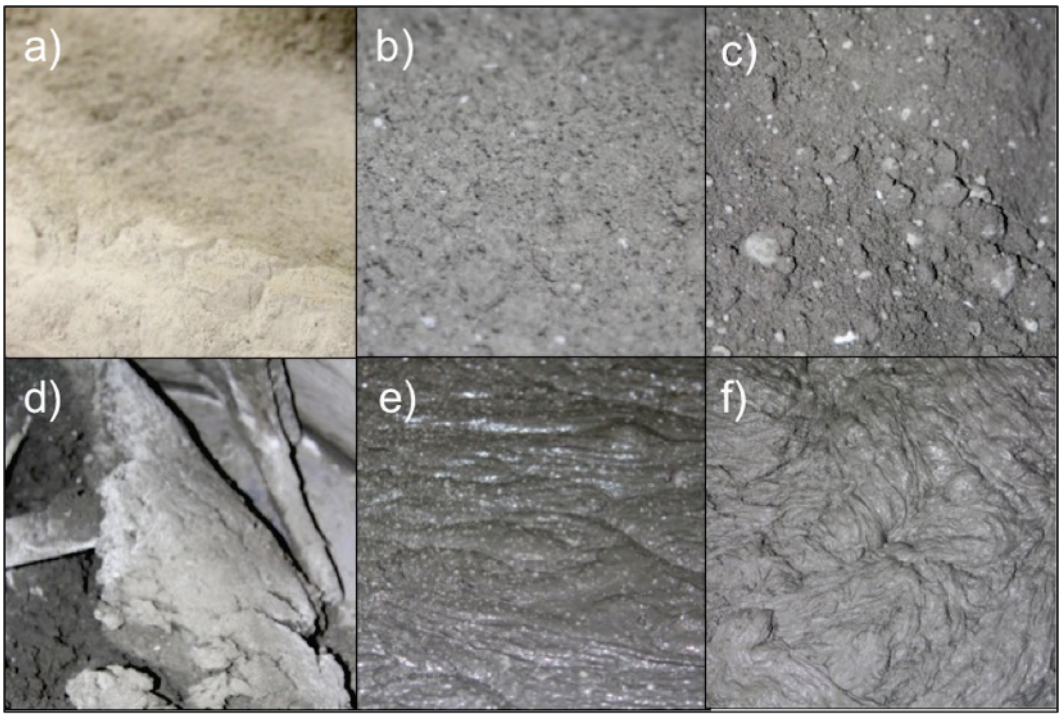

4.4 Placement techniques

In its fresh state, HSHDC will be semi-fluid. All specimens are cast by pouring the mix in the center of the specimen mold using a vibration table meeting ASTM C 1170 (ASTM 2014) to consolidate the material in the

mold (Ranade et al. 2012). Specimen geometries and dimensions for standardized test methods are discussed in Chapter 5. Chapter 6 discusses the specimens used for quasi-static and dynamic pressure loading of simply supported one-way panels.

4.5 Finishing techniques

In this study, a smooth finished surface is desired to prevent variation in specimen thickness. One of the best ways to prevent difficulties in finishing is to make sure that molds are not overfilled. If molds are overfilled, be sure to remove excess material from the edges of the mold so that the test region of the panel maintains uniform fiber dispersion. Once filled, the specimen is finished with a steel trowel. After specimens have been finished as desired, they should be sprayed with Euclid Eucobar (Euclid Chemical Company 2014) evaporation retardant to prevent moisture loss as shown in Figure 4.4. Once the specimens reach initial set, wet burlap was placed on top and then sealed with plastic sheeting.

Figure 4.4. Finished HSHDC samples being sprayed with evaporation retardant to prevent moisture loss.

4.6 Curing regime and specimen preparation

The following curing regimen was followed for all HSHDC samples:

Elevated temperature curing was used for all the HSHDC specimens. After casting the fresh HSHDC mixture into specimen molds, they were sealed with plastic sheets and cured for two days at room temperature (23 ± 3°C [73 ± 5°F]). Due to a high dosage of HRWRA and the use of Class H cement that is slow setting, the specimens require more than 24 hours for attaining the stiffness necessary for demolding. Subsequently,

the hardened specimens were removed from the molds and kept in a water tank for curing at room temperature for 7 days. This was followed by elevated-temperature curing for 5 days in water at 90°C (194°F) and for 3 days in air at 90°C (194°F). The purpose of the elevated-temperature curing was mainly to accelerate the primary and secondary hydration reactions. The temperatures below 100°C (212°F) are generally not enough to initiate significant morphological changes to the microstructure of hydration products of Class H cement with low calcium aluminate contents. The HSHDC specimens were further kept in air at room temperature until 28 days after casting (Ranade et al. 2013).

After demolding and subsequent curing, samples specimens were stored in open-air conditions at room temperature until testing was completed at a minimum specimen age of 28 days. Specimen preparation for testing included smoothing rough edges with a grinding block as needed. A surface grinder was used to smooth out cylindrical specimens and the finished surface of tension specimens. Although simply supported one-way panel specimens had some variation in thickness and surface roughness, all panels were nominally 25.4 mm (1 in.) thick. This dimension was achieved by using a steel trowel against the smooth top surface of precision-machined molds. It was not feasible to grind these larger specimens to a more precise thickness because of the time required using the small grinding wheel on the precision surface grinder.

5 Quasi-Static

5.1 Introduction

Standardized concrete test methods were used to compare the materials prepared in this study to materials prepared in previous work found in the literature. These test methods include measurements of compressive, tensile and flexure strengths. Direct tension tests were conducted on an MTS servo-hydraulic universal testing machine with a 22-kip load cell (nonlinearity: 0.8 percent of full scale) and 22-kip hydraulic wedge grips. Load and deflection data was collected using Test Works 4 software from MTS. All other data presented in this section was collected on a Tinius Olsen servo-hydraulic universal testing machine with a 400-kip pressure transducer. This data was collected using Instron's Partner software.

5.2 Compressive strength

Compressive strength tests were conducted on VHSC and HSHDC. VHSC specimens were cast as 102x203 mm (4x8 in.) cylinders due to the size of steel fibers included in the material. In order for direct comparison with data presented in the literature, HSHDC specimens were cast as 2 in. cubes. The cylindrical specimens were ground to meet tolerances and tested in accordance with ASTM C 39 (ASTM 2012). Cube specimens were cast in standardized molds and tested in accordance with ASTM C 109 (ASTM 2013). Figure 5.1 shows tested HSHDC compressive specimens and the experimental setup. Compressive strength results are presented in Figure 5.2 and Table 5.1.

Figure 5.1. Tested uniaxial compressive specimen of VHSC (a), HSHDC (b), and test setup (c).

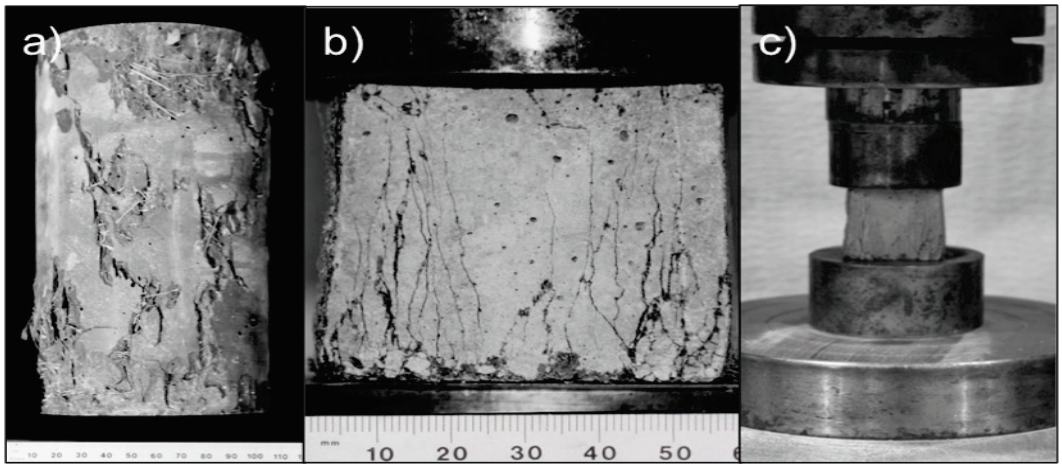

Figure 5.2. Compression data from VHSC 102x203 mm (4x8 in.) cylinders (a) and HSHDC 51 mm (2 in.) cubes (b).

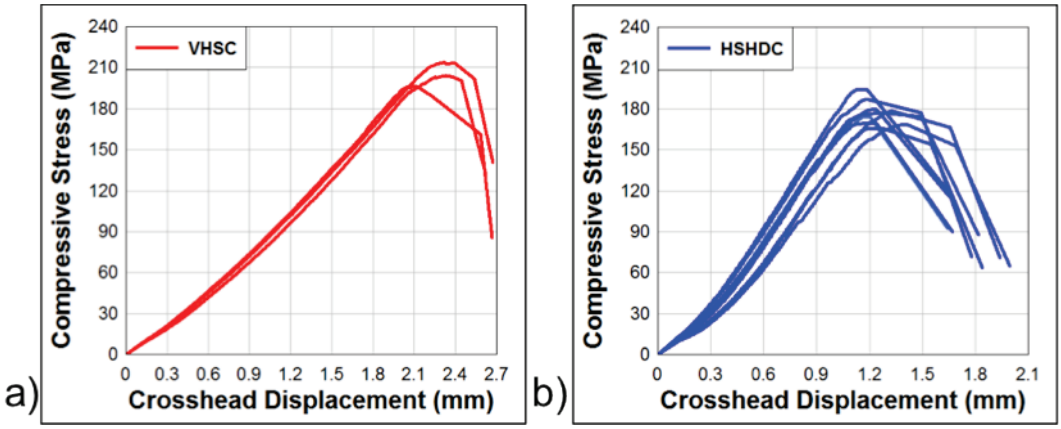

Table 5.1. Uniaxial compression test results.

Specimen Number	Uniaxial compression strength, MPa (ksi)	
	VHSC 102x203 mm (4x8 in.) cylinders	HSHDC 51 mm (2 in.) cubes
1	213 (31.0)	187 (27.1)
2	196 (28.5)	179 (26.0)
3	204 (29.6)	168 (24.4)
4	---	174 (25.2)
5	---	166 (24.0)
6	---	169 (24.5)
7	---	194 (28.1)
8	---	177 (25.6)
9	---	178 (25.9)
Average	204 (29.7)	177 (25.7)
Standard deviation	9 (1.3)	9 (1.3)
Coefficient of variation, %	4.2	5.2

5.2.1 Comparison between VHSC and HSHDC

As shown in Table 5.1, the average compressive strength of VHSC is 15 percent higher than HSHDC. The reduction in compressive strength is comparable with data presented for VHSC and HSHDC in prior work (Ranade et al. 2012). This reduction in compressive strength is a trade-off required to provide the required fresh properties to achieve uniform fiber dispersion (Ranade et al. 2013). However, HSHDC is substantially stronger than most strain-hardening cementitious composites including

ECC (30-70 MPa) (Ranade et al. 2013), which was used as a benchmark in development of HSHDC.

5.2.2 Comparison to previous HSHDC data

Previous research presented the average peak compressive stress of HSHDC cubes as 166 MPa (24.1 ksi) (Ranade et al. 2013). Based on the data presented in Table 5.1, average compressive strength is 6.6 percent stronger than the average compressive strength data presented in the literature.[11]

5.3 Splitting tensile strength

Splitting tensile tests were conducted in accordance with ASTM C 496 (ASTM 2012). Although this is a common method for determining the tensile properties of concrete, this method is not ideal for SHCCs such as HSHDC. This test method was originally designed for brittle materials. As shown in Figure 5.3, these samples fail in a combination of splitting tension and compressive crushing. Splitting tensile strength results are presented in Figure 5.4 and Table 5.2.

Figure 5.3. VHSC (a) and HSHDC (b) split tensile specimens, HSHDC specimen displays failure modes compressive crushing (flattened region at the bottom of specimen); ASTM test setup (c) (ASTM 2012).

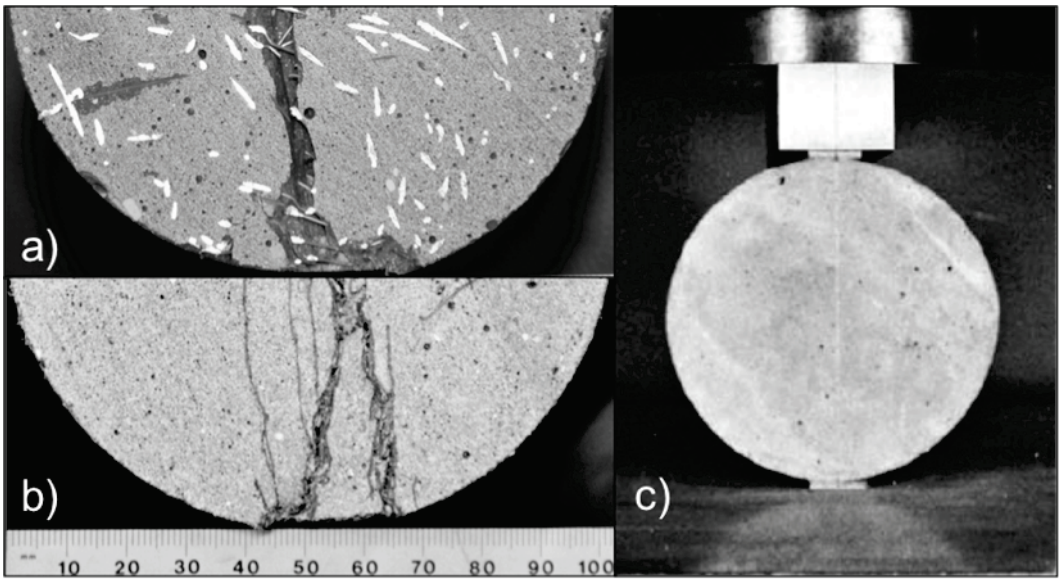

Figure 5.4. Splitting tensile data from VHSC and HSHDC 102x203 mm (4x8 in.) cylinders.

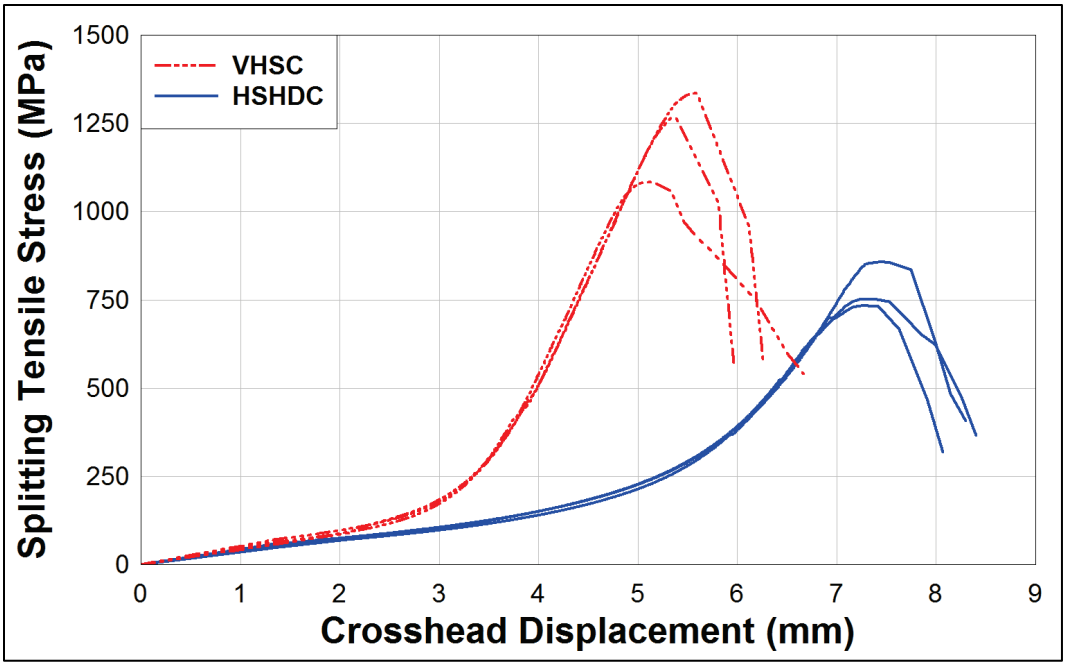

Table 5.2. Splitting tensile test results.

Specimen Number	Splitting tensile stress, MPa (ksi) 102x203 mm (4x8 in.) cylinders	
	VHSC	HSHDC
1	25.8 (3.7)	15.3 (2.2)
2	27.2 (3.9)	17.5 (2.5)
3	22.1 (3.2)	15.0 (2.2)
Average	25.0 (3.6)	15.9 (2.3)
Standard deviation	2.6 (0.4)	1.4 (0.2)
Coefficient of variation, %	10.4	8.6

5.3.1 Comparison between VHSC and HSHDC

In the splitting tensile test results shown in Table 5.2, the average splitting tensile stress is 25.0 MPa (3.6 ksi) for VHSC and 15.9 MPa (2.3 ksi) for HSHDC. VHSC has a tensile capacity 86 percent higher than HSHDC.

5.3.2 Comparison to previous HSHDC splitting tensile data

The average peak splitting tensile stress of HSHDC reported in previous research was 17.0 MPa (2.5 ksi) with a COV of 8.5 percent (Ranade et al. 2013). Based on the data presented in Table 5.2, the average material made in this study is 6.5 percent lower than data presented in the literature (Ranade et al. 2013).

5.4 Direct tensile strength

Direct tensile specimens were prepared and subsequent mechanical tests conducted in accordance with the appendix "Testing Method for Uniaxial Tensile Strength" from the Japanese Society of Civil Engineering (JSCE 2008). The direct tension test specimen is dumbbell shaped as shown in Figure 5.5. The cross-section dimensions are 30x30 mm (1.18x1.18-in.) with an 80 mm (3.15-in.) gauge length. Tensile loading was applied at a displacement rate of 0.5mm/min (0.02 in./min). Two LVDTs are placed on diagonally opposite corners of the gauge length in order to capture strain and rotation as shown in Figure 5.6. Quantifying any rotation verifies that the test is truly uniaxial. This method is discussed in more detail in previous ERDC publications (Scott et al. 2014). Although the method list a specimen thickness of either 13 mm or 30 mm, previously reported data on HSHDC used 13 mm specimens. However, in these previous studies at the ERDC, thicker specimens were required due to the fiber in VHSC. Specimen size is discussed further in Section 5.4.3. A pin-connection (hinged) load end was also included rather than fixed-fixed support conditions used previously.

Figure 5.5. Direct tension setup from Japanese Society of Civil Engineers (JSCE) "Testing Method for Uniaxial Tensile Strength" showing a dimensioned drawing (a) (JSCE 2008) and the actual test setup (b) (Scott et al. 2014); 30 mm (1.18-in.) thickness used in this study.

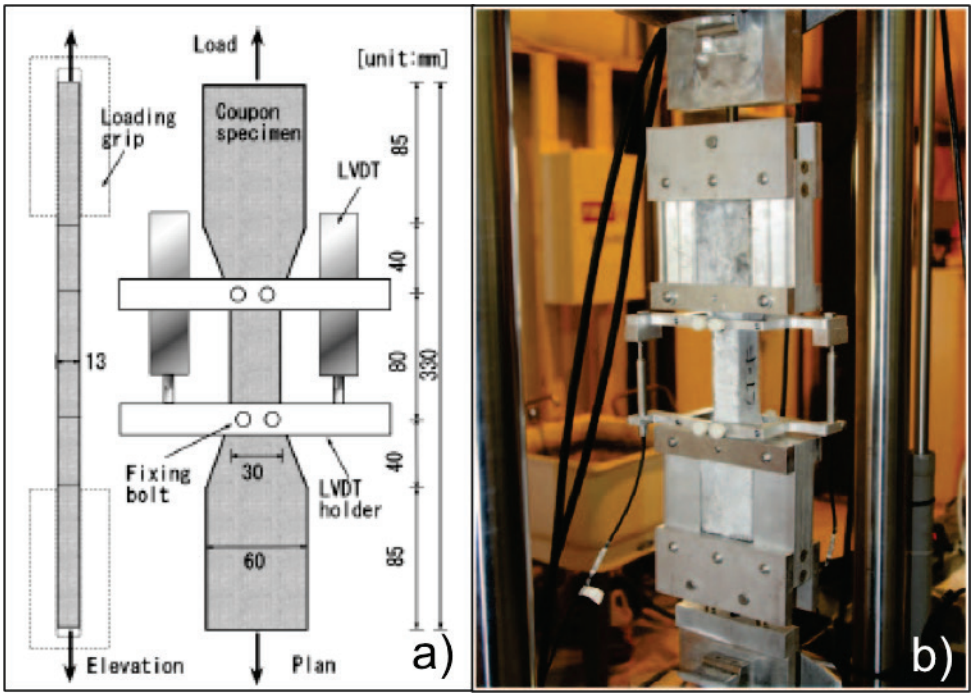

Figure 5.6. LVDT setup used for JSCE "Testing Method for Uniaxial Tensile Strength."

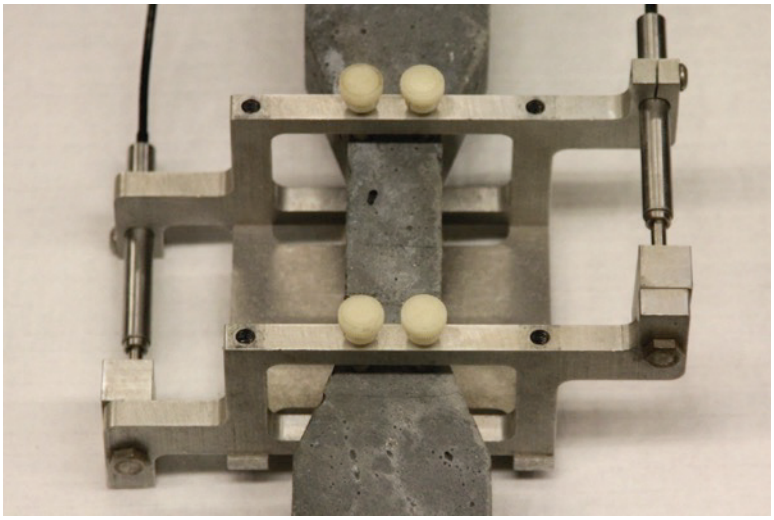

Multiple cracking behaviors observed in HSHDC are shown in Figure 5.7. Direct tensile strength results from current study are presented in Figure 5.8 and Table 5.3.

Figure 5.7. VHSC (top) and HSHDC (bottom) direct tension specimens, HSHDC specimen exhibits multiple parallel cracking pattern causing pseudo-strain-hardening behavior.

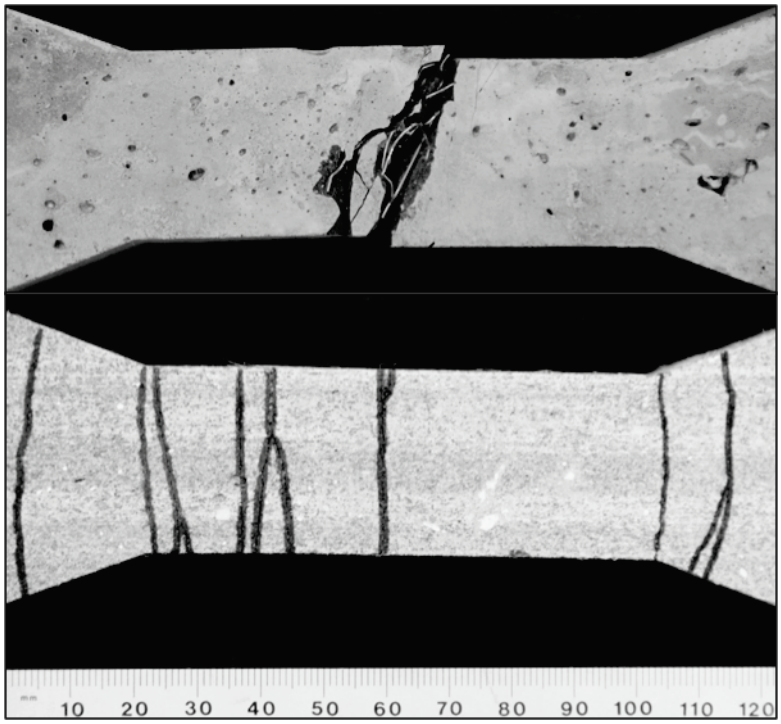

Figure 5.8. Direct tension data for VHSC and HSHDC specimens.

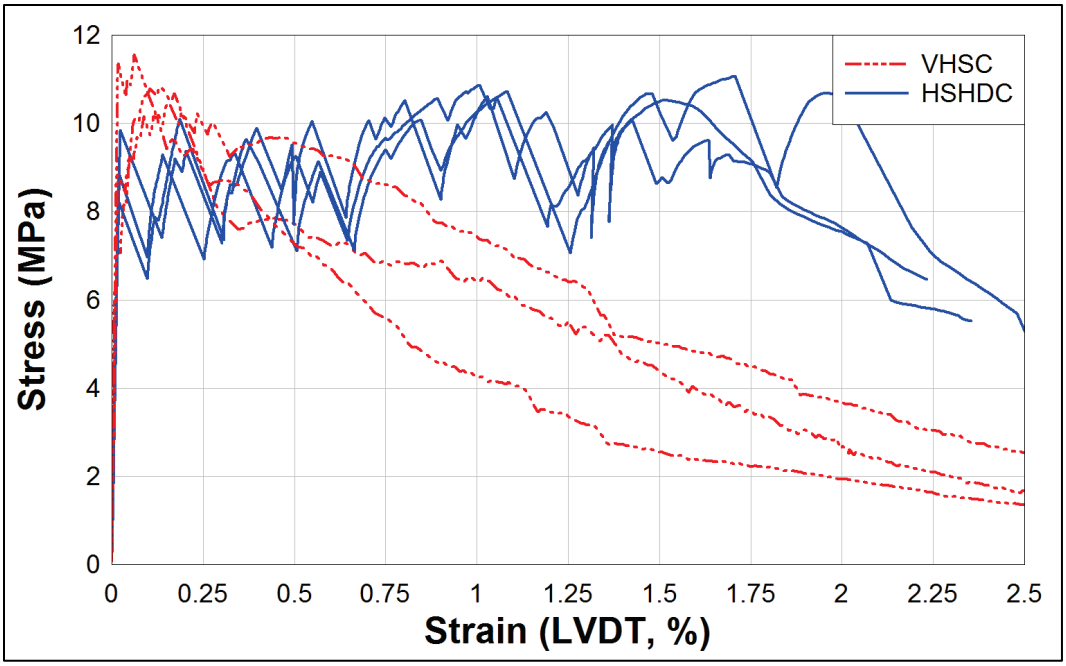

Table 5.3. Direct tension test results.

	Direct tensile strength, MPa (ksi) at % strain	
	30x30 mm (1.2-in.) cross section	
Specimen Number	VHSC	HSHDC
1	10.8 (1.57) @ 0.13%	11.1 (1.61) @ 1.71%
2	10.5 (1.52) @ 0.16%	10.5 (1.52) @ 1.51%
3	11.6 (1.68) @ 0.06%	10.1 (1.46) @ 1.42%
Average	10.9 (1.59) @ 0.12%	10.6 (1.53) @ 1.54%
Standard deviation	0.56 (0.08); 0.05	0.50 (0.08); 0.14
Coefficient of variation, %	5.15; 44.0	5.17; 9.6

5.4.1 Comparison between VHSC and HSHDC

The direct tension test of VHSC and HSHDC allow the tensile strength and strain capacities of VHSC and HSHDC to be compared under the same test conditions. VHSC has approximately the same tensile strength as HSHDC, but its tensile strain capacity at the recorded stress is approximately 12 times less. These data are in Table 5.3.

5.4.2 Comparison to previous HSHDC data

Published HSHDC data show an average direct tensile stress of 14.5 MPa (2.1 ksi) and strain of 3.4 percent (Ranade et al. 2013). In the current study, direct tension tests were conducted on both HSHDC and VHSC

specimens. The published results from previous tests may vary from those reported here for the following reasons:

1. Specimen Size – Specimens tested in the current study were 30 mm (1.18-in.) thick rather than 13 mm (0.51-in.) in previous studies of HSHDC in the literature. Both thicknesses are acceptable for the test method. However, the thicker specimens were used due to the longer fibers present in VHSC. In the current study, both VHSC and HSHDC specimens were cast with the same dimensions (30 mm thick). The larger specimens typically provide lower strengths due to an increased probability of large internal flaws (Lamond 2006).
2. Fiber Orientation – As specimen size increases relative to fiber size, fiber orientation becomes more randomized. In this cast the fibers have room to align perpendicular to the axis of loading and therefore not provide tensile capacity (Oesch 2015). In the published data for 13 mm (0.51-in.) thick HSHDC specimens using 12.7 mm (0.50-in) long fibers, the fibers have a probability to align more in the direction of loading based on geometrical constraints. This provides idealized fiber orientations to support more tensile stress.
3. Support Conditions – Data for a more recent study (Ranade et al. 2013) was obtained with fixed-fixed support conditions. This support condition restricts specimen rotation during tests. In the current study, hydraulic wedge grips were not available that could directly grip the thicker specimens. Direct tension data observed in previous work records lower ultimate stress in specimens with rotational degrees of freedom that averaged 11.8 MPa (1.7 ksi) (Ranade et al. 2013) while specimens with fixed-fixed support conditions averaged 14.5 MPa (2.1 ksi) (Ranade et al. 2014).

5.5 Third-point flexure strength

Third-point flexure tests were performed because the panels ultimately tested in the BLS are loaded in bending. These tests are discussed in Chapters 6 and 7. Third-point flexure tests were conducted in accordance with ASTM C 1609 (ASTM 2012) using a beam specimen cast into 102x102x356 mm (4x4x14 in.) plastic molds. Along with load, two external LVDTs were mounted at the centerline of the specimen to measure mid-point deflection. Third-point flexure test specimens are presented in Figure 5.9. Results are presented in Figure 5.10 and Table 5.4.

Figure 5.9. Tested third-point flexure specimens of VHSC (a) and HSHDC (b), HSHDC specimen shows multiple cracking radiating back to the center of the beam.

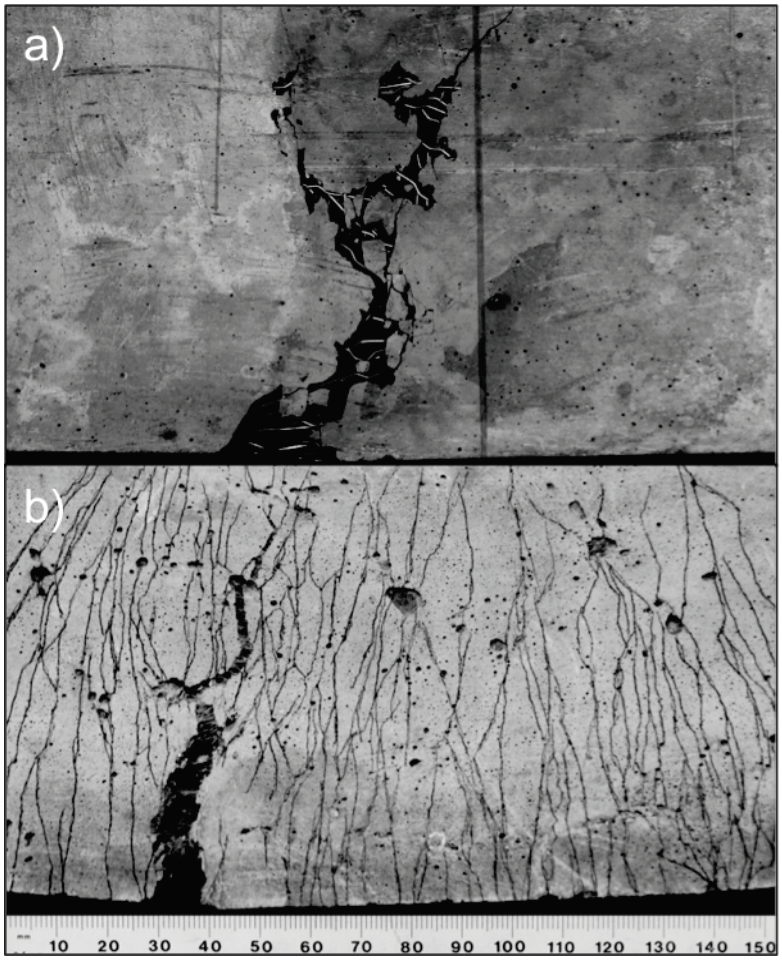

Figure 5.10. Flexure data comparing VHSC to HSHDC.

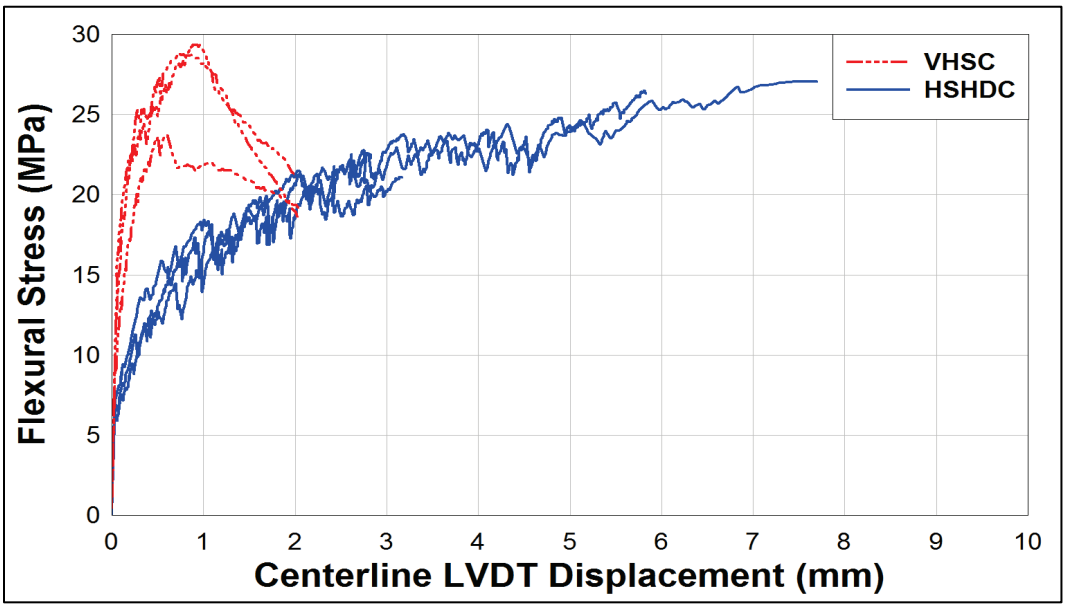

Table 5.4. Third-point flexure test results.

Specimen Number	Third-point flexural strength, MPa (ksi)	
	102x102x356 mm (4x4x14 in.) beams	
	VHSC	HSHDC
1	28.9 (4.2)	28.1 (4.1)
2	28.3 (4.1)	21.0 (3.1)
3	23.4 (3.4)	26.4 (3.8)
Average	26.9 (3.9)	25.2 (3.6)
Standard deviation	3.0 (0.4)	3.7 (0.5)
Coefficient of variation, %	11.1	14.6

5.5.1 Flexure tests of VHSC and HSHDC

Both VHSC and HSHDC exhibit similar strength, but HSHDC exhibits greater ductility through higher deflections at peak loads. In ASTM C 1609 Section 9.6, the endpoint of a flexure test is achieved when specimens reach a deflection of the span (102 mm) divided by 150. This criterion was used as the end point for tests of VHSC. However, HSHDC specimens were tested until peak loads were reached. Peak loads for VHSC occur at average displacements over seven times lower than the peak loads for HSHDC. For comparison purposes, toughness was calculated for tests of both materials by integrating the data sets to obtain area under the load vs. displacement curve up to the peak load. Toughness values for VHSC tests were more than seven times lower than toughness of HSHDC.

5.5.2 Comparison to previOus HSHDC data

Previous research presented the average peak flexural stress of HSHDC as 31.8 MPa (4.6 ksi) (Ranade et al. 2013). Based on the data presented in Table 5.4, HSHDC in the current study is 20 percent weaker. This presents a substantial difference in materials properties, although the values for coefficient of variation are high in both the published (14 percent) and current (15 percent) datasets.

6 Equipment and Test Method Development

6.1 Introduction

New equipment and test methods were developed for:

1. Quasi-static loading of simply supported, pressure-loaded one-way panels to obtain load-deflection data and subsequent resistance functions.
2. Dynamic loading of simply supported, pressure-loaded one-way panels.

6.2 Simply supported, pressure-loaded one-way panels

One potential application for HSHDC includes its use in a protective armor panel or panel component in a current protective system. In this application the panels are installed in a way that is best represented as a simply supported one-way panel as shown in Figure 6.1. Blast loading is one of the major concerns for these protective structures. As a result, pressure loading is more representative of anticipated loading conditions rather than point loads as commonly used in standardized flexural test methods for concrete beams.

Figure 6.1. Modular Protective System (MPS) utilizing armor panels for rapidly deployable blast and ballistic protection.

The panel specimen selected for tests was 305x305x25 mm (12x12x1-in.) square panel. This panel approaches the maximum size panel that can be tested in the ERDC's small-scale blast load simulator (BLS). It is also the standard dimension used at the ERDC's penetration research facility. A

water chamber test apparatus was developed to test these square panels. This apparatus was developed to replicate the support conditions in the blast testing, but uses a quasi-static pressure load. Data from this test is used to develop a resistance function as described in Section 6.3.

6.3 Importance of resistance function for dynamic calculations

A resistance function for the panel in the current study is the function fitting of the load and centerline displacement. A resistance function varies with specimen geometry, material, support condition, and loading. The resistance function can be applied to calculations using a single degree-of-freedom (SDOF) model such as Wall Analysis Code (WAC) (Slawson 1995). Obtaining an accurate resistance function for the appropriate support conditions and sample geometry allows for the prediction of deflection based on the dynamic load-time history that will be applied to the panel. The resistance function is discussed in more detail in Section 2.6 and WAC is discussed further in Chapter 7.

6.4 Water chamber equipment and test method development

Quasi-static water chamber tests can provide accurate pressure vs. deflection data, which are used to develop resistance functions in dynamic analysis. Although some researchers have used vacuum chambers (Salim et al. 2013), water pressure loading is preferred in this study since water is a nearly incompressible fluid (especially as compared to air). In vacuum tests, a quasi-static test is slow and controlled until the sample reaches the peak pressure at which failure occurs. In hydrostatic loading of the type used in the current study, the volume of the water remains the same after the peak pressure drops and allows continual quasi-static observation of post-peak behavior.

6.4.1 Physical design and setup

Design of the water chamber is such that a quasi-static pressure loading is applied to a pliable rubber bladder. The design was based on using city water pressure. This concept came from a larger testing apparatus designed at the ERDC for testing vertical concrete masonry unit (CMU) walls (Dennis et al. 2002). In the current research, cast concrete panels can be tested in horizontal orientation. In the final design a panel is placed horizontally over a neoprene bladder (Dennis et al. 2002). This allowed

the tensile face of the sample to be easily observed in a dry state for high quality photographs.

The initial design (WC1) focused on the testing apparatus being lightweight so that it could be easily transported. WC1 consisted of a base milled from a solid block of high-density polyethylene (HDPE). A groove in the top edge provided for an O-ring to seal against the lid. WC1 included a steel lid with a series of clamps to hold it in place. Lastly there were pin connections used to secure the support rails to the lid. WC1 is shown in Figure 6.2. This unit proved to be adequate for standard high strength concretes, but could not withstand the pressures required to fail VHSC. This design also tended to trap air underneath the bladder, which caused an accumulator effect, producing dynamic failure after peak pressure was reached. This is caused by the expansion of air as pressure decreases, whereas water is nearly incompressible.

Figure 6.2. Initial water chamber design (WC1) for quasi-static pressure loading capable of testing a 305x305x25 mm (12x12x1 in.) square specimen underneath the support rails at the top of the chamber.

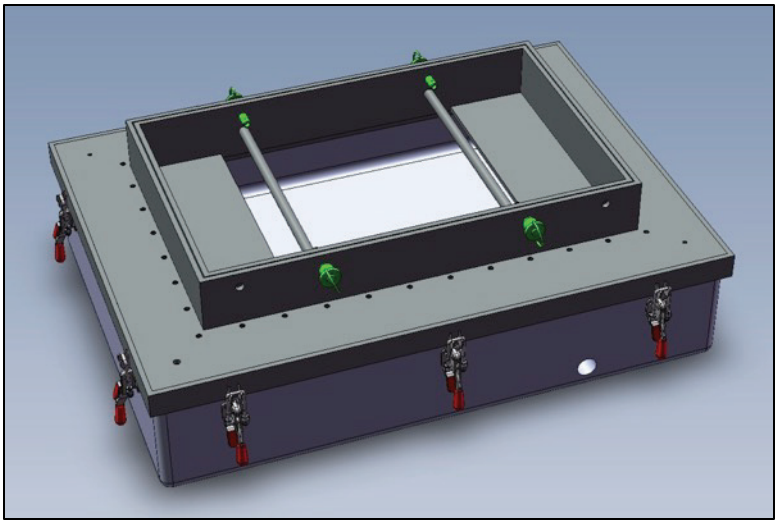

As a result, the water chamber was redesigned for the pressure required to fail VHSC. The second version of the design is referred to as WC2. WC2 added a large aluminum plate to the base of the milled HDPE block to provide a rigid reaction for steel clamps that were placed around the lid. These clamps are shown in Figure 6.2. Large bolts were added to replace the pin connections securing the support rails to the steel lid. Steel handles were added across the top of the support rails. The steel handles stiffened the support rails and made the lid easier to lift. To eliminate the trapped

air, the device was mounted to a rotating engine stand. This stand allowed the entire apparatus to be turned upside down. The bottom of the device had been milled out to a drain point as shown in Figure 6.3. When the apparatus was turned over, trapped air migrated to the drain point and escaped. As a result, trapped air in the system was eliminated. The WC2 design is illustrated in Figure 6.4.

Figure 6.3. Drain milled in the bottom of the high-density polyethylene (HDPE) base of water chamber.

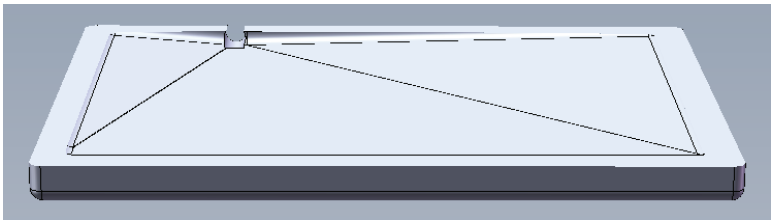

Figure 6.4. Water chamber test fixture (WC2) capable of flexure testing 305x305x25-mm (12x12x1-in.) concrete panel with a 254 mm (10-in.) span.

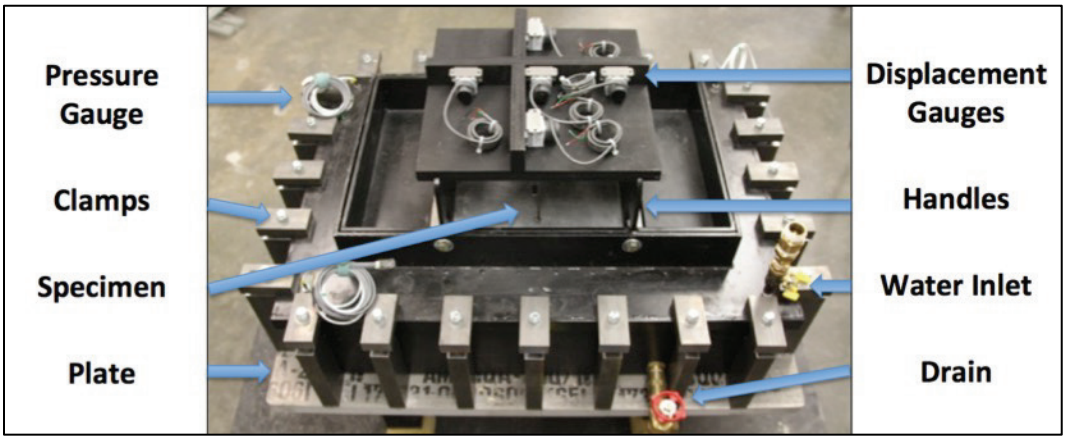

6.4.2 Data acquisition and instrumentation

The water chamber instrumentation consists of three Kulite pressure gauges (XTM-190-100A), five Measurement Specialties displacement gauges (SM2-2, 2-in., miniature string pots) and one Omega flowmeter (FTB-1311). These devices are monitored throughout the test using a customized virtual instrument set up with National Instruments LabVIEW software. The virtual instrument is the program within LabVIEW that manages data collection through a graphical user interface as shown in Figure 6.5. This program incorporates the calibration factors for each gauge and converts electrical signals to the appropriate units in terms of displacement, pressure or flow. Active control of the test is attained by first using the flowmeter to correlate water flow rate with displacement rate obtained with the

displacement gauges. Although displacement rate can be actively observed during the test, the measured displacements are very small and begin to change unpredictably as cracks begin to form. The flowmeter provides a smoother signal for active feedback when using the manual valve to control the speed of the test. The resulting data file is used to establish the resistance function (pressure vs. displacement). Subsequently, the resistance function is used for selecting the appropriate impulse load for achieving a prescribed damage level in blast testing. This process is discussed in greater detail in Chapter 7.

Figure 6.5. Graphical user interface showing customized virtual instrument in National Instruments LabVIEW program.

6.5 Blast load simulator equipment and test method development

The ERDC's small-scale blast load simulator (BLS) was modified to provide the same support conditions during tests as the water chamber. As a result, the quasi-static and dynamic tests could be compared directly.

6.5.1 Physical design and setup

In the BLS, dynamic flexural strength of VHSC and HSHDC panels were tested under blast pressure loading conditions. Panel flexure is measured as a function of strain rate. Due to the compact size of the small-scale BLS, several panels can be tested in a day at a cost much less than that incurred with larger-scale testing that has been traditionally done at the ERDC. However, this BLS had previously only been used for calibration shots and proof-of-concept for the large (1/3-scale) BLS. Since this was the case, a target vessel was designed to incorporate the appropriate support

conditions with room for gauges, lighting and cameras. Cylindrical rods (12.7 mm (0.5 in.) in diameter) are used as simple supports with a 254 mm (10 in.) flexural span. The pressure vessel (tank) volume was 3.53 L (0.125 ft^3). The complete test setup is shown in Figure 6.6. An expanded view is shown in Figure 6.7.

Figure 6.6. Complete test setup for small-scale blast load simulator (BLS).

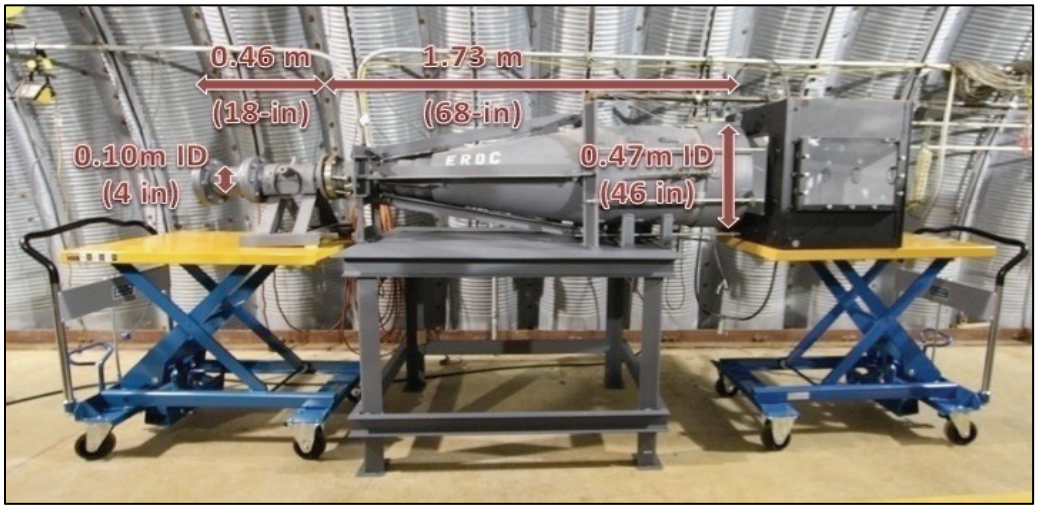

Figure 6.7. Reaction frame providing simply supported loading conditions with appropriate cutouts and windows for instrumentation, lighting, and video (dimensions in inches).

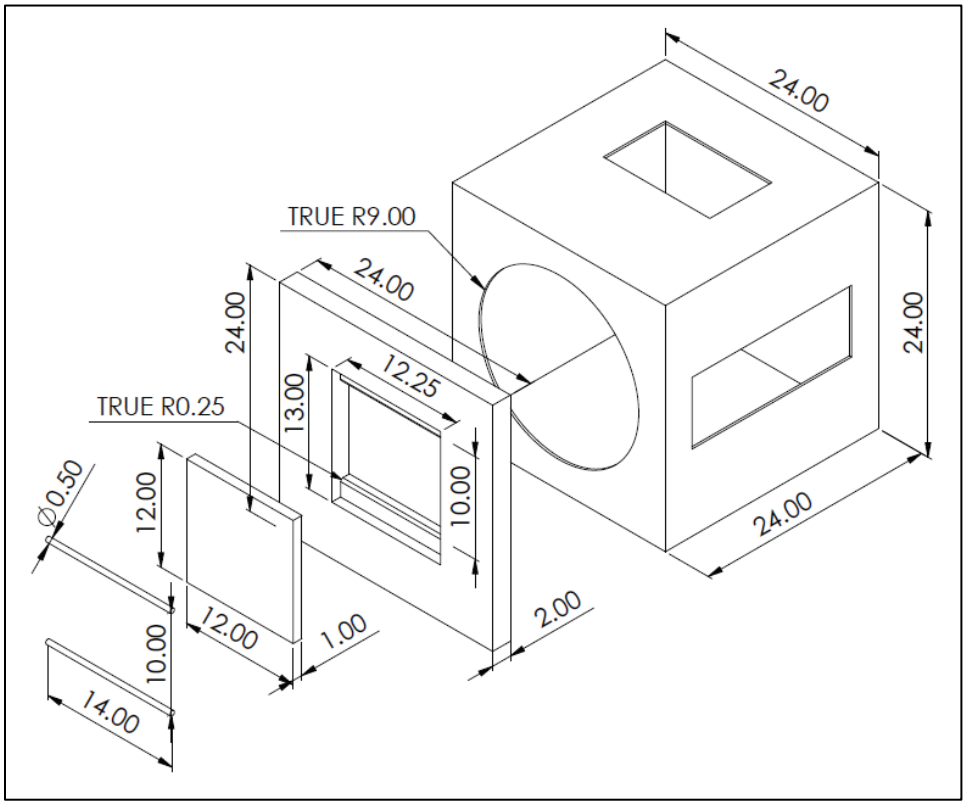

Once testing began, several shortcomings were noted about the setup. Higher pressures caused the entire setup (table/carts/frame) to shift during the test. Energy from the blast was being dissipated through the entire system. As a result, displacement data was inaccurate. In order to resolve this issue several steps were taken:

- Blast load simulator was welded to the table and the air tank was welded to the cart
- Weights were added to the table to increase mass
- Larger diameter horizontal tension members (all-thread) were added between vertical supports to increase stiffness
- Table was permanently attached to the floor using Red Head Tapcon (ESR-2202 2014) anchors and angle iron
- Wheel locks were enabled on the carts

Once these changes were made, the system was rigid and no longer moved during testing (even at maximum pressures). Images of these updates are shown in Figure 6.8.

Figure 6.8. Modified BLS with stiffened supports and tension members (a) and Red Head Tapcon anchors through angle iron into the slab (b).

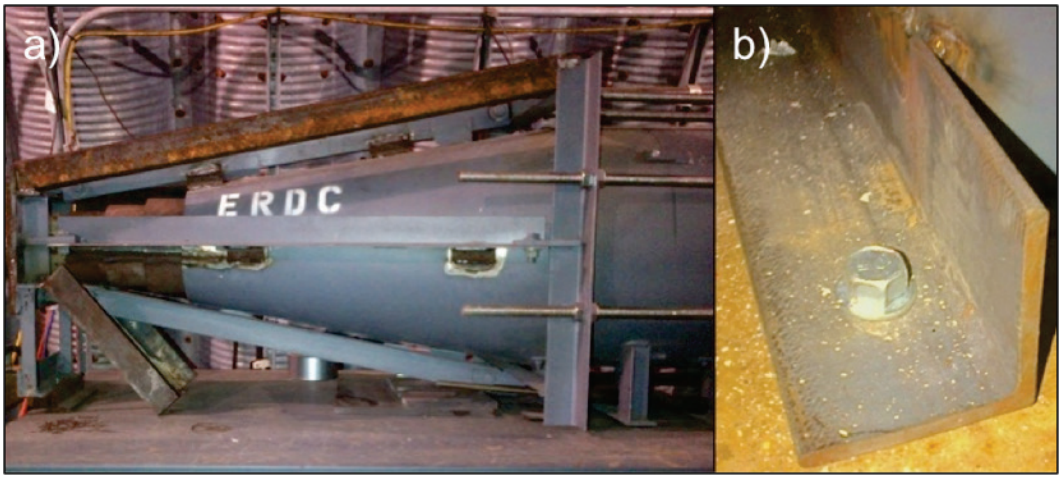

An additional problem with the setup included the length of the shock tube. Although, its current setup was adequate for lower strength materials, higher pressures required for failing VHSC caused the blast wave to jet rather than being applied uniformly. As tank pressures increased beyond 7.00 MPa (1,015 psi), the blast wave did not have adequate distance to become uniform by the time it reached the panel. This was determined by recording higher pressures at the center of the calibration plate (Figure 6.9) as compared to the outer gauge pressures.

Since changing the length and design of the shock tube fell outside of the scope of this work, all pressures used in this study fell at or below a tank pressure of 7.0 MPa (1,015 psi).

Figure 6.9. Pressure gauge layout showing gauges P1-P9 as configured for calibration shots, gauges P1, P2, P8, and P9 were used during concrete panel testing.

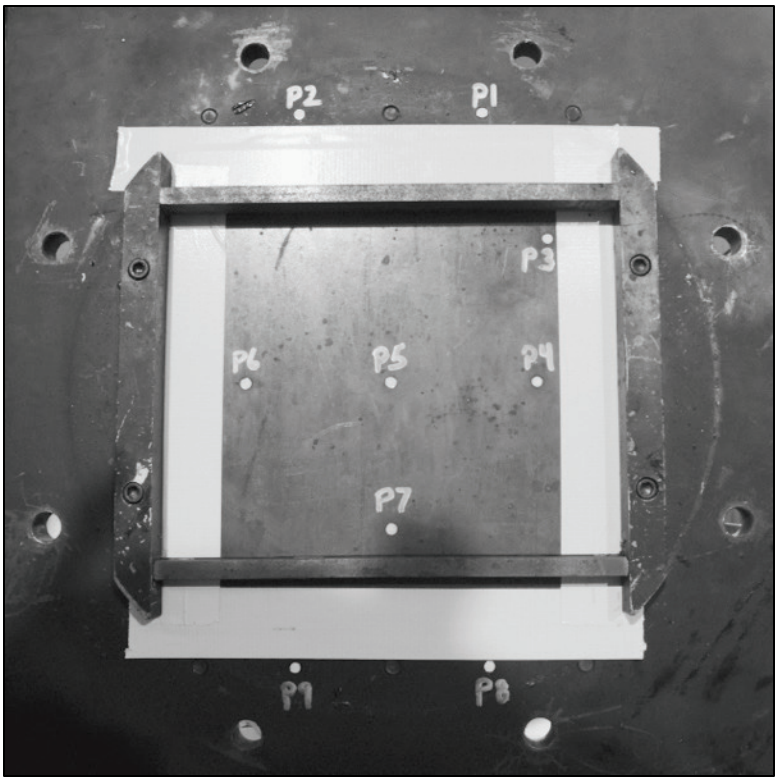

6.5.2 Achieving consistent test pressures for replicates

Several methods were investigated for achieving consistent pressure-time loading histories during tests. Rupture plates (commonly referred to as diaphragms) are typically used in blast load simulator experiments to cause air to be uniformly released from a pressurized tank (Robert et al. 2011). These diaphragms can be made of various types and thicknesses of aluminum or steel with rupture pressures estimated based on material strengths and thicknesses. Although this provides a uniform pressure wave, rupture pressures vary due to material inclusions, variations in thickness and scratches. In order to produce replicate tests, the rupture of the diaphragms needs to be triggered at the same tank pressure for each test.

Initial rupture techniques focused on remotely triggered projectiles fired at the diaphragms to cause premature failure of the diaphragms at a specified

tank pressure. These attempts were unsuccessful and either resulted in no rupture or caused a large hole that allowed pressure to bleed out without rupturing the diaphragm fully. Ultimately, a small blasting cap was adhered to the surface of the diaphragm. Remote triggering was used to detonate the blasting cap, causing rupture at the specified tank pressure. By causing the diaphragms to rupture at a specified tank pressure for each test, the blast pressures recorded at the specimen surface were very similar for replicate tests. Pressure data from replicate tests are presented in the following chapter in Table 7.3.

6.5.3 Data acquisition and instrumentation

Pressure data was collected with four Kulite HKS pressure gauges surrounding the panel (P1, P2, P8, P9 as shown in Figure 6.9 above). Displacement was calculated with accelerometers (Endevco Model 7270A) and measured with high-speed video. Acceleration measurements from accelerometers were double integrated to calculate displacement. One accelerometer was mounted on the frame to record any movement of the setup during the test. The other accelerometer was mounted on the center of the panel. High-speed Phantom cameras (v710 and v9.1) were used to confirm displacement readings taken from accelerometers. Figure 6.10 shows the test setup including accelerometer positions and scales used for reference measurements in high-speed videos.

Figure 6.10. Small-scale BLS test setup showing accelerometer positions and scales used for high-speed video measurements.

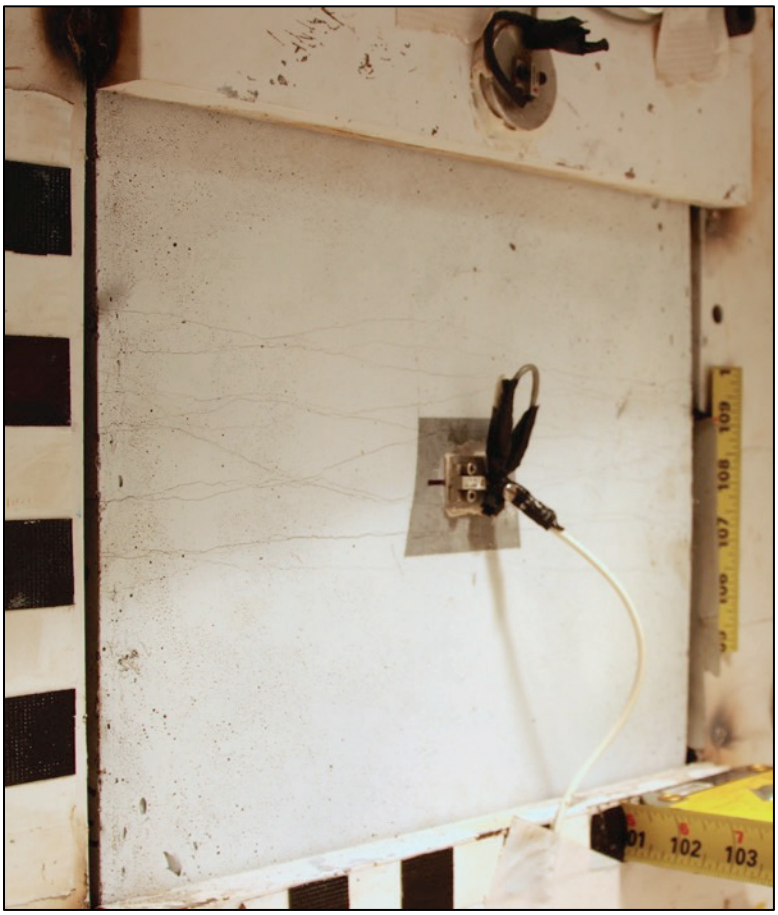

7 Testing of Simply Supported Pressure-Loaded Panels

7.1 Introduction

After developing the equipment and test methods described in Chapter 7, tests were conducted on VHSC and HSHDC panel specimens. This chapter describes the centerline displacement measurements that are used for determining strain and strain rates. Strain rate calculations provide a means to compare results of quasi-static and dynamic testing of simply supported one-way panels. Quasi-static water chamber results are presented and the data is used to develop a resistance function for each material. Lastly, dynamic testing results are presented and discussed.

7.2 Centerline displacement measurements

In quasi-static and dynamic tests of panels discussed in this chapter, centerline displacement is a key response of the panels measured during testing. This measurement is made for the tension face relative to the simple supports. An HSHDC specimen is shown in Figure 7.1 exhibiting the deformed shape after testing.

Figure 7.1. Centerline displacement of HSHDC simply supported one-way panel specimen.

7.3 Strain and strain rate calculations

Strain was calculated for dynamic loading through the use of images from high-speed cameras. Both types of loading are applied to simply supported, pressure-loaded one-way panels. In order to compare the strain rates, the strain must be calculated. Strain is obtained by measuring a change in gauge length when a specimen is loaded. The first measurement is the distance across the gauge length before testing. The second measurement is taken as the peak centerline deflection once crack saturation has occurred. In the course of study a gauge length of 102mm (4-in) was selected since this is the primary region where micro-cracking occurs. This calculation is based off of previous work reported in the literature (Ranade et al. 2014).

Quasi-static tests could not be recorded with video since displacement gauges blocked the field of view. This removes the possibility of directly calculating strain for these tests. Therefore, strains are presented for dynamic tests first.

Dynamic strains were recorded using high-speed cameras. The yellow line shown in Figure 7.2 represents the gauge length (left). As the panel is loaded, it bends; the surface away from the loaded surface lengthens. The maximum length is recorded at the peak pressure (as shown on the right). A strain value is obtained by dividing the change in lengths by the original (unloaded) length. Specimen HSHDC-24 had a strain of 3.47 percent (on the tensile face of the sample). Since the strain occurs over a time period of 3.6 msec, the resulting strain rate is 9.65/s.

Figure 7.2 shows specimen HSHDC-24, which had a peak centerline deflection of 6.86 mm (0.27-in.). This level of deflection corresponds to the reported strain of 3.47 percent. In quasi-static a deflection of 6.86 mm (0.27-in.) was achieved in 6 min (360 sec) compared to 3.6 msec in dynamic tests. These times of tests represent a displacement rate increase of five orders of magnitude from quasi-static to dynamic loading. Assuming that strain directly correlates to displacement, the quasi-static strain rate is approximately 10-4/s. Although strain rates presented here are not exact, they give a good frame of reference to better understand the effects of strain for the two types of loading (quasi-static and dynamic).

Figure 7.2. High-speed video length measurements (yellow lines), pretest image (left), and peak centerline deflection image (right).

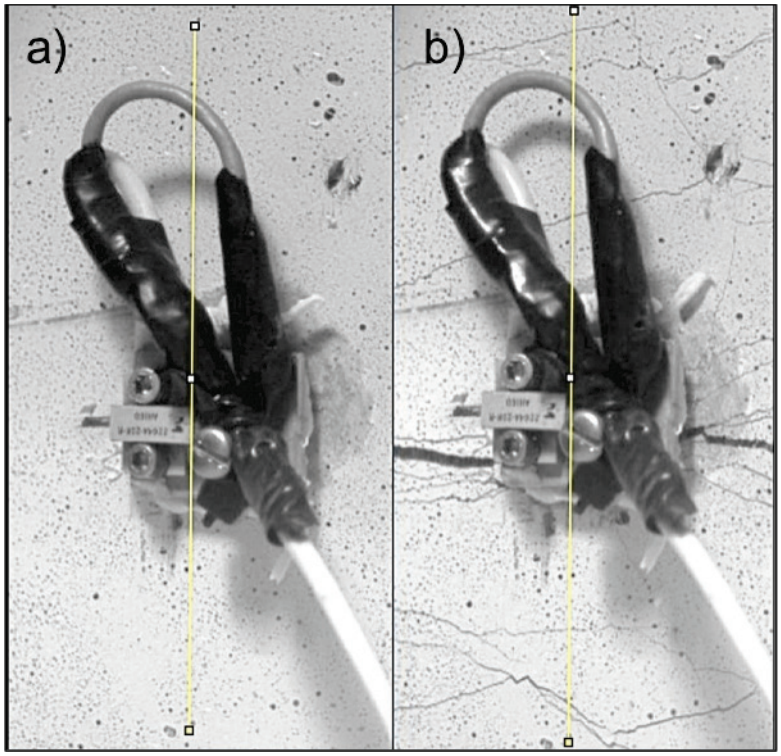

7.4 Quasi-static water chamber tests

Quasi-static water chamber tests were conducted using the experimental setup described in Chapter 6. The quasi-static strain rate was approximately 10^{-4}/s. All panels tested have nominal dimensions of 305x305x25 mm (12x12x1 in.). Quasi-static pressure loadings were conducted to provide the same pressure loading and support conditions designed for blast experiments. However, lower strain rates were possible by using water pressure rather than air pressure. Consistent loading type and support conditions at different rates provide a means to account for strain-rate effects in the materials. The quasi-static test results used to develop the resistance functions used in the SDOF code in analyzing walls exposed to blast loadings as discussed in Section 7.5.

7.4.1 Results

Quasi-static peak pressures and centerline displacements are presented for VHSC and HSHDC panels in Table 7.1 and Table 7.2, respectively. Raw data is plotted in Figure 7.3. Large crack openings become the predominant failure mode after peak pressure has been reached.

Table 7.1. VHSC results from quasi-static testing of simply supported one-way panels.

Specimen #	Peak Pressure, kPa (psi)	Centerline Displacement at Peak Pressure, mm (in)
VHSC-10	467 (67.7)	2.92 (0.115)
VHSC-15	407 (59.1)	2.88 (0.113)
VHSC-20	465 (67.4)	2.76 (0.109)
Average	446 (64.7)	2.82 (0.111)
Standard deviation	34 (4.9)	0.08 (0.003)
Coefficient of variation, %	7.6	3.0

Table 7.2. HSHDC results from quasi-static testing of simply supported one-way panels.

Specimen #	Peak Pressure, kPa (psi)	Centerline Displacement at Peak Pressure, mm (in)
HSHDC-18	428 (62.0)	17.11 (0.674)
HSHDC-19	337 (48.9)	7.93 (0.312)
HSHDC-23	374 (54.3)	12.96 (0.510)
Average	380 (55.1)	12.52 (0.493)
Standard deviation	45 (6.6)	6.49 (0.256)
Coefficient of variation, %	12	51.8

Figure 7.3. Quasi-static positive water pressure loading of simply supported one-way panels.

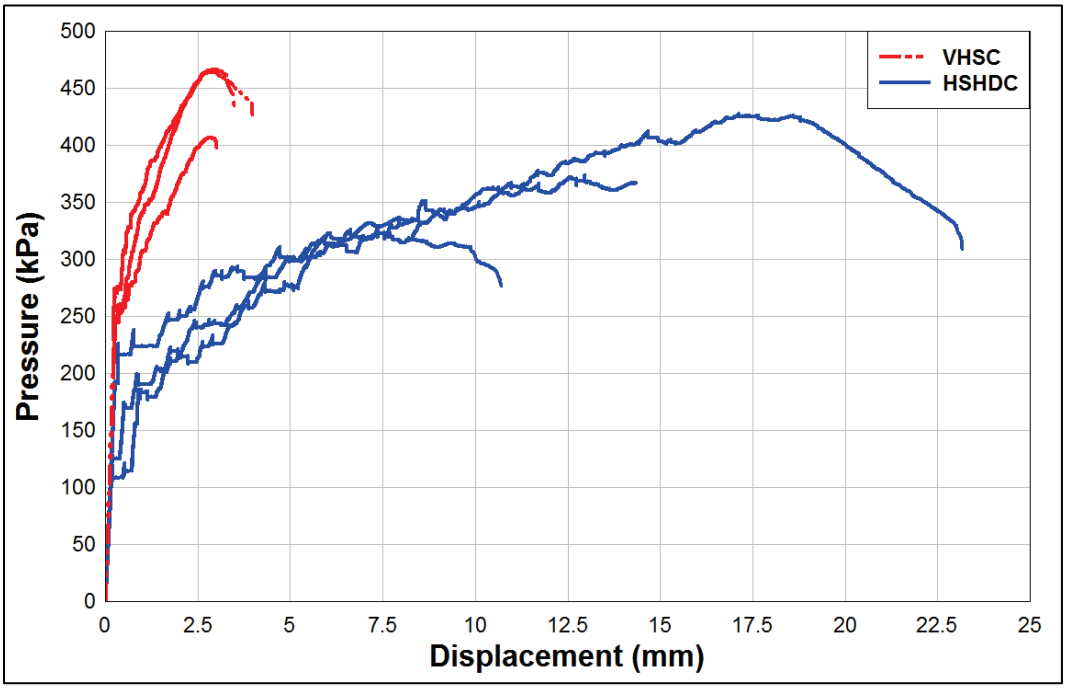

7.4.2 Discussion

Recorded centerline displacements at peak pressures are higher for HSHDC than for VHSC. This is consistent with flexure tests as discussed in Section 5.5. In water chamber tests, the average VHSC deflection at peak pressure is approximately four times lower with a 17 percent higher average peak pressure compared to HSHDC. It is important to note that panels displayed cracking in the center of the span, except for HSHDC-19 (which developed cracking close to the supports). In general, once the peak pressure was reached for HSHDC specimens, a critical crack began to widen and to become a macro-crack that continued to open until the specimen failed. Failure in VHSC panels was dominated by a single macro-crack. Representative images of failed HSHDC and VHSC specimens are shown in Figure 7.4 and Figure 7.5, respectively. Images of each panel tested are included in Appendix A.

Figure 7.4. Image of HSHDC-18 panel after testing with quasi-static pressure loading.

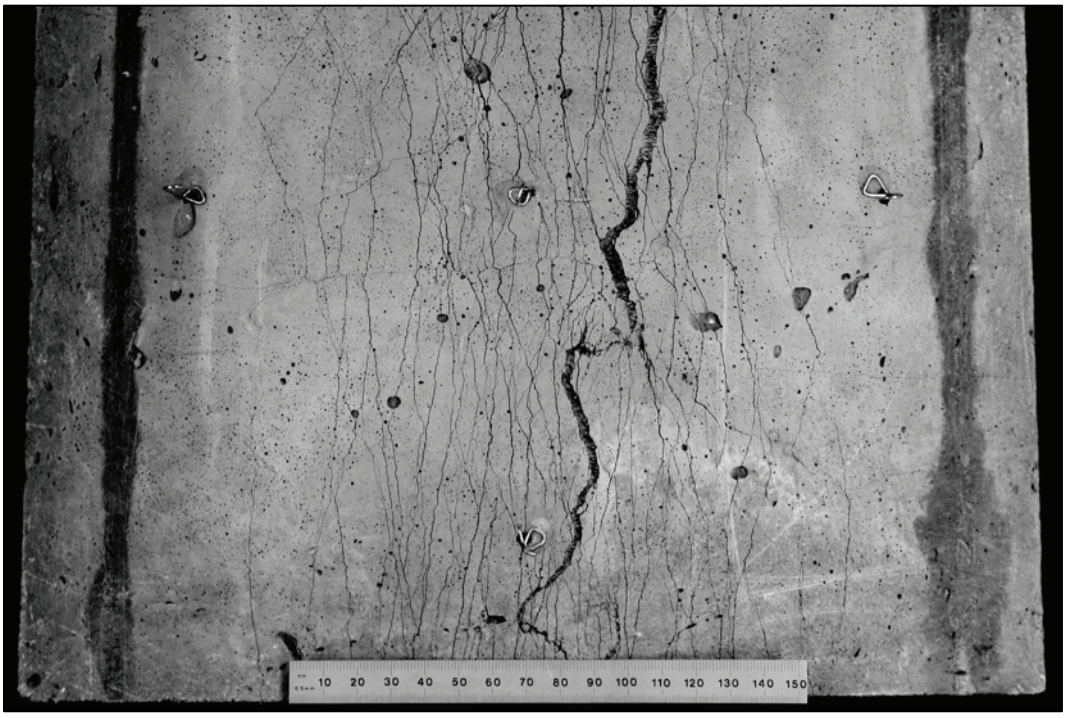

Figure 7.5. Image of VHSC-20 panel after testing with quasi-static pressure loading.

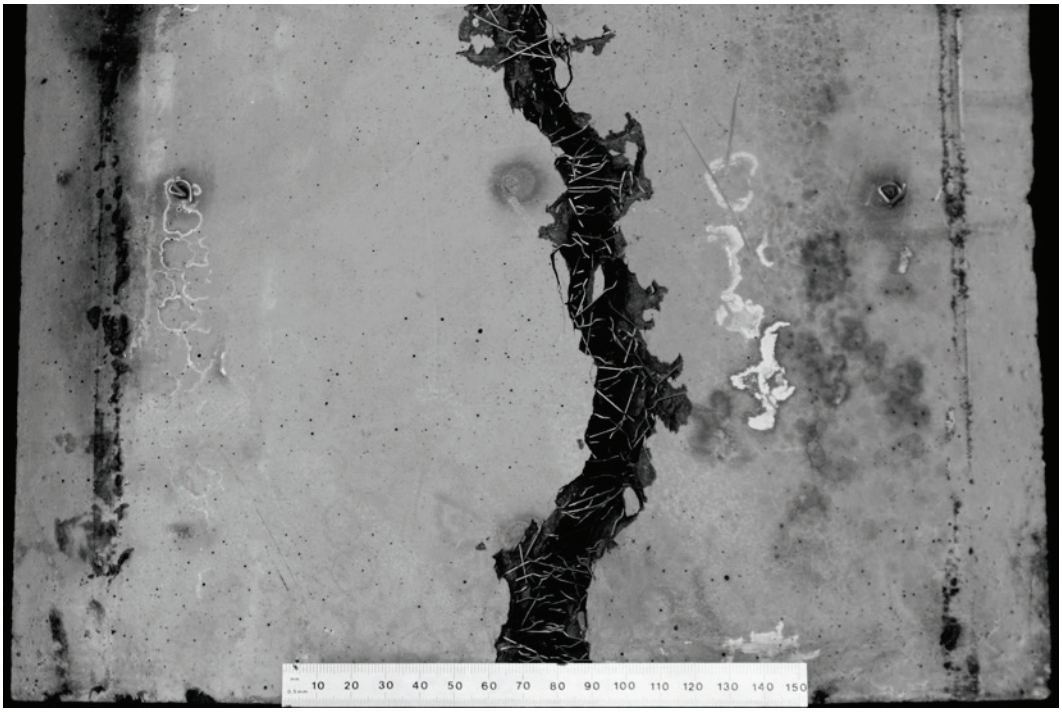

7.5 Resistance function

A resistance function is an x,y dataset representing the relationship between displacement (x) and pressure (y). In the current study, resistance functions were obtained for simply supported pressure-loaded panels of both HSHDC and VHSC and are shown in Figure 7.6. The functions are used in the Wall Analysis Code (WAC) as further described in Chapter 7.

Data used in defining the resistance functions are based on consideration of initial modulus, first-crack, and median displacement. Initial modulus is the linear region at the beginning of the pressure vs. displacement curve. Non-linearity at low pressures in this region was considered a result of settling in the test fixture and therefore was not included in the resistance function. This non-linear section was removed by fitting a straight line through first-crack strength and then shifts the data back to a starting point with zero load and displacement. The next parameter to consider is first-crack strength, which marks the location at which the specimen transitions from elastic to plastic. The average first-crack strength from three specimens was selected for each material's resistance function. Lastly, the median displacement at peak pressure was used as the displacement value where the peak pressure occurred in the resistance function.

Figure 7.6. Quasi-static positive water pressure loading of simply supported panels and calculated resistance functions (RF).

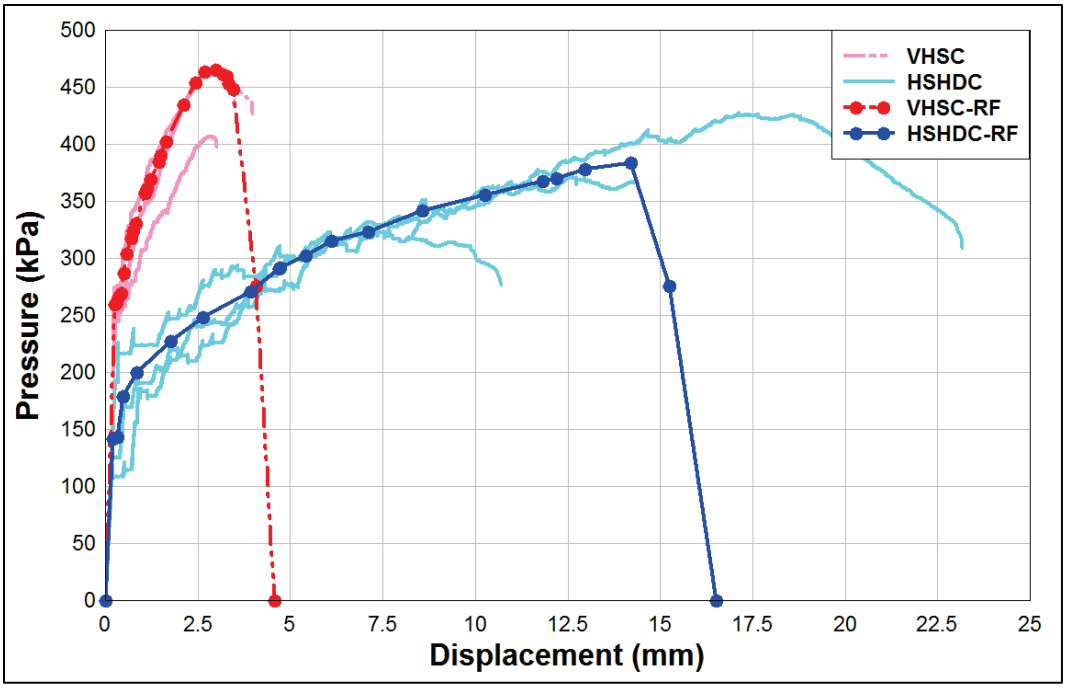

7.6 Dynamic blast data

Dynamic tests were conducted using the small-scale Blast Load Simulator (BLS) described in Chapter 7. This design was used to test at dynamic strain rates of approximately 10/s. All panels tested had nominal dimensions of 305x305x25 mm (12x12x1 in.).

7.6.1 Results

Table 7.3 summarizes the results from dynamic blast load simulator experiments. In initial tests, all panels were tested with a maximum tank pressure of 7.00 MPa (1,015 psi). This pressure caused minimal damage to VHSC, but resulted in fairly large deformations in HSHDC. To reduce the deformation of HSHDC, additional tests were conducted with a tank pressure of 5.86 (850 psi) was used to test HSHDC specimens. Three replicates were tested for both VHSC and HSHDC. Tank pressures above 7.00 MPa were avoided for reasons discussed in Chapter 7.

Table 7.3. Dynamic blast data.

Specimen #	Tank Pressure, MPa (psi)	Peak Pressure, kPa (psi)	Impulse, MPa-msec (psi-msec)	Centerline Deflection at Peak Pressure, mm (in.)
VHSC-1	7.00 (1015)	306 (44.4)	1.44 (208)	0.55 (0.022)
VHSC-6	7.00 (1015)	353 (51.2)	1.65 (239)	0.43 (0.017)
VHSC-9	7.00 (1015)	334 (48.5)	1.47 (213)	0.41 (0.016)
HSHDC-2	5.86 (850)	295 (42.8)	1.39 (202)	2.41 (0.095)
HSHDC-11	5.86 (850)	308 (44.6)	1.38 (200)	1.97 (0.078)
HSHDC-14	5.86 (850)	282 (40.9)	1.37 (198)	2.31 (0.091)
HSHDC-1	7.00 (1015)	315 (45.7)	1.51 (220)	3.05 (0.120)
HSHDC-16	7.00 (1015)	327 (47.5)	1.52 (221)	4.29 (0.169)
HSHDC-24	7.00 (1015)	347 (50.4)	1.57 (228)	6.86 (0.270)

7.6.2 Discussion

There was no visible damage of tested VHSC panels. Minimal cracking was observed at the time of peak deflection and then the cracks closed after the loading dissipated and the panels nearly returned to their original geometry. The high-speed cameras focused on the centerline of the panel were beneficial in capturing the damage levels for these specimens. An example image of VHSC during the high-speed video is presented in Figure 7.7.

Figure 7.7. Panel VHSC-6 image taken from high-speed video showing hairline cracking (inside the boxed region) observed during dynamic testing.

An important observation of this study is that HSHDC remains ductile at higher rates of loading. The same multiple-cracking patterns observed in quasi-static testing (Figure 7.4) were present in dynamic tests. An image from high-speed video during tests of an HSHDC panel is shown in Figure 7.8. Images of each panel are included in Appendix A.

Figure 7.8. Panel HSHDC-16 image taken from high-speed video showing multiple, parallel cracks from dynamic testing.

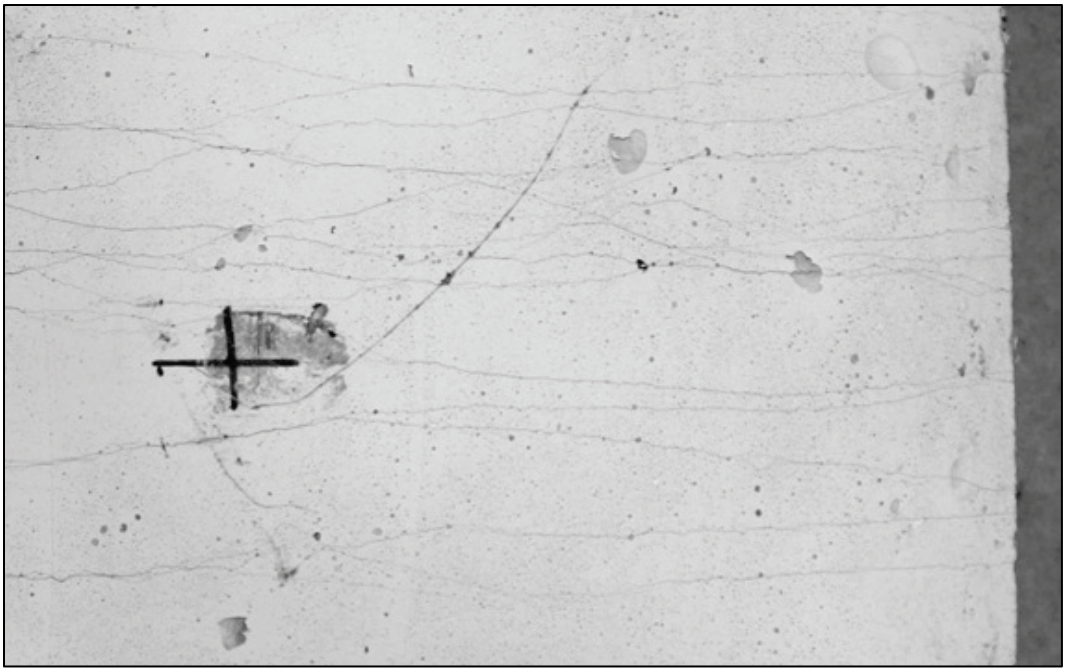

8 Wall Analysis Code (WAC)

8.1 Introduction to WAC

The Wall Analysis Code (WAC) (Slawson 1995) is a single degree-of-freedom (SDOF) model that solves the equations of motion for a wall using the central difference numerical integration technique. One of the primary inputs for this program is an accurate resistance function that relates displacement and pressure for a given specimen geometry, material, and support condition. This study developed resistance functions using quasi-static positive water pressure loading as described in Chapter 7. Through the use of transformation factors for load, resistance, and mass, the wall (reinforced, unreinforced, or user-defined) is represented by an equivalent SDOF system used for deflection calculations and predictions for a given load case and material type.

8.1.1 Procedure for using WAC

Values inputted into WAC are required to be in English units as shown in the graphical user interface (GUI) presented in Figure 8.1. This figure shows the WAC prompts used to input wall parameters. The concrete panels being tested in this study are represented in the software as a scaled wall.

The following steps were followed in the WAC analysis conducted for this study and further describes the inputs shown in Figure 8.1.

1. Wall clear height (ft) – 1.0 representing the 305 mm support span.
2. Wall width (ft) – 1.0 representing the total panel width of 305 mm.
3. Wall thickness (in.) – Nominally 1 inch, but varies slightly from panel to panel.
4. Unit weight of wall (pcf) – 159.7 lb/ft^3 (2,558 kg/m^3) for VHSC and 139.2 lb/ft^3 (2,230 kg/m^3) for HSHDC (as determined by ASTM C 642 (ASTM 2013)).
5. Wall types – In the current case, “user defined” is selected. This allows the user to define section properties (x,y data relating displacement and pressure) by inputting a data file from the resistance functions calculated in Chapter 7.
6. Load-mass factor represents a relationship between load factor and mass factor to provide an equivalent system equation of motion. For pressure-loaded, simply supported one-way panels with a uniform mass in the

plastic failure regime, the load-mass factor is set to 0.66 based formation of a perfect hinge in the center of the span as described in structural dynamics (Biggs 1964). This is appropriate for the failure mechanisms observed in VHSC. However, HSHDC calculations use a load-mass factor of 0.78 (Biggs 1964). This is done because the failure shape is rounded, which is more similar to the assumptions of elastic bending. This failure shape is illustrated in Figure 7.1.

7. Material type – Concrete.
8. Wall failure criterion is the rotation angle at which a specimen has failed by exceeding the maximum rotation permitted for a given requirement. This input requires values in degrees. The solution of the equation of motion is stopped if this value is reached (Slawson 1995). Samples tested in this study maintain some level of structural integrity after being tested so this parameter can be set arbitrarily high (45 deg was chosen for all samples).
9. Calculation duration – An input of zero allows the software to predict the appropriate amount of time required for the calculations. However, an exact time can be inputted in milliseconds if a particular duration needs to be specified. In the current study, an input of zero was selected and the software automatically ran calculations until steady-state conditions were achieved.

8.1.2 Specified load case

Figure 8.2 illustrates the data required for defining a specified load case in WAC. This data is taken from the pressure gauges surrounding the concrete specimen during blast load simulator testing. The figure shows the pressure data (averaged from four gauges) and corresponding impulse. However, the dataset must be a DAT file with less than 100 points so that it can be inputted into WAC.

In order to reduce the data set to the 100 point limit, DPlot software and internal functions described in the *DPlot user manual* (HydeSoft Computing, LLC 2014) were used to depopulate pressure-time histories. The WAC load case curve shown in Figure 8.2 is a down-sampled fit of the pressure data curve. This is calculated by using a backbone fit operation to trace the shape of the curve within an x-axis bin size of 0.1 msec. Next, the Welch depopulation scheme operation within DPlot was used to depopulate the curve while maintaining fidelity within 2 percent of the original dataset. A conventional explosives blast curve with the same peak and arrival time is shown as a reference. This is included to compare the simulated air blasts used in this study to the shape of a conventional pressure-time history that would be observed from the use of actual explosives.

Figure 8.1. Wall Analysis Code (WAC) graphical user interface (GUI).

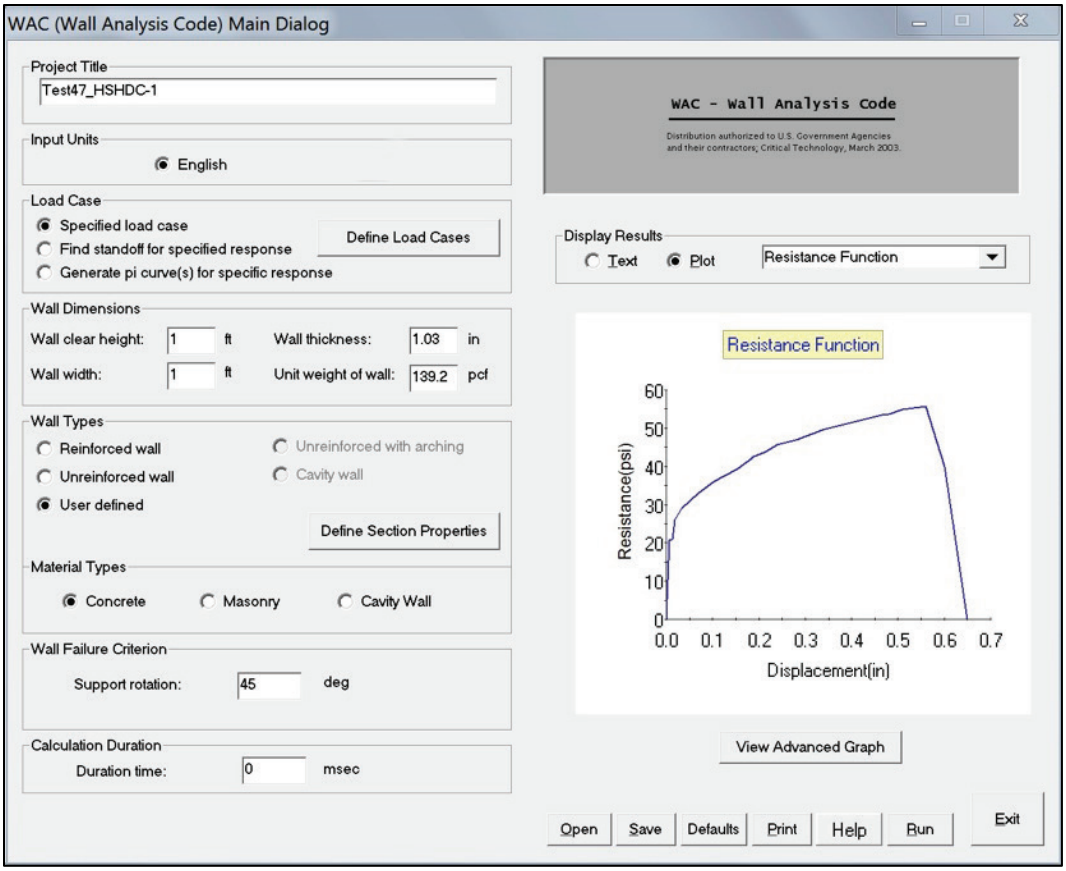

Figure 8.2. Difference in quasi-static (dotted) and dynamic (solid) resistance functions calculated for material response of VHSC and HSHDC.

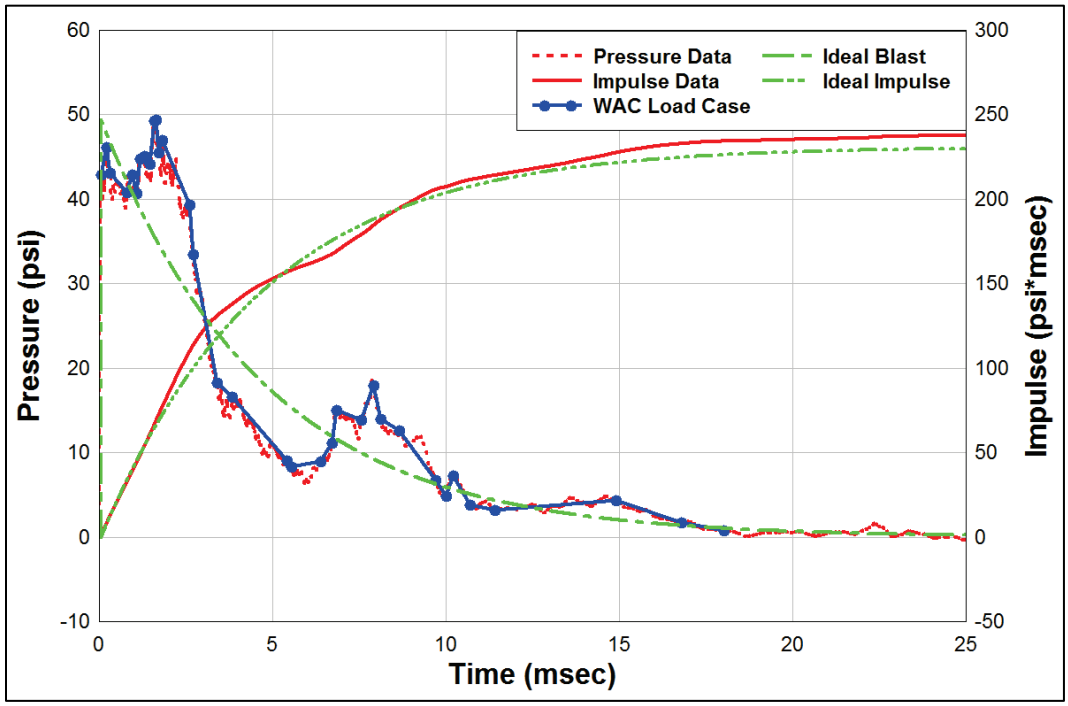

8.2 WAC calculations with quasi-static resistance function

Using the procedure described above, each sample that was tested dynamically was subsequently analyzed using WAC. A unique specified load case (pressure-time history) and the corresponding user-defined wall type (resistance function) were inputted to predict centerline panel deflections.

8.2.1 Results

After conducting analysis with WAC, predicted and actual displacement values were compared. Results from WAC analysis are presented in Table 8.1 and Figure 8.3. The diagonal lines in Figure 8.3 are included as a visual reference. If the model perfectly predicted the response of each specimen, all data values would lie on the 1:1 line. Additional reference lines for 2:1 and 3:1 are included to show the magnitude of over prediction for centerline deflections calculated in WAC.

Table 8.1. Results from WAC analysis using quasi-static resistance function.

Specimen #	Centerline Deflection, mm (in.)	WAC Predicted Centerline eflection, mm (in.)	Error, %
VHSC-1	0.55 (0.022)	1.09 (0.043)	98%
VHSC-6	0.43 (0.017)	1.45 (0.057)	237%
VHSC-9	0.41 (0.016)	1.24 (0.049)	202%
HSHDC-2	2.41 (0.095)	6.27 (0.247)	160%
HSHDC-11	1.97 (0.078)	6.20 (0.244)	215%
HSHDC-14	2.31 (0.091)	5.26 (0.207)	128%
HSHDC-1	3.05 (0.120)	7.57 (0.298)	148%
HSHDC-16	4.29 (0.169)	7.54 (0.297)	76%
HSHDC-24	6.86 (0.270)	8.20 (0.323)	20%

8.2.2 Discussion

The results in Figure 8.3 show that WAC over predicted dynamic displacement by a factor of 2-3 in most cases. However, the quasi-static resistance function used for these calculations does not account for any type of strain-rate effect associated with the flexural capacity of these materials. Strain-rate considerations are discussed in the following section.

Figure 8.3. WAC predicted deflections vs. measured deflections for individual test panels from dynamic testing using quasi-static resistance functions.

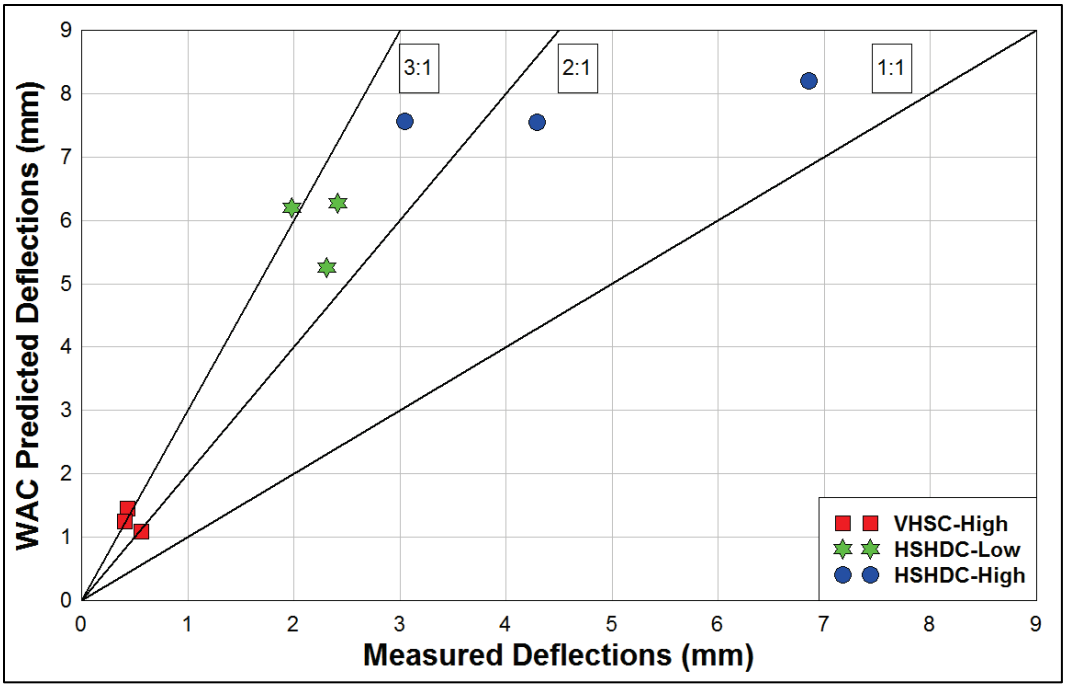

Three replicate specimens were tested for each combination of material (VHSC and HSHDC) and pressure (low and high). Referencing Figure 8.3, replicate tests showing variations in measured deflections (x-axis) are due to variability in specimens. This variability is especially high for HSHDC specimens tested at higher pressures. This noise is consistent with variability observed in quasi-static testing at similar deflections as observed in Figure 7.3. Since all WAC predicted deflections use the same nominal thickness and resistance function, variability in the predicted deflection (y-axis) for replicate tests are due to variation in the pressure-time histories from specimen-to-specimen.

8.3 WAC calculations with dynamic resistance function

Strain-rate effects are important when developing deflection predictions for blast testing. The WAC predictions should become more accurate if the resistance functions can account for these strain-rate effects by creating dynamic resistance functions and then re-analyzing the data in WAC.

8.3.1 Developing dynamic resistance function

Ranade recently published a paper discussing the tensile rate effects for HSHDC (Ranade et al. 2014). This paper is relevant to the current

experiments since concrete in flexure fails in cracking. The referenced paper presents data at the same strain rates observed in this study for the quasi-static (10^{-4}/s) and dynamic (10/s) tests presented. Ranade determined that the following changes occur from the increase in strain rate (Ranade et al. 2014):

- First-crack strength increases by 53 percent
- Ultimate strength increases by 42 percent

These observed increases in first-crack strength and ultimate strength are then applied to the quasi-static resistance functions as shown in Figure 8.4. Since HSHDC and VHSC have a very similar cementitious matrix, both dynamic resistance functions are developed using the strain-rate data from HSHDC.

Figure 8.4. Difference in quasi-static (dotted) and dynamic (solid) resistance functions calculated for material response of VHSC and HSHDC.

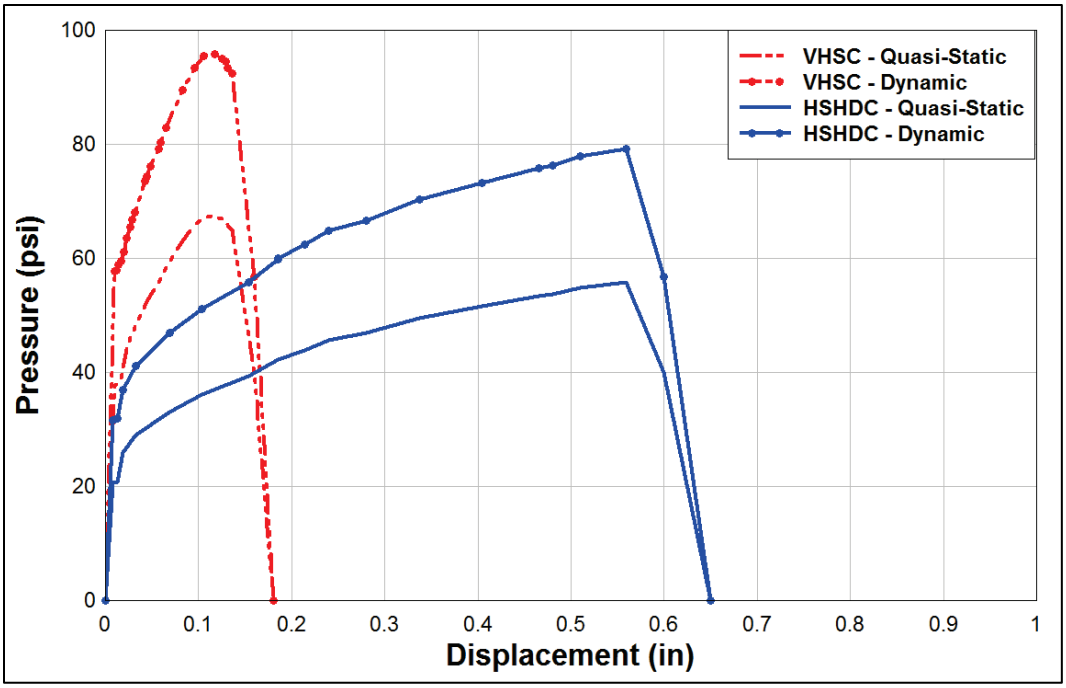

8.3.2 Results

Table 8.2 shows the WAC predicted centerline displacement values of each specimen based on the dynamic resistance functions from Figure 8.4. Figure 8.5 shows predictions using quasi-static and dynamic resistance functions for direct comparison.

Table 8.2. Results from WAC analysis using dynamic resistance function.

Specimen #	Centerline Deflection, mm (in.)	WAC Predicted Centerline Deflection, mm (in.	Error, %
VHSC-1	0.55 (0.022)	0.48 (0.019)	13%
VHSC-6	0.43 (0.017)	0.56 (0.022)	30%
VHSC-9	0.41 (0.016)	0.56 (0.022)	37%
HSHDC-2	2.41 (0.095)	2.01 (0.079)	17%
HSHDC-11	1.97 (0.078)	1.98 (0.078)	1%
HSHDC-14	2.31 (0.091)	1.83 (0.072)	21%
HSHDC-1	3.05 (0.120)	2.36 (0.093)	23%
HSHDC-16	4.29 (0.169)	2.54 (0.100)	41%
HSHDC-24	6.86 (0.270)	2.87 (0.113)	58%

Figure 8.5. WAC predicted deflections vs. measured deflections from dynamic testing using quasi-static resistance functions and dynamic resistance functions.

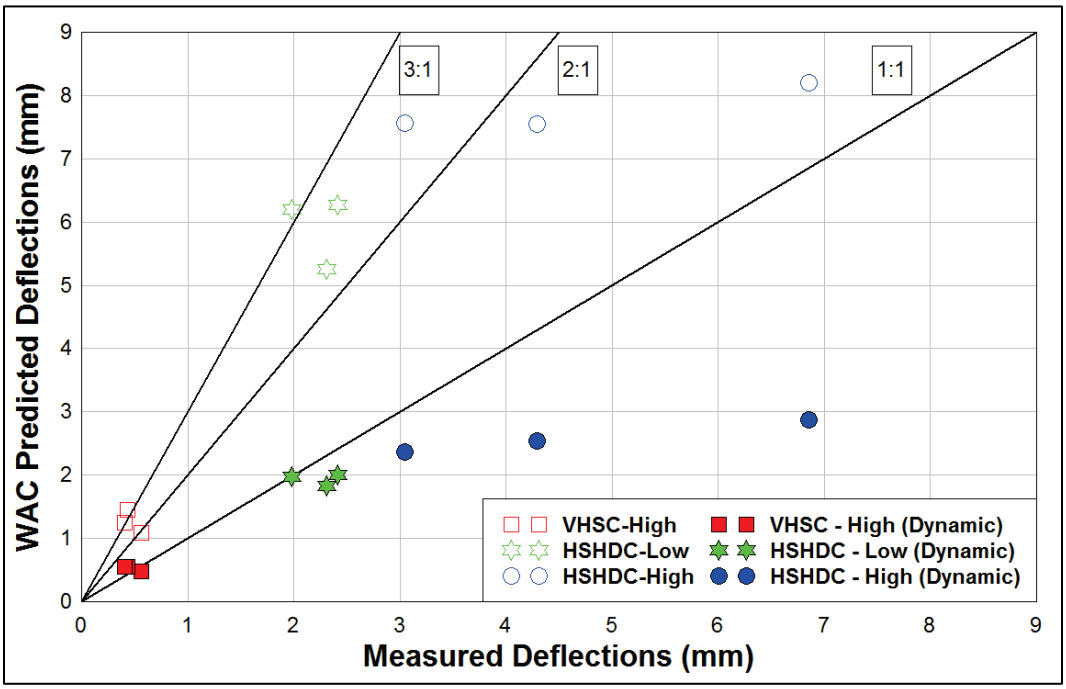

8.3.3 Discussion

After considering the strain-rate effects for these materials, WAC is more accurate in predicting the deflection of a panel based on the load case that is applied (as shown in Figure 8.5). By using the dynamic resistance functions, WAC predictions for displacements up to 2.54 mm (0.1 in.) have minimal error. These displacements occur in the initial portion of the resistance function where low levels of apparent plasticity are observed.

This analysis process using WAC provides a way to estimate small deflections observed for a given resistance function without having to perform a series of expensive blast experiments.

However, large deflection predictions in WAC for HSHDC are still unreliable with large discrepancies between predicted and measured deflections. These larger deflections are observed well into the apparent plastic region of the resistance functions where relatively small increases in impulse can lead to relatively large changes in deflection. The assumptions within WAC based on beam theory and plastic hinge formation may not hold true for these types of large deformations. Poor predictions in the apparent plastic region of the resistance function may also be related to the change in failure modes as strain rate increases, which has been observed in prior research (Ranade et al. 2014). This research observed that crack width decreases as strain rate increases. This phenomenon provides an explanation as to why the WAC predictions are lower than the measured deflections.

Overall, WAC predictions were improved using dynamic resistance functions. However, several variables should be considered when analyzing the final dataset:

- Dynamic increase factors used to develop dynamic resistance functions are based on direct tension data and then applied to flexural response. Although behavior of the tensile face is the primary mode for failure in flexure, compressive rate effects also influence material response.
- Tensile data is based on a constant strain rate, whereas the strain rate under blast loading is non-uniform.
- Higher deflections in HSHDC specimens recorded in Figure 8.5 are in the apparent plastic region of the resistance function where large deformations occur. Data in this region is highly sensitive to small changes in impulse. Future work should consider a sensitivity study incorporating modifications to the dynamic resistance function.

In future work, a sensitivity study will be conducted to determine how modifications to dynamic resistance functions affect the predicted deflection values in WAC. The analysis presented in the current research is based on strain rate data for HSHDC specimens in tension. Although this provides a reasonable starting point for obtaining dynamic resistance functions, the dynamic increase factors related to first-crack strength and

ultimate strength should be analyzed further. These parameters will be adjusted to develop a resistance function that provides a better correlation to the reported experimental data. Through the use of a sensitivity study focused on fitting experimental data, the resulting resistance function will also account for any complexities of the experimental setup and changes in dynamic failure mechanisms.

9 Conclusions and Recommendations

9.1 Scope

This chapter presents conclusions and recommendations for quasi-static testing, dynamic test method development, dynamic testing, and analysis.

9.2 Conclusions

9.2.1 Quasi-static material properties

- Quasi-static testing included compression, flexure, splitting tension, and direct tension. Results from these tests were similar to published values indicating that materials in this study were produced as desired.

9.2.2 Dynamic test method development

- The newly developed/constructed water chamber apparatus provides a unique capability for quasi-static pressure loading of simply supported concrete panels in one-way bending. From these tests, resistance functions can be developed for small-scale samples to develop pressure-displacement relationships.
- Upgrades made to the existing small-scale Blast Load Simulator allow tests of panel specimens at this scale. Such tests determine dynamic properties of materials at reduced cost.

9.2.3 Testing of simply supported, pressure-loaded one-way panels

- Specimen size of 305x305x1 mm with a 254 mm span worked well for both quasi-static and dynamic tests.
- In quasi-static water chamber tests, very-high-strength concrete (VHSC) has a peak flexural strength approximately 7 percent higher than high-strength high-ductility concrete (HSHDC). However, water chamber tests of HSHDC indicate increased ductility. Displacement of VHSC at peak stress is approximately eight times lower than that of HSHDC specimens.
- Dynamic blast load simulator tests of HSHDC specimens indicate ductility at higher strain rates occurs through development of parallel microcracks.

9.2.4 Wall Analysis Code (WAC)

- Quasi-static resistance functions can be modified using dynamic increase factors (DIF) from the literature to create dynamic resistance functions for improved accuracy in deflection predictions from the Wall Analysis Code (WAC).
- WAC can be paired with an accurate resistance function and a unique load case to accurately predict deflections up to approximately 2.54 mm (0.1 in.) in both VHSC and HSHDC. However, larger deflections recorded in some HSHDC samples proved to have a high degree of variability and were difficult to predict accurately.
- Utilizing WAC in conjunction with blast load simulator experiments can provide cost savings by reducing the number of experiments required to validate material response.

9.3 Recommendations

9.3.1 Quasi-static material properties

- Quasi-static test methods should be conducted on samples cured with steam (rather than the method presented in this study) to determine if the same material properties can be produced on a larger scale. It is not feasible to cure full-size slabs using a water bath and oven as prescribed in the current curing methods.
- Direct tension methods require additional data to compare the effects of support conditions (fixed-fixed vs. rotational degrees of freedom) to relate prior data reported using different supports. Sample thickness should also be investigated since larger specimens allow for more uniform fiber dispersion.

9.3.2 Test method development

- The quasi-static positive water pressure apparatus could be redesigned based on the peak pressures required for testing. An optimized design for specific peak pressures should be able to reduce the size and weight of the testing apparatus.
- Dynamic pressure loading method – Increase the functional pressure range by lengthening the shock tube so that there is more time/distance for higher pressure waves to become uniform prior to reaching the panel. This will allow for the testing of VHSC to higher displacements.

- Add modular components to allow various sizes and locations of air gaps so that impulse can be controlled. This would provide further investigation into the pressure-dominant and impulse-dominant regions of blast response.

9.3.3 Testing of simply supported, pressure-loaded one-way bending panels

- Quality control should be improved during placement to confirm that all test panels have the same geometry to minimize specimen-to-specimen variation. Specimens should also achieve initial set on a level surface to minimize variations in thickness across a given specimen.
- Additional replicates of simply supported panels tested (both quasi-statically and dynamically) are desirable for presenting more confident statistical information (such as average values, standard deviations, and outliers).

9.3.4 Wall Analysis Code (WAC)

- Improve resistance functions by collecting a larger quasi-static dataset to provide average material response with a higher confidence so that deflection calculations in WAC will be more accurate.
- Explore ways to modify loading conditions (pressure-time histories) to quantify material performance in both pressure and impulse dominated failure regions. This would produce a larger data set to determine the effectiveness of WAC in different portions of the failure envelope.

9.4 Summary

The testing equipment and protocols developed for this study provide a viable technique for evaluating structural response modes of small-scale panel specimens. Additionally, the documented protocols are effective and economical techniques for performing sensitivity studies regarding the effects of variations in material properties on structural response of panels. More data are needed to validate the use of SDOF analysis to predict panel response to the dynamic loading of the small-scale BLS.

References

American Society for Testing and Materials (ASTM). 2012. *Standard test method for compressive strength of cylindrical concrete specimens*. ASTM C 39. C09 Committee. West Conshohocken, PA: ASTM International; doi:10.1520/C0031_C0031M.

_____. 2012. *Standard test method for splitting tensile strength of cylindrical concrete specimens*. Designation: ASTM C 496. C09 Committee. West Conshohocken, PA: ASTM International; doi:10.1520/C0031_C0031M.

_____. 2012. *Standard test method for flexural performance of fiber-reinforced concrete*. Designation: C 1609. C09 Committee. West Conshohocken, PA: ASTM International; doi:10.1520/C0031_C0031M.

_____. 2013. *Standard test method for compressive strength of hydraulic cement mortars*. Designation: ASTM C 109. C01 Committee. West Conshohocken, PA: ASTM International; doi:10.1520/C0091.

_____. 2013. *Standard test method for density, absorption, and voids in hardened concrete*. Designation: ASTM C 642. C09 Committee. West Conshohocken, PA: ASTM International.

_____. 2014. *Standard test method for determining consistency and density of roller-compacted concrete using a vibrating table*. Designation: C 1170. C09 Committee, West Conshohocken, PA: ASTM International.

Biggs, J. M. 1964. Introduction to Structural Dynamics. New York, NY: McGraw-Hill Companies.

Dennis, S. T., J. T. Baylot, and S. C. Woodson. 2002. Response of 1/4-scale concrete masonry unit (CMU) walls to blast. *Journal of Engineering Mechanics* 128(2):134-142. doi:10.1061/(ASCE)0733-9399(2002)128:2(134).

Eirich Mixing Technology. 2015. http://www.eirich.com/en/mixers, 1-1.

ESR-2202. 2014. ITW Red Head Tapcon screw anchors. http://www.tapcon.com/documents/esr-2202.pdf.

Euclid Chemical Company. 2014. Eucobar evaporation retardant. http://www.euclidchemical.com/fileshare/ProductFiles/techdata/Eucobar.pdf.

Hobart. 2015. Mixer with bowl and paddle. http://img0045.popscreencdn.com/127371411_hobart-a200-20-quart-dough-mixer-w-bowl-hook-paddle-ebay.jpg, 1-1.

HydeSoft Computing, LLC. 2014. DPlot User Manual. http://dplot.swmirror.com/1e65d.

Johnson, C. F. 2013. Concrete masonry wall retrofit systems for blast protection. PhD diss., Texas A&M University.

Japan Society of Civil Engineers. 2008. *Recommendations for design and construction of high performance fiber reinforced cement composites with multiple fine cracks*. Tokyo: JSCE.

Lamond, J. F. 2006. *Significance of tests and properties of concrete and concrete-making materials*. ASTM STP 169 C. West Conshohocken, PA: ASTM International.

Lin, Z., T. Kanda, and V. C. Li. 1999. On interface property characterization and performance of fiber-reinforced cementitious. *Concrete Science and Engineering* 1:173–174.

Li, V. C. 1993. From micromechanics to structural engineering-The design of cementitous composites for civil engineering applications. *JSCE Journal of Structural Mechanics and Earthquake Engineering* 10(2):37-48.

Li, V. C., S. Wang, and C. Wu. 2001. Tensile strain-hardening behavior of polyvinyl alcohol engineered cementitious composite (PVA-ECC). *ACI Materials Journal* 98(6):483-492.

Li, V. C., C. Wu, S. Wang, A. Ogawa, and T. Saito. 2002. Interface tailoring for strain-hardening polyvinyl alcohol-engineered cementitious composite (PVA-ECC). *ACI Materials Journal* 99(5):463-472.

Li, V. C. 2003. On engineered cementitious composites (ECC). *Journal of Advanced Concrete Technology* 1(3):215-230.

Oesch, T. S. 2015. Investigation of fiber and cracking behavior for conventional and ultra-high performance concretes using x-ray computed tomography. PhD diss., University of Illinois at Urbana-Champaign.

O'Neil, E. F. 2008. On engineering the microstructure of high-performance concretes to improve strength, rheology, toughness, and frangibility. PhD diss., Northwestern University.

Ranade, R., M. D. Stults, V. C. Li, T. S. Rushing, J. Roth, and W. F. Heard. 2012. *Development of high strength high ductility concrete.* 2nd International RILEM Conference on Strain Hardening Cementitious Composites. Rio de Janeiro, Brazil.

Ranade, R., V. C. Li, M. D. Stults, W. F. Heard, and T. S. Rushing. 2013. Composite properties of high-strength, high-ductility concrete. *ACI Materials Journal* 110:413-422.

Ranade, R., V. C. Li, M. D. Stults, T. S. Rushing, and J. Roth. 2013. Micromechanics of high-strength, high-ductility concrete. *ACI Materials Journal* 110:375-384.

Ranade, R., V. C. Li, and W. F. Heard. 2014. Tensile rate effects in high strength-high ductility concrete. *Cement and Concrete Research* 68(C):1–11. doi:10.1016/j.cemconres.2014.11.005.

Robert, S. D., C. F. Johnson, and S. C. Woodson. 2011. Effects of high-strength materials on blast response of reinforced concrete panels. *ACI Special Publication* 281:1-16.

Roth, J., T. S. Rushing, O. G. Flores, D. K. Sham, and J. W. Stevens. 2010. *Laboratory investigation of the characterization of Cor-Tuf flexural and splitting tensile properties*. ERDC/GSL TR-10-46. Vicksburg, MS: U.S. Army Engineer Research and Development Center.

Rushing, T. S., J. F. Burroughs, B. A. Williams, and W. F. Heard. 2012. *Both high strength and high ductility achieved with concrete*. International SAMPE Technical Conference. New York, NY: Elsevier Inc.

Salim, H., S. Roberts, and A. Saucier. 2013. *Experimental evaluation of static resistance function using a vacuum chamber*. American Society of Civil Engineers; 2013:137–147. Reston, VA: ASCE. doi:10.1061/9780784412848.013.

Scott, D. A., W. R. Long, R. D. Moser, B. H. Green, J. L. O'Daniel, and B. A. Williams. 2014. *Impact of steel fiber size and shape on the mechanical properties of ultra-high performance concrete*. ERDC/GSL TR-15-22. Vicksburg, MS: U.S. Army Engineer Research and Development Center.

Slawson, T. R. 1995. *Wall response to airblast loads: The wall analysis code (WAC)*. Contract DACA39-95-C-0009, ARA-TR-95-5208. Vicksburg, MS: U.S. Army Engineer Waterways Experiment Station.

Williams, E. M., S. S. Graham, P. A. Reed, and T. S. Rushing. 2009. *Laboratory characterization of Cor-Tuf concrete with and without steel fibers*. ERDC/GSL TR-09-22. Vicksburg, MS: U.S. Army Engineer Research and Development Center.

Yokel, F. Y., R. G. Mathey,and R. D. Dikkers. 1971. *Strength of masonry walls under compressive and transverse loads*. Volume 34 of Building Science Series. Washington, DC: U.S. National Bureau of Standards.

Appendix A: Photographs of Tested Panels

A.1 Quasi-static simply supported one-way panels

Figure A1. VHSC-1.

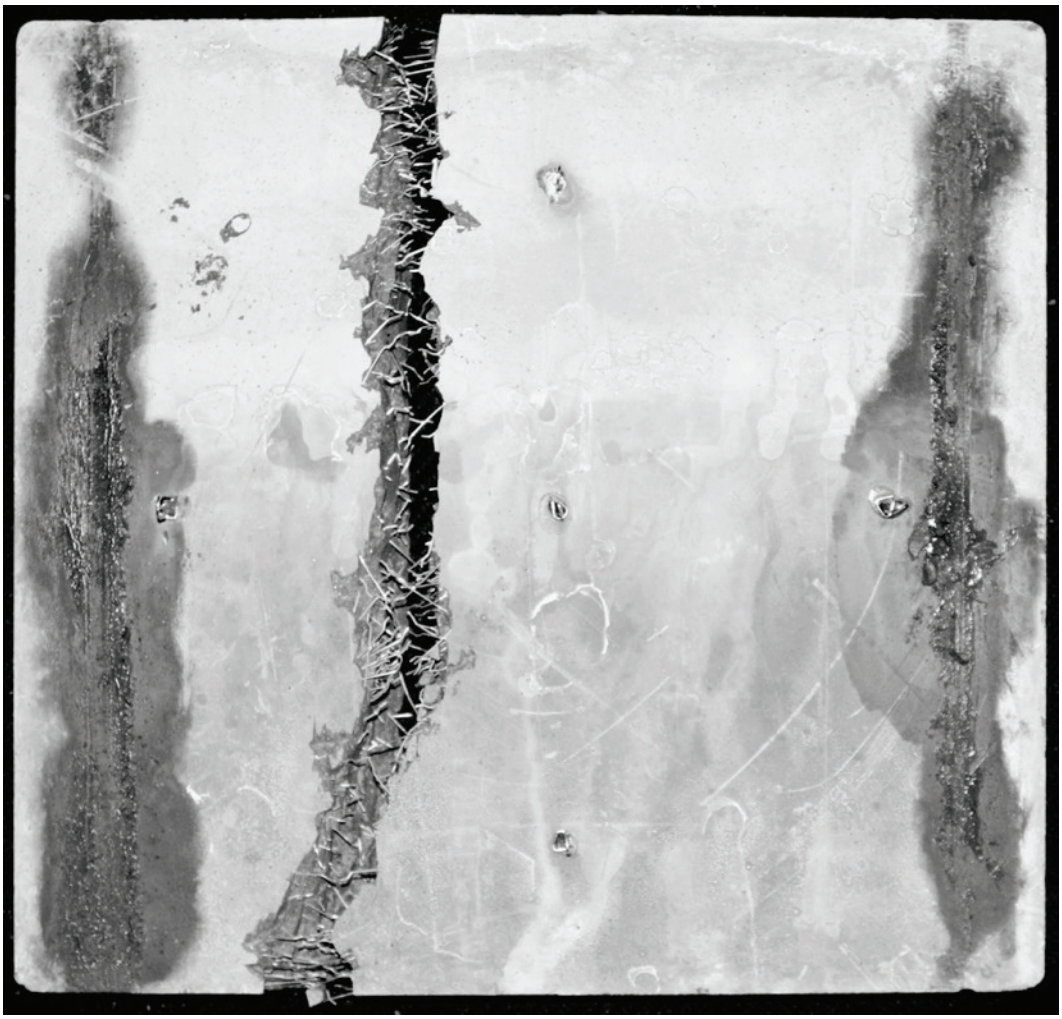

Figure A2. VHSC-10.

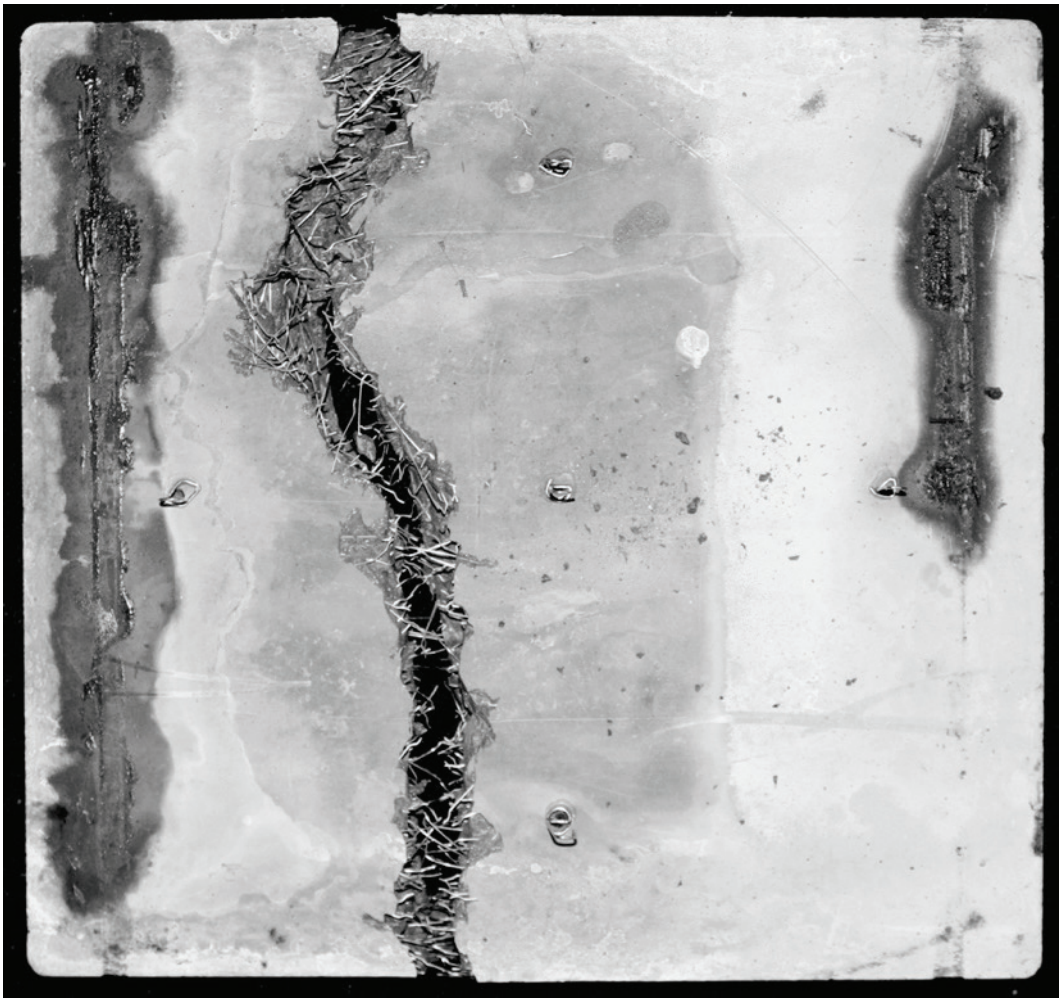

Figure A3. VHSC-20.

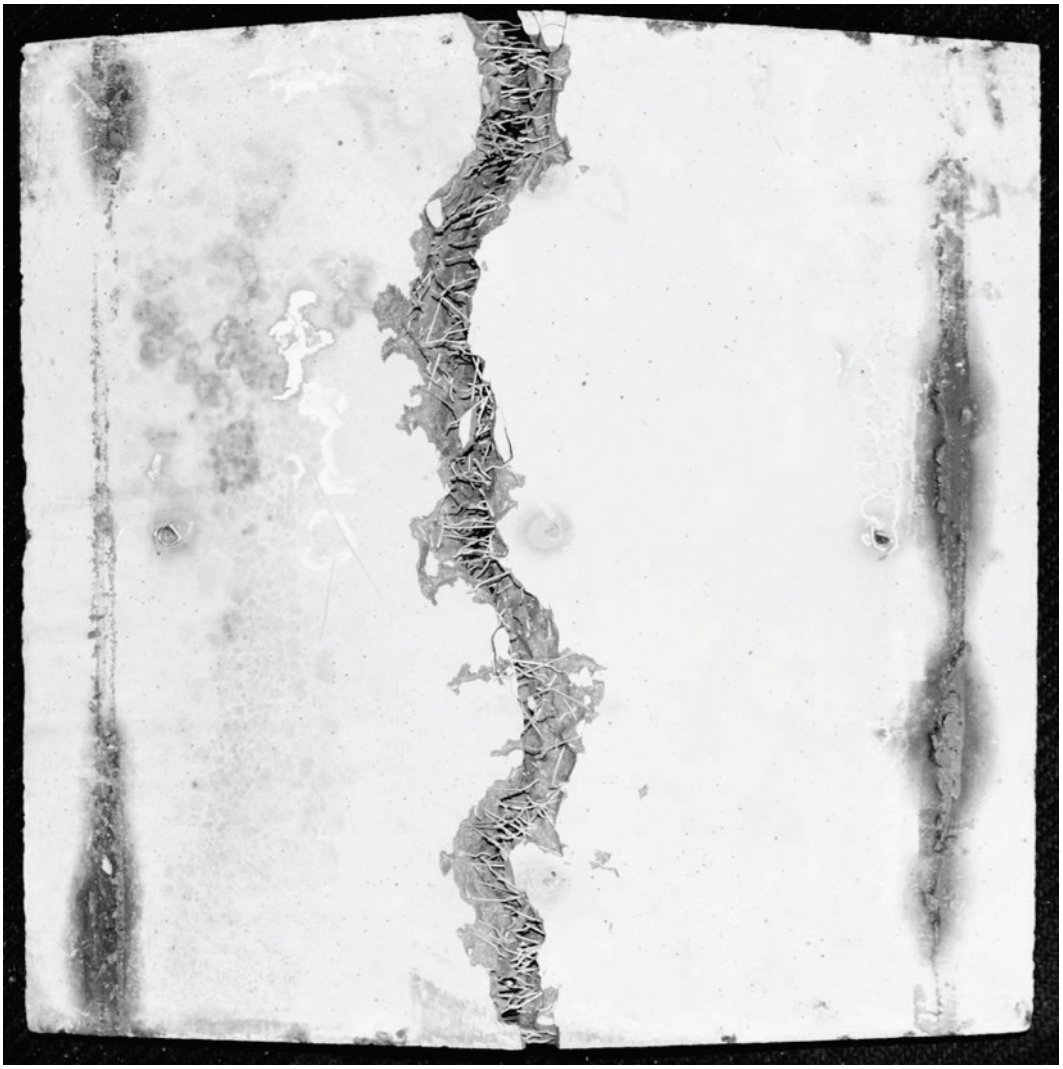

Figure A4. HSHDC-18.

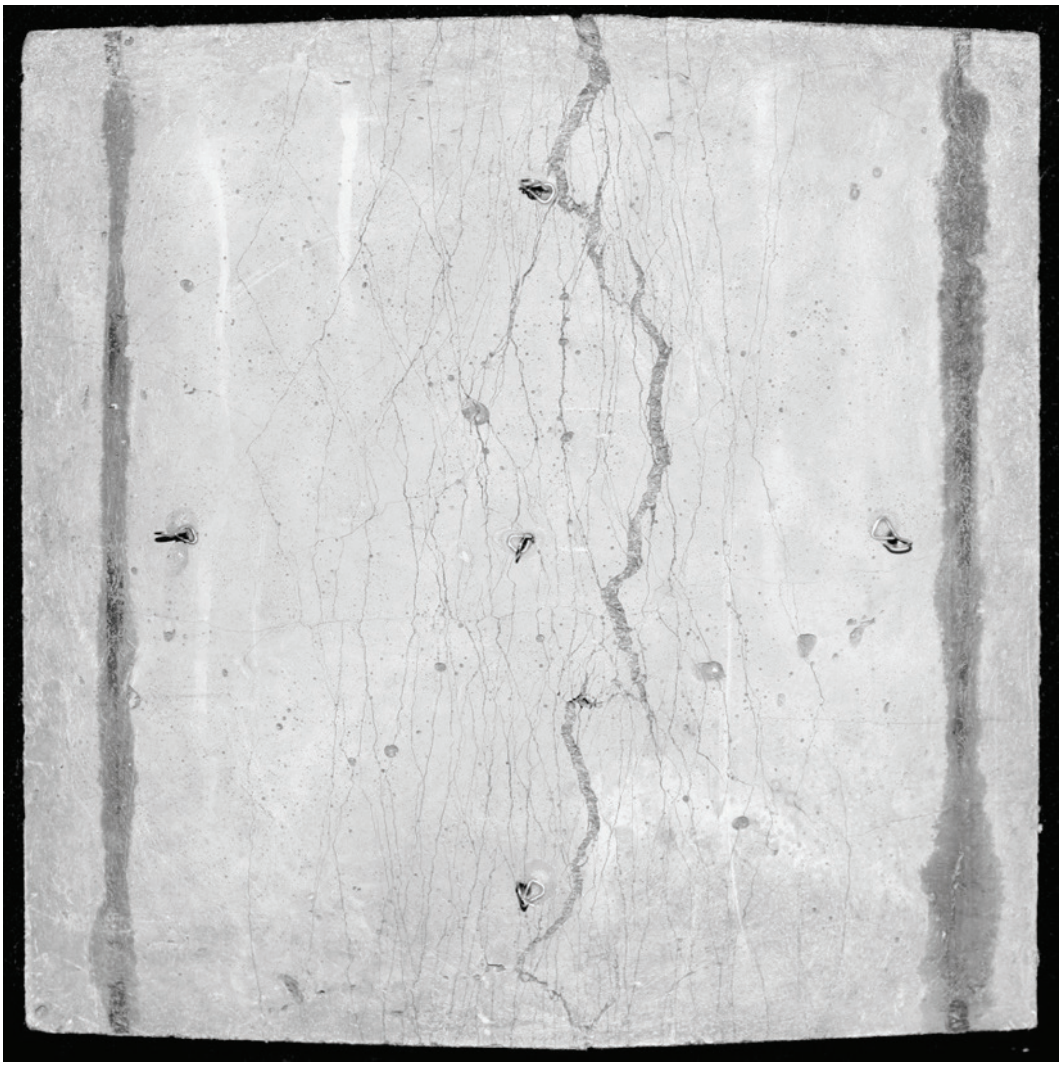

Figure A5. HSHDC-19.

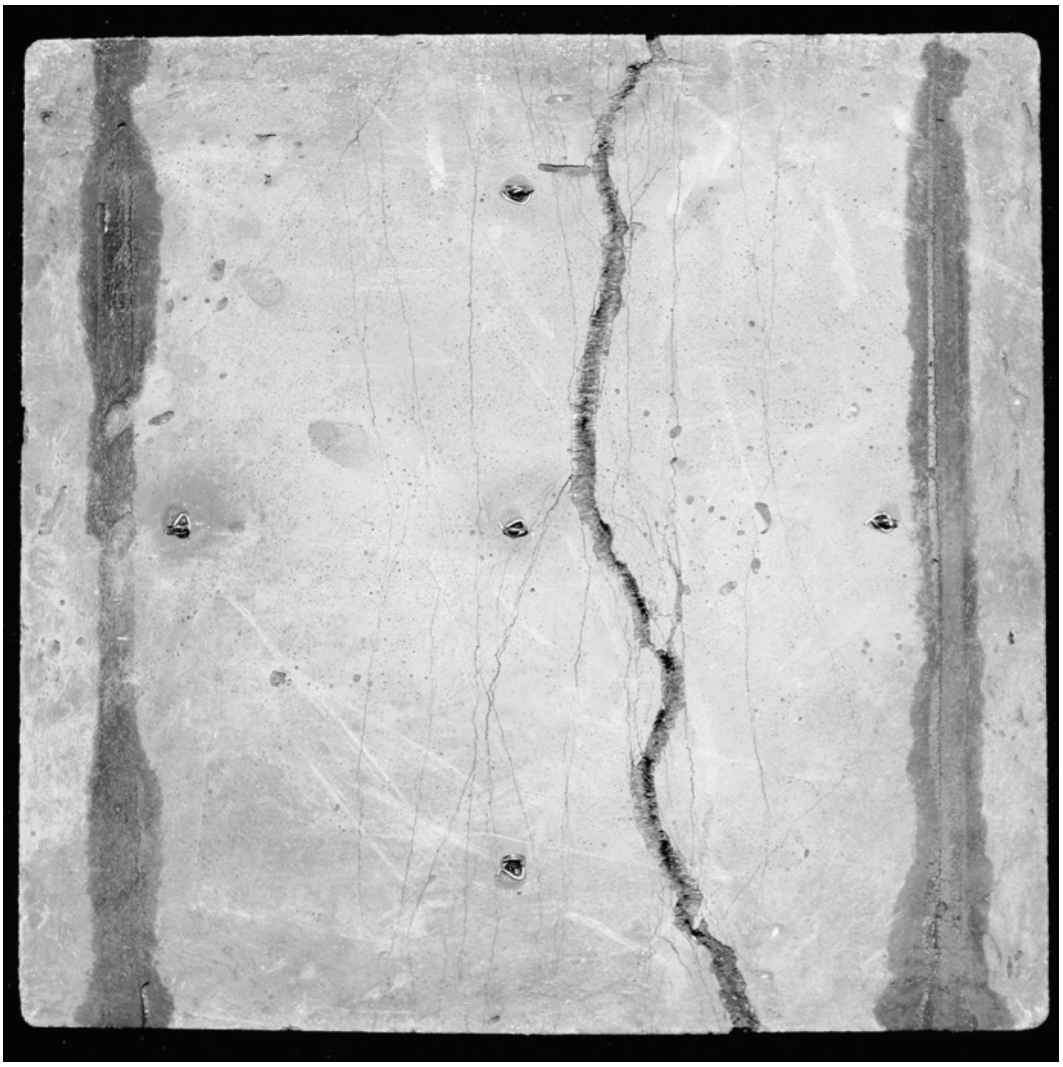

Figure A6. HSHDC-23.

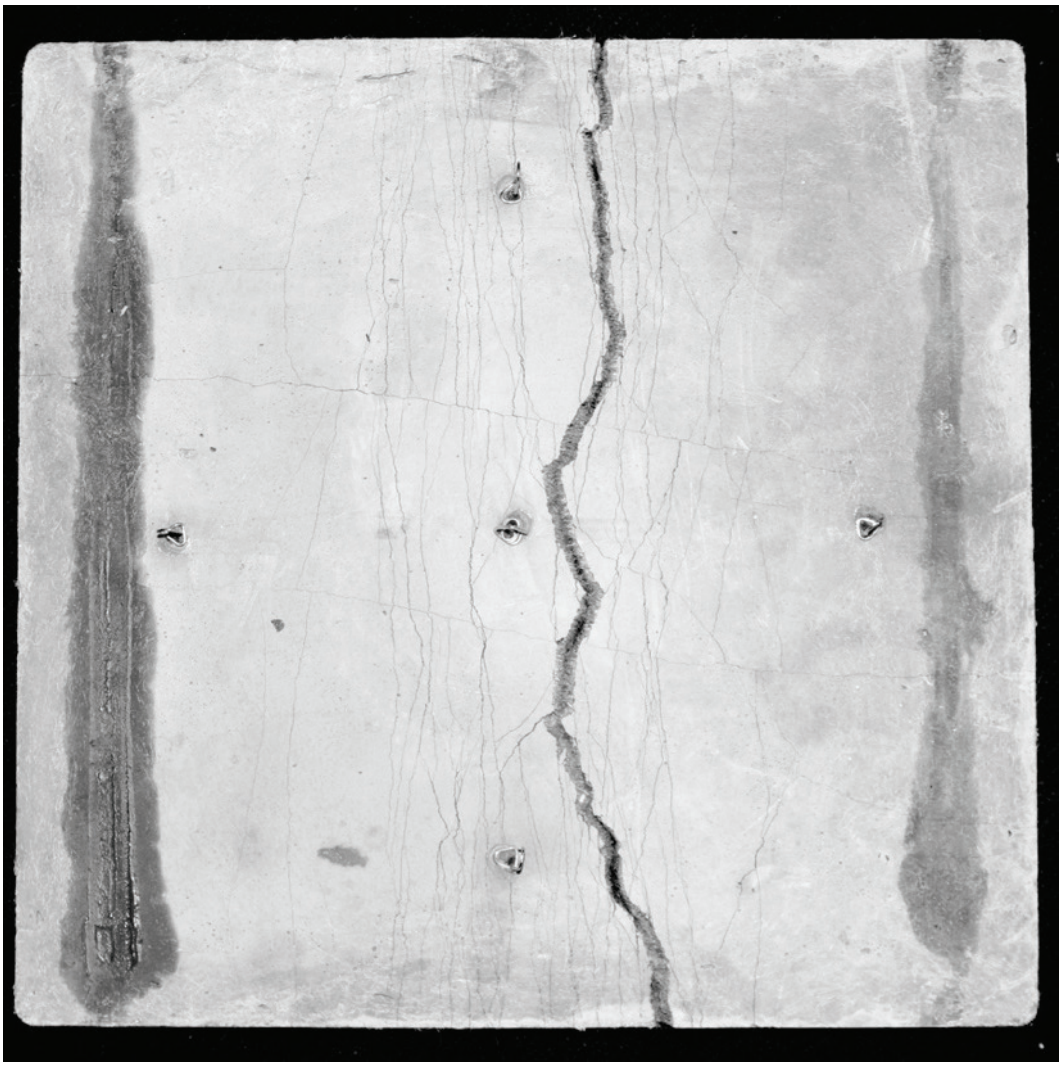

A.2 Dynamic simply supported one-way panels

A.2.1 Low pressure

Figure A7. HSHDC-2.

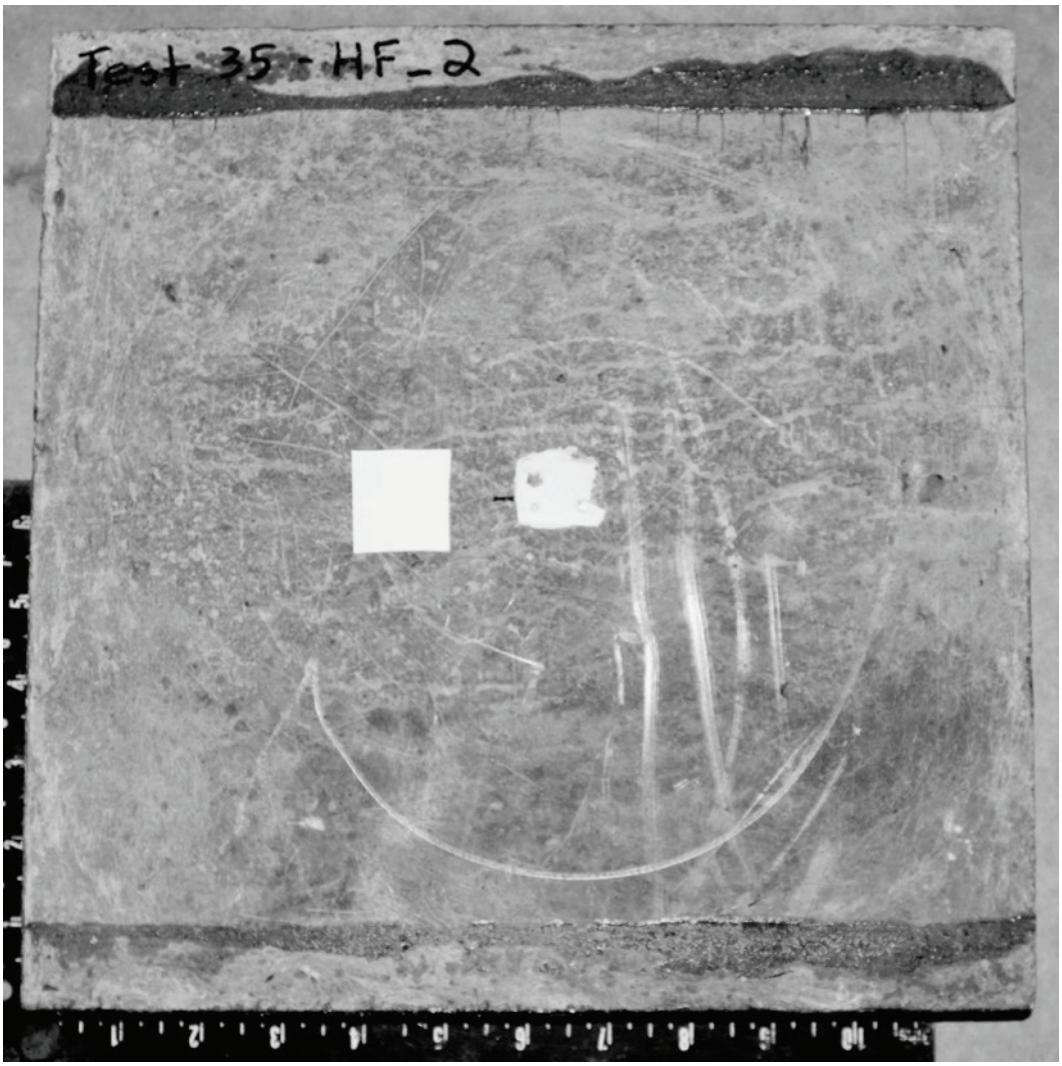

Figure A8. HSHDC-11.

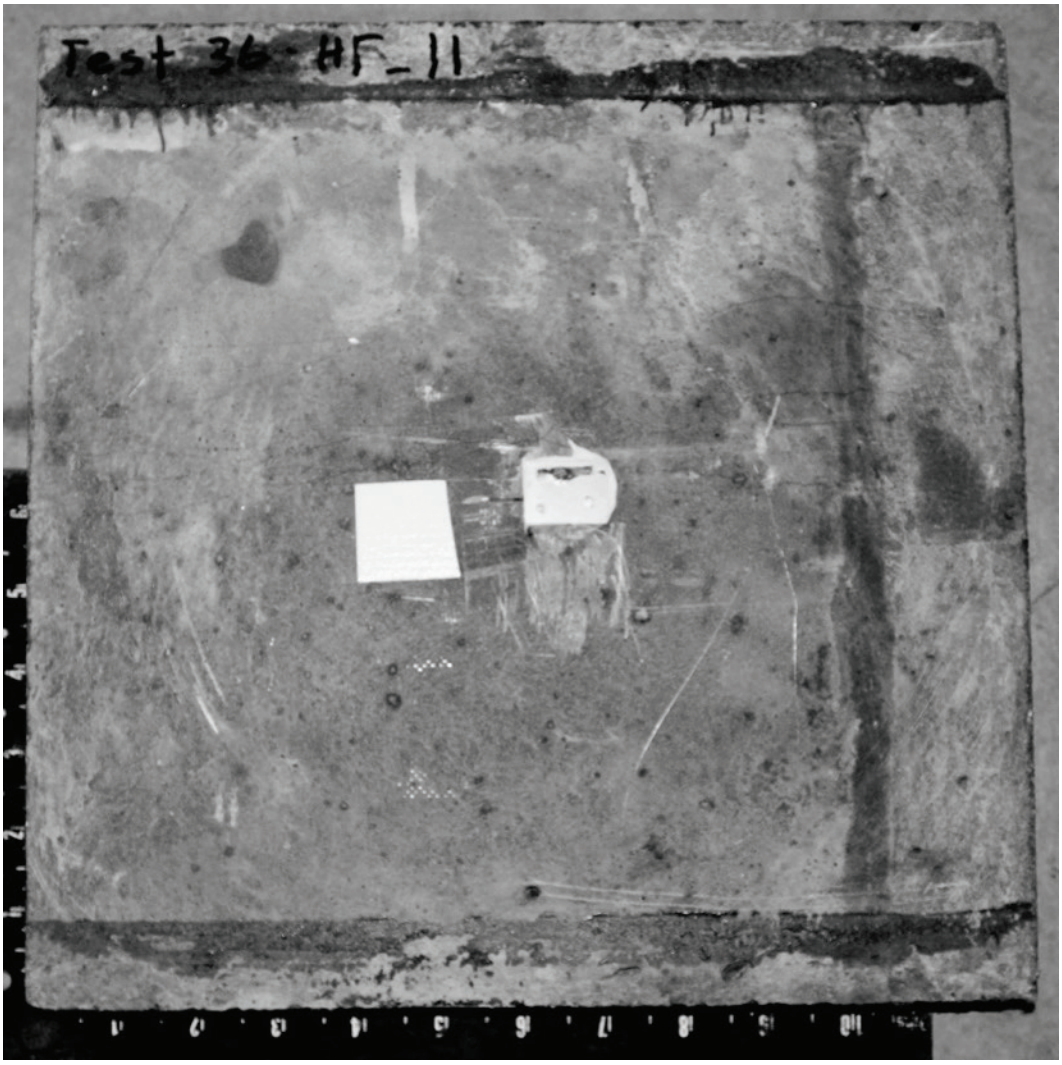

Figure A9. HSHDC-14.

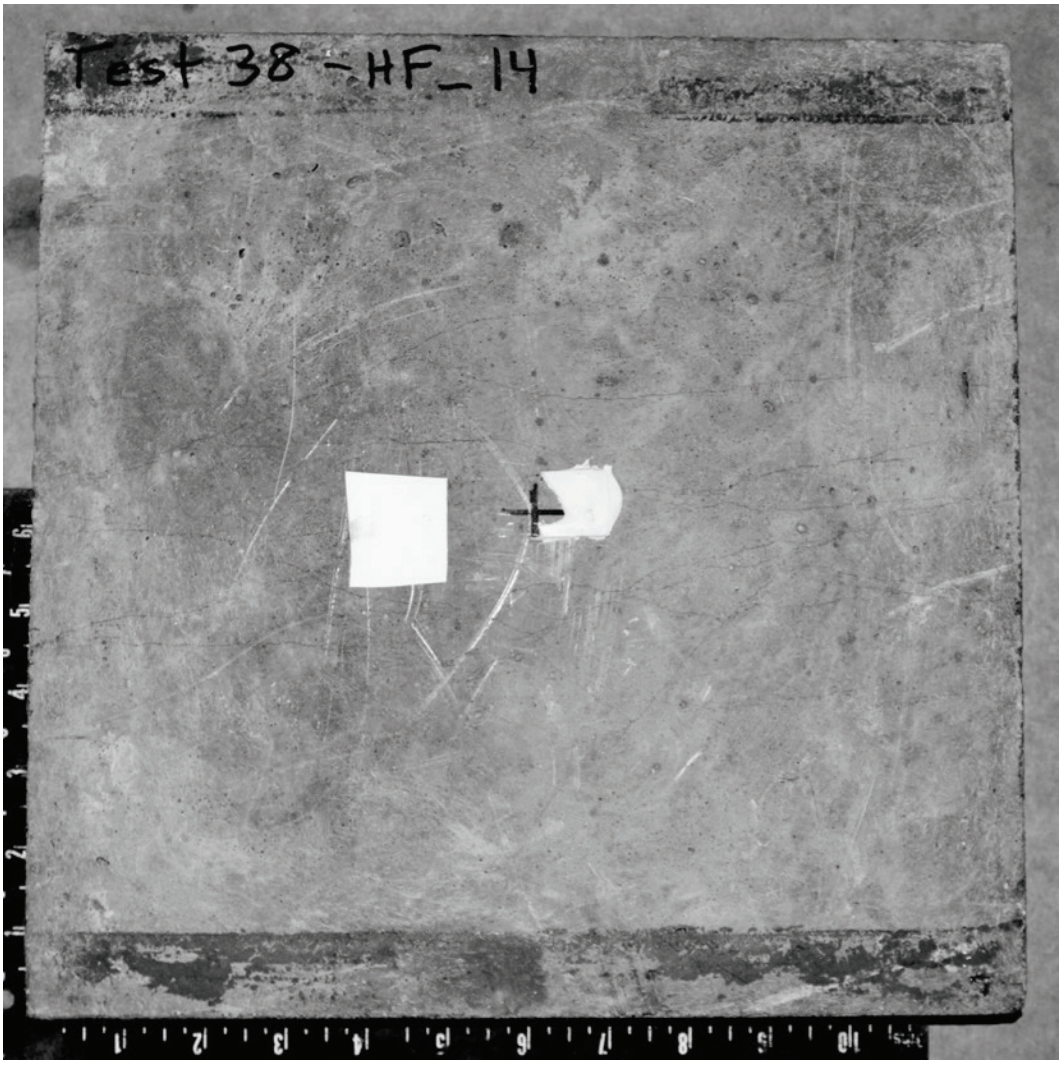

A.2.2 High pressure

Figure A10. VHSC-1-1.

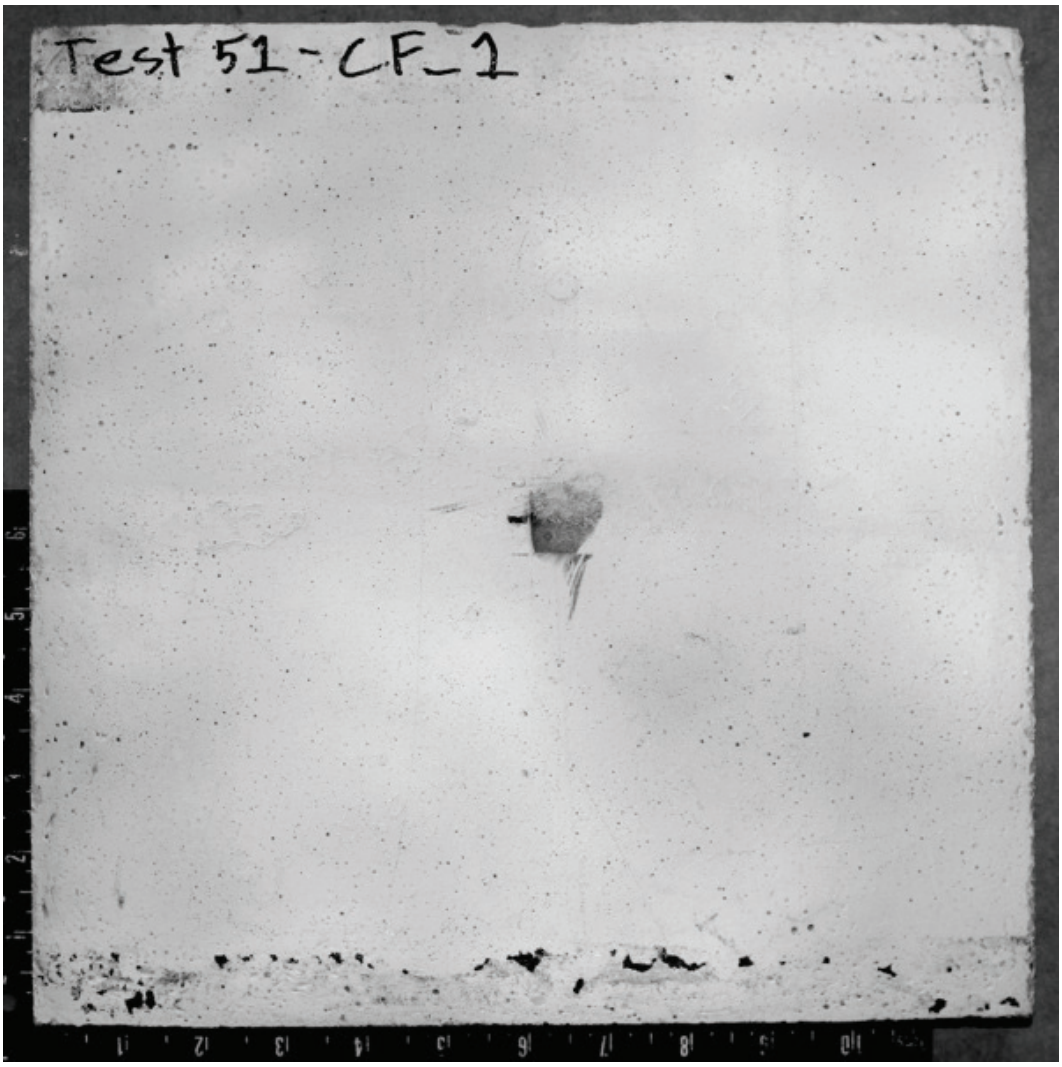

Figure A11. VHSC-1-2.

Figure A12. VHSC-6-1.

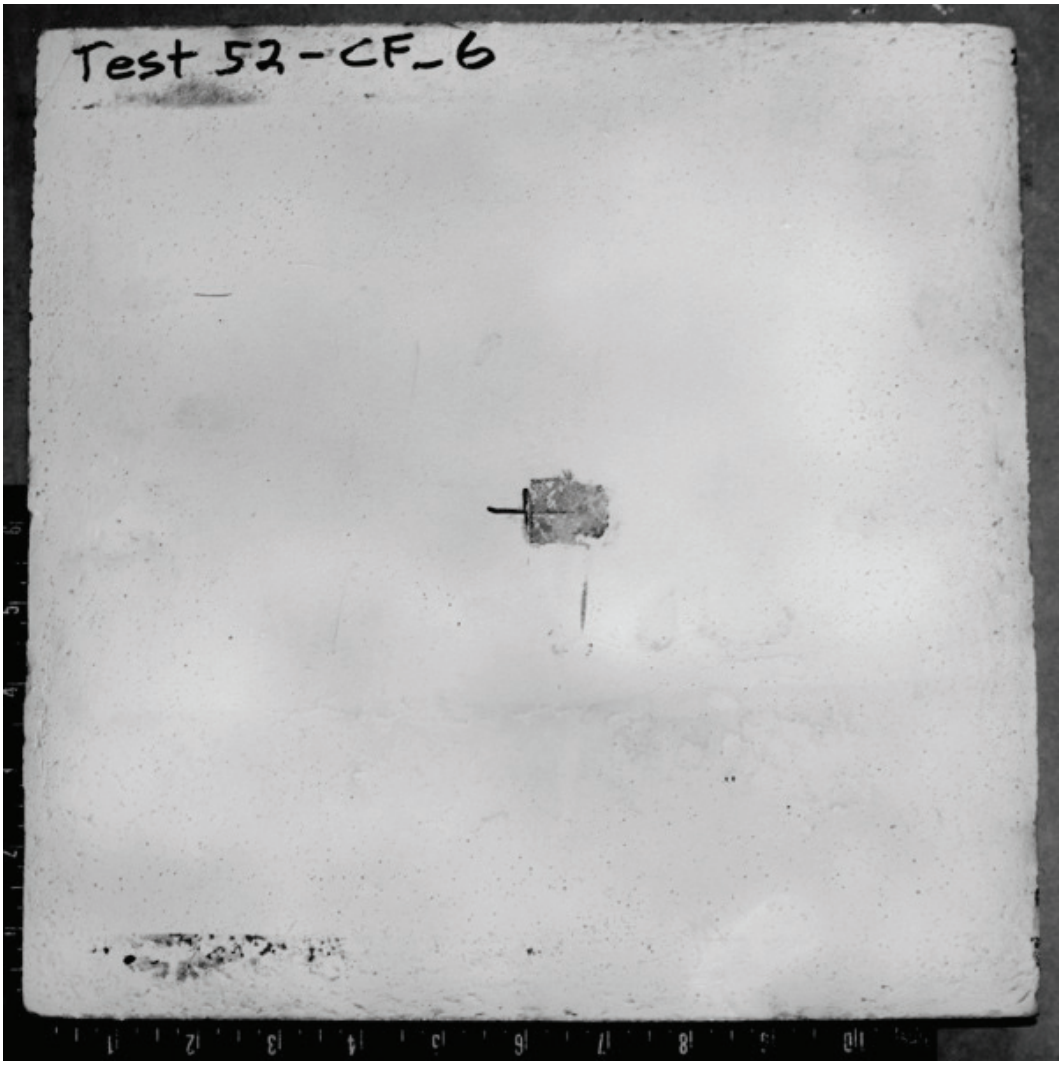

Figure A13. VHSC-6-2.

Figure A14. VHSC-9-2.

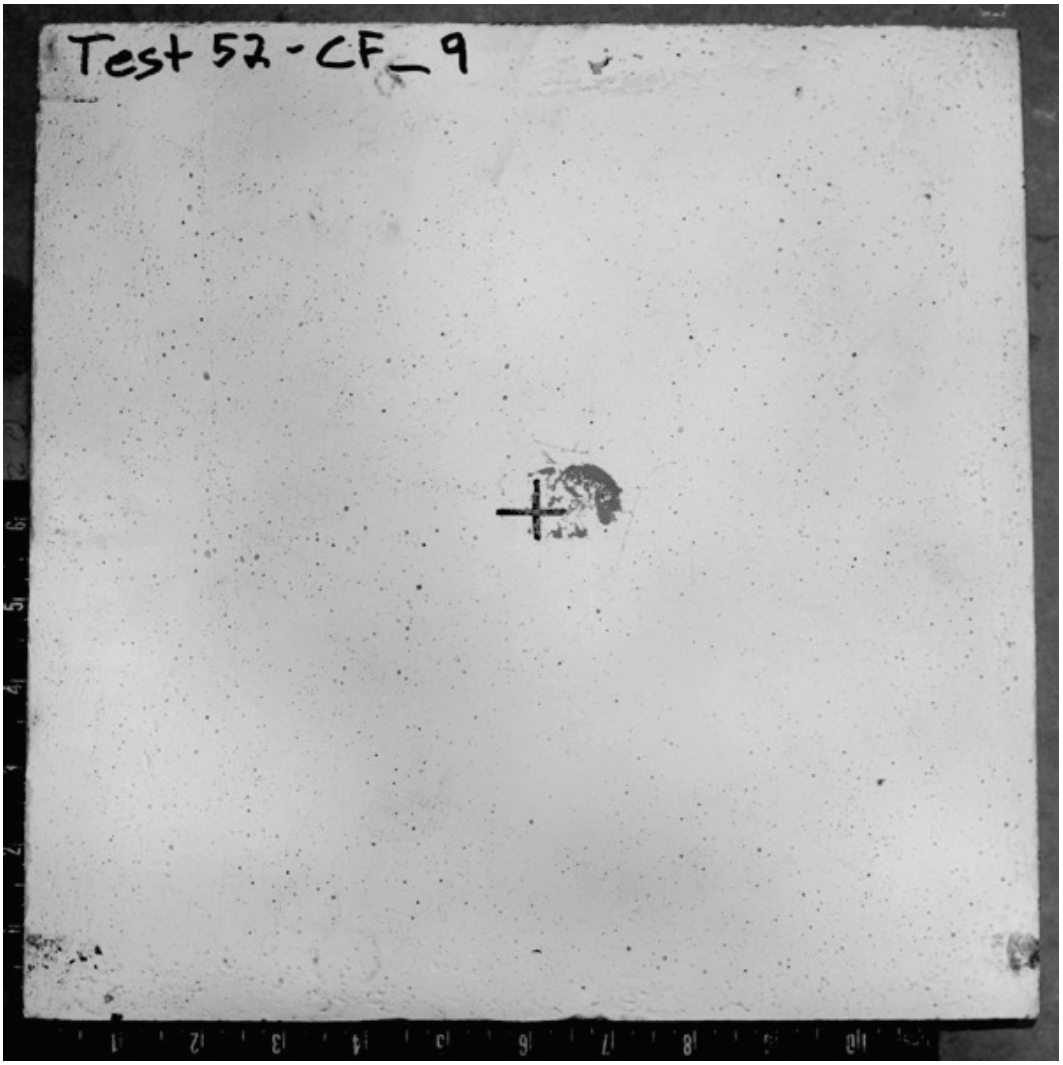

Figure A15. VHSC-9-1.

Figure A16. HSHDC-1.

Figure A17. HSHDC-16.

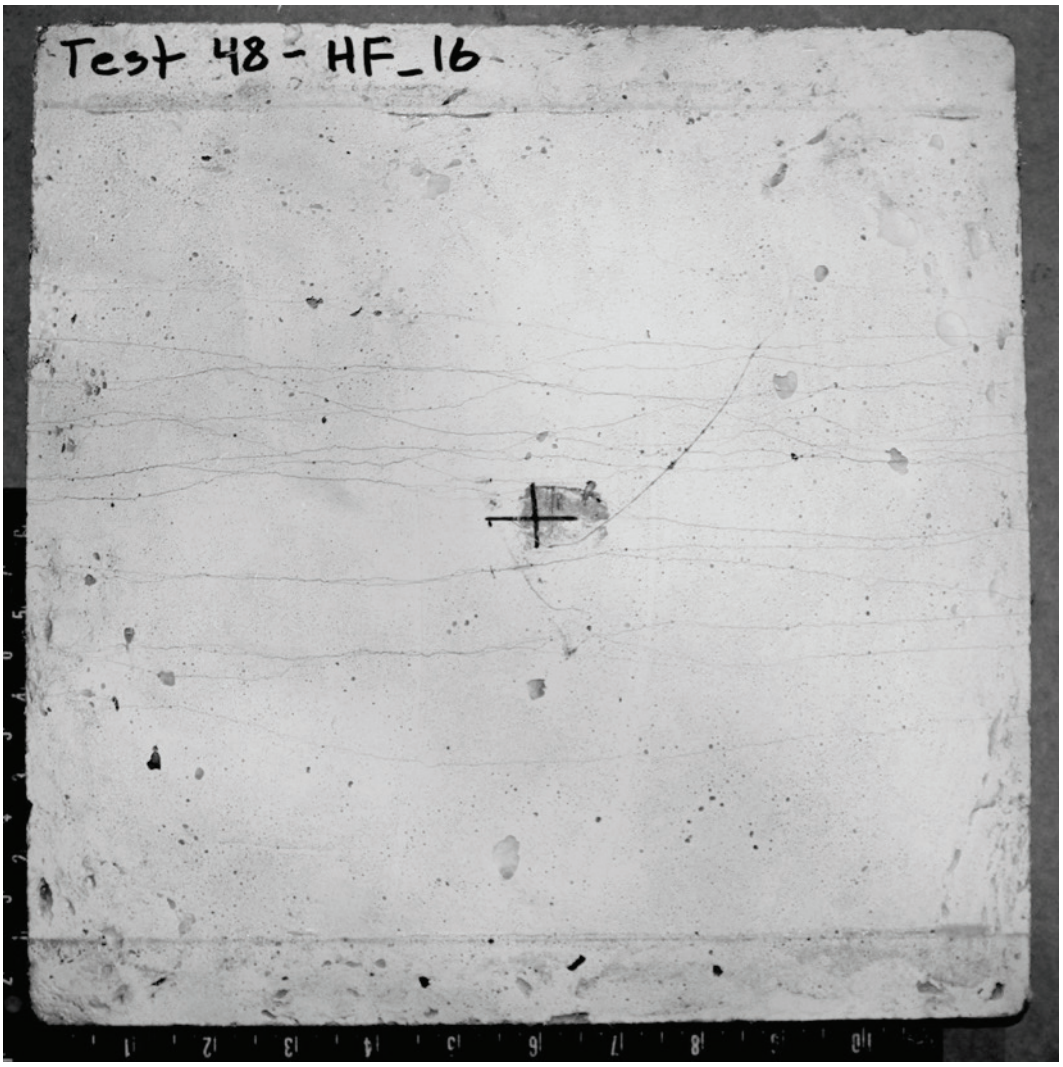

Figure A18. HSHDC-2.

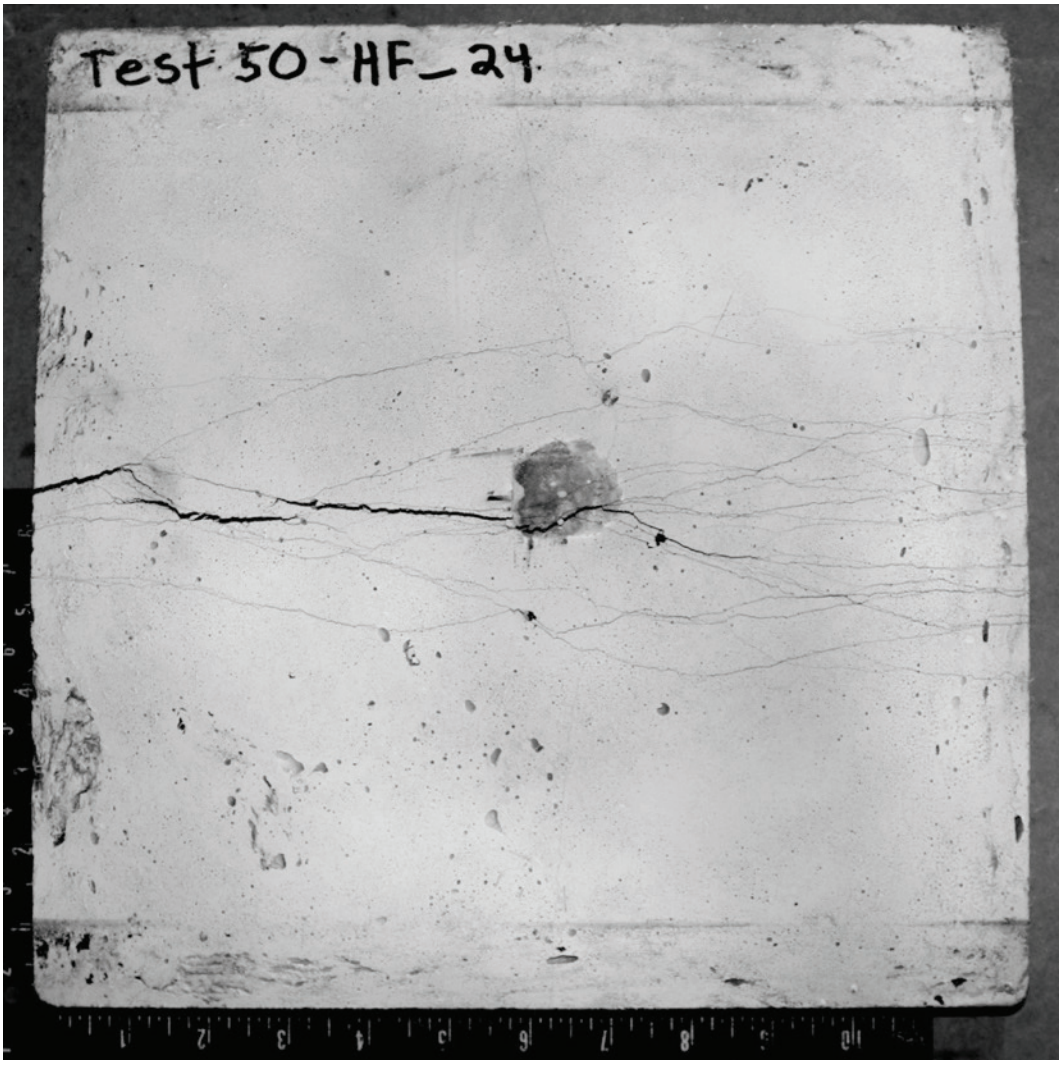

REPORT DOCUMENTATION PAGE

Form Approved
OMB No. 0704-0188

1. REPORT DATE ***(DD-MM-YYYY)***
August 2016

2. REPORT TYPE
Final

3. DATES COVERED ***(From - To)***

4. TITLE AND SUBTITLE

Equipment and Protocols for Quasi-Static and Dynamic Tests of Very-High-Strength Concrete (VHSC) and High-Strength High-Ductility Concrete (HSHDC)

5a. CONTRACT NUMBER

5b. GRANT NUMBER

5c. PROGRAM ELEMENT NUMBER

6. AUTHOR(S)

Brett A. Williams, Robert D. Moser, William F. Heard, Carol F. Johnson, Dylan A. Scott, Thomas R. Slawson, Henry L. Blake, R. Nicholas Boone, and Thomas D. White

5d. PROJECT NUMBER

5e. TASK NUMBER

5f. WORK UNIT NUMBER
BT007

7. PERFORMING ORGANIZATION NAME(S) AND ADDRESS(ES)

Geotechnical and Structures Laboratory
Information Technology Laboratory
U.S. Army Engineer Research and Development Center
3909 Halls Ferry Road
Vicksburg, MS 39180-6199

8. PERFORMING ORGANIZATION REPORT NUMBER

ERDC TR-16-13

9. SPONSORING / MONITORING AGENCY NAME(S) AND ADDRESS(ES)

Office of the Assistant Secretary of the Army for Acquisition, Logistics and Technology, Research and Technology
Washington, DC 20310-1500

10. SPONSOR/MONITOR'S ACRONYM(S)
SAAL-ZT

11. SPONSOR/MONITOR'S REPORT NUMBER(S)

12. DISTRIBUTION / AVAILABILITY STATEMENT
Approved for public release; distribution is unlimited.

13. SUPPLEMENTARY NOTES

14. ABSTRACT

This research developed the quasi-static and dynamic equipment and protocols for tests of both very-high-strength concrete (VHSC) and high-strength high-ductility concrete (HSHDC) to predict blast performance. VHSC was developed for high compressive strength (> 200 MPa). Using VHSC as the baseline material, HSHDC was developed and exhibits comparable compressive strength (> 150 MPa) and high tensile ductility (> 3 percent tensile strain). This research investigated quasi-static material properties including compression, tension, and flexure (third-point and pressure loadings). Additionally, dynamic blast load simulator (shock tube) tests were performed on simply supported one-way panels in flexure. Subsequently, the material response in flexure was predicted using the Wall Analysis Code (WAC). Although VHSC has a higher peak flexural strength capacity, HSHDC exhibits higher ductility through multiple parallel micro-cracks transverse to loading. The equipment and test protocols proved to be successful in providing ways to test scaled concrete specimens quasi-statically and dynamically.

15. SUBJECT TERMS

16. SECURITY CLASSIFICATION OF:			**17. LIMITATION OF ABSTRACT**	**18. NUMBER OF PAGES**	**19a. NAME OF RESPONSIBLE PERSON**
a. REPORT	**b. ABSTRACT**	**c. THIS PAGE**			**19b. TELEPHONE NUMBER** ***(include area code)***
Unclassified	Unclassified	Unclassified		90	

15. SUBJECT TERMS (concluded)

Blast Load Simulator
High-Performance Concrete
Mechanical properties
Strain rate sensitivity
High strength concrete – Ductility
Concrete panels – Blast effect
Explosives – Military aspects – Testing
Strength materials
Soil mechanics
Dynamic testing
Cratering